Dynamics of Guests Bound to Biomolecules

by

Tamara Catherine Selina Pace
B.Sc., McMaster University, 2003

A Dissertation Submitted in Partial Fulfillment
of the Requirements for the Degree of

DOCTOR OF PHILOSOPHY

in the Department of Chemistry

# Supervisory Committee

Dynamics of Guests Bound to Biomolecules

by

Tamara Catherine Selina Pace
B.Sc., McMaster University, 2003

**Supervisory Committee**

Dr. Cornelia Bohne (Department of Chemistry)
**Supervisor**

Dr. Frank C. J. M. van Veggel (Department of Chemistry)
**Departmental Member**

Dr. Lisa Rosenberg (Department of Chemistry)
**Departmental Member**

Dr. Alisdair Boraston (Department of Biochemistry and Microbiology)
**Outside Member**

# Abstract

**Supervisory Committee**
Dr. Cornelia Bohne (Department of Chemistry)
**Supervisor**
Dr. Frank C. J. M. van Veggel (Department of Chemistry)
**Departmental Member**
Dr. Lisa Rosenberg (Department of Chemistry)
**Departmental Member**
Dr. Alisdair Boraston (Department of Biochemistry and Microbiology)
**Outside Member**

Supramolecular systems are held together by non-covalent forces, and include systems involving the interaction of small molecules with biomolecules such as DNA and proteins. The inherent reversibility of supramolecular systems means that dynamic processes are important for many of the functions achieved.

The first objective of this work was to develop methodology to study the dynamics and binding mechanism of small molecules with DNA. Though there is a great deal known about the thermodynamics of molecules binding to DNA there is much less known about the binding dynamics. Aminoxanthones were chosen as appropriate guest molecules, and their photophysics were examined in a number of solvents, showing that both the singlet and triplet excited states are strongly affected by solvent polarity, with the excited state energies decreasing in polar solvents. Laser flash photolysis experiments for quenching of the triplet excited state by nitrite anions in the absence and presence of DNA allowed a residence time of microseconds to be estimated for these guests. These experiments also showed that this methodology is not widely applicable when studying the binding dynamics of small molecules with DNA, and that other fast kinetic techniques are necessary.

Laser temperature jump experiments allow measurement of dynamics in supramolecular systems, while avoiding the problems encountered in laser flash photolysis experiments. A custom-built system was developed as an adaptation of systems described in the literature, with the main difference being a laser optimized for the excitation of water, and the ability to operate across a wide dynamic range. The laser and the detection systems for absorbance and fluorescence were successfully implemented and a number of artifacts were eliminated. The expected temperature jump was obtained and signals were detected by both fluorescence and absorption; the signal-to-noise ratio still needs improvement before systematic studies can be carried out.

The second objective of this work was to study bimolecular reactions in proteins. Using biomolecules to effectively modulate reactivity in bimolecular reactions requires knowledge of the reaction mechanism. When the dimerization of 2-anthracenecarboxylate (AC) takes place in serum albumin proteins enantiomeric excess (ee) is obtained for the chiral products. There are a number of binding sites for AC in these proteins and it has been shown that a balance between strength of binding and mobility of the reactants is essential to achieve high ee's. In human serum albumin remarkable ee's of more than 80% are achieved. It is important to differentiate between reactant molecules bound to different binding sites so that the binding sites where reaction preferentially forms one enantiomer can be identified. Steady-state and time-resolved fluorescence studies identified two types of 2-anthracenecarboxylate bound to HSA: one that has a short lifetime and is very protected from the bulk aqueous solution, and one that has a longer lifetime, but is exposed to the bulk solution. Further work using binding site inhibitors allowed identification of a third type of molecule that has a longer

lifetime, but is very protected from the bulk solution, which is likely the species responsible for the majority of the observed ee.

# Table of Contents

# List of Tables

# List of Figures

# List of Schemes

# List of Abbreviations

| | |
|---|---|
| Å | Angstrom |
| A | absorbance |
| $A_i$ | pre-exponential factor for species *i* |
| AC | 2-anthracenecarboxylate |
| AT | adenine-thymine base pair |
| ΔA | absorbance difference |
| BSA | bovine serum albumin |
| °C | degrees Celsius |
| CD | cyclodextrin |
| CD | circular dichroism |
| $CH_3NO_2$ | nitromethane |
| cm | centimetre |
| *ct* | calf thymus |
| $C_v$ | heat capacity at constant volume |
| DAX | 2,7-diaminoxanthone |
| DNA | deoxyribonucleic acid |
| $D_2O$ | deuterated water |
| $E_s$ | singlet excited state energy |
| $E_T$ | triplet excited state energy |
| ee | enantiomeric excess |
| eq. | equivalents |
| ε | absorption coefficient |
| $F_i$ | fraction of integrated fluorescence spectra corresponding to species *i* |
| G | guest |
| H | host |
| HG | host-guest complex |
| HH | head-to-head |
| HPLC | high performance liquid chromatography |

| | |
|---|---|
| HT | head-to-tail |
| HSA | human serum albumin |
| $H_2O$ | water |
| I | light intensity |
| I | fluorescence intensity |
| 4-IB | 4-iodobenzoate |
| IRF | instrument response function |
| $\Delta I$ | change in fluorescence intensity |
| $k_+$ | association rate constant |
| $k_+^*$ | association rate constant for an excited state |
| $k_-$ | dissociation rate constant |
| $k_-^*$ | dissociation rate constant for an excited state |
| $k_i$ | decay rate constant for species *i* |
| $k_o$ | decay rate constant for guest in bulk solution |
| $k_o^H$ | decay rate constant for guest in host |
| $k_{obs}$ | observed rate constant |
| $k_q$ | quenching rate constant for guest in bulk solution |
| $k_q^H$ | quenching rate constant for guest in host |
| $K$ | equilibrium constant |
| $K_{SV,i}$ | Stern-Volmer constant for species *i* |
| kJ/mol | kilojoules per mole |
| kΩ | kiloohms |
| l | pathlength |
| $L_{bound}$ | concentration of bound guest |
| $L_{free}$ | concentration of free guest |
| LAAPD | large-area avalanche photodiode |
| lfp | laser flash photolysis |
| ltj | laser temperature jump |
| λ | wavelength |
| $\lambda_{em}$ | emission wavelength |
| $\lambda_{ex}$ | excitation wavelength |

| | |
|---|---|
| m | mass |
| M | molar |
| MAX | 2-aminoxanthone |
| mL | millilitre |
| mm | millimetre |
| mM | millimolar |
| ms | millisecond |
| mV | millivolts |
| MΩ | megaohms |
| μM | micromolar |
| μs | microsecond |
| *n* | number of base pairs per binding site |
| NaCl | sodium chloride |
| NaOH | sodium hydroxide |
| Nd:YAG | neodymium-doped yttrium aluminum garnet |
| nm | nanometre |
| NMR | nuclear magnetic resonance |
| ns | nanosecond |
| $N_2O$ | nitrous oxide |
| PMT | photomultiplier tube |
| *r* | ratio between concentration of bound guest and the concentration of DNA base pairs |
| s | second |
| SDS | sodium dodecyl sulfate |
| $<\tau>$ | average lifetime |
| *t* | time |
| T | transmittance |
| $T_i$ | initial temperature |
| ΔT | change in temperature |
| UV-Vis | ultraviolet-visible spectroscopy |
| ΔU | change in internal energy |
| V | volts |

| | |
|---|---|
| VSF | vacuum spatial filter |
| w/v | weight per volume |

## Acknowledgments

I would like to thank my supervisor, Dr. Cornelia Bohne, for all the guidance and opportunities she has provided for me throughout my time at UVic, Luis Netter for all his help in development of the laser temperature jump system, and otherwise, and the various members of, and visitors to, the Bohne research group who have given great variety to my experience.

I would like to thank Professor Yoshihisa Inoue at Osaka University, Japan, for the productive AC collaboration, and the opportunities to spend time in his lab, Dr. Masaki Nishijima for his help with product studies, and all the other members of the Inoue research group for their warm welcome during my times in Japan.

I would like to thank my family and friends for all their support, especially my parents, Phil and Linda, for their unwavering belief in me.

Finally, I would like to express my gratitude for the generous funding I have received during my studies from NSERC, UVic and its donors, and the COE programs at Osaka University.

# 1. GENERAL INTRODUCTION

## 1.1 Dynamics in supramolecular systems

Supramolecular systems consist of two or more molecular components held together by intermolecular forces.[1] The properties of the supramolecular system are different than those of its components, and a supramolecular system has the capability of achieving functions that molecular systems cannot. The intermolecular forces involved in these systems can include hydrogen bonding, hydrophobic effects, π-stacking, electrostatic interactions, and van der Waals forces. These forces are relatively weak when compared to covalent bonds, and as a result supramolecular systems are reversible. This inherent reversibility is essential for many of the functions that are achieved. Many supramolecular systems have been synthesized, but one may also consider many naturally occurring biological systems. Supramolecular interactions are the basis of many highly specified biological processes including protein complexation, transport of small molecules, cellular recognition, and reading or copying of DNA.[1]

Detailed knowledge of both the dynamics and thermodynamics of supramolecular systems is needed in order to understand how they function. Thermodynamic studies provide information about what complexes are present at equilibrium and how efficiently they are formed, while structural studies show how these systems are organized at equilbrium. Kinetic studies allow measurement of association and dissociation rate constants, providing information on how fast a complex is formed and how fast it falls apart. Thermodynamic information can be inferred from dynamic studies, but no information on the kinetics of a system can be obtained from thermodynamic or structural

studies. Two host-guest systems may have the same equilibrium constant, which means that the ratio of the association and dissociation rate constants is the same, but the absolute values of the rate constants could be very different. Direct kinetic measurements must be made in order to understand dynamic processes in supramolecular systems.

The structural complexity of supramolecular systems that has been achieved far exceeds what is known about dynamics in these systems. In general kinetics can be measured using real time measurements to measure absolute rate constants, or by relative rate measurements. Measuring relative rates requires comparison to a system with the same mechanism for which rate constants are known. Dynamics in supramolecular systems are not well enough understood to find appropriate standard reactions, and kinetic measurements need to be carried out in real time. This has provided challenges because the dynamics are generally faster than were accessible early on, and suitable techniques had to be developed.[2,3] The timescale for the association and dissociation processes involving the various components of a supramolecular system is influenced by the size and complexity of the system. The shortest timescale on which encounter between two components can occur in solution is limited by the rate of diffusion. Generally association and dissociation processes in supramolecular systems are expected to occur on a timescale of nanoseconds or longer.

### 1.2 Techniques to study dynamics in supramolecular systems

Real time kinetic measurements are most commonly carried out using methods that involve perturbing a system that is at equilibrium, though there are some methods that do not require perturbation of an equilibrium. The perturbation must be faster than

the relaxation of the system to its new equilibrium. The relaxation kinetics are measured, from which the rate constants for the relevant association and dissociation processes can be obtained (Section 1.3). There are a number of ways in which a system can be perturbed, with creation of a new chemical species (excited state) or changes in temperature, pressure or concentration being the most common. Each technique has advantages and disadvantages and the choice of technique depends on a number of factors including the required timescale and the experimental observable. These techniques are described here briefly, with the techniques used in this work given first in more detail.

### 1.2.1 Photophysical techniques

Perturbation of a supramolecular system can be achieved by using photophysical techniques, where formation of an excited state provides the fast perturbation. The movement of an excited state guest between the host system and bulk solution can then be monitored directly, or indirectly with the use of quenchers. The ability to measure binding dynamics depends in part on the excited state lifetime.[2,3] If the binding dynamics are slower than the excited state lifetime then the excited state will not have the opportunity to relocate during its lifetime, and no information on the association and dissociation rate constants can be obtained. Photophysical techniques necessitate the use of molecules containing chromophores, and it is important for the excited state molecule to be non-reactive towards itself and other components in the system. It should be noted that photophysical methods measure the association and dissociation rate constants of the

excited state guests, which can differ significantly from those observed for the ground state guest.[4]

### 1.2.1.1 Fluorescence

#### 1.2.1.1.1 Time-resolved fluorescence

Singlet excited state lifetimes are measured using time-correlated single photon counting. An excitation source with a high repetition rate is used to excite the fluorophore and the time for emission of a single photon is measured. A histogram of the number of photons detected against time is built, relying on the concept that the probability distribution for emission of a single photon after excitation follows the statistical distribution of all photons emitted as a result of excitation. A large dynamic range is obtained for the intensity, which helps in differentiation of fluorescence species with different lifetimes.

Fluorescence decay functions are generally exponential or a sum of exponentials (Equation 1.1):

$$I(t) = \sum_{1}^{i} A_i e^{-k_i t} \qquad (1.1)$$

The parameter $k_i$ is the decay rate constant of each fluorescent species, and its inverse value is equal to the singlet excited state lifetime of the emissive species ($\tau_i = 1/k_i$). $A_i$ is the pre-exponential factor for each emissive species, $i$, with a different lifetime, where the sum of all pre-exponential factors is equal to 1.

In general the singlet excited states of organic molecules have lifetimes that are shorter than 100 ns. Information on dynamics can therefore only be obtained from time-resolved fluorescence measurements if the association and dissociation rate constants are

very fast, and in most cases the lifetime of the singlet excited state is too short for the guest to move between the bulk solution and the host system.

#### 1.2.1.1.2 Steady-state fluorescence

Steady-state fluorescence experiments measure the fluorescence intensity as a function of wavelength. Fluorescence measurements can provide information on the binding environment of the fluorophore and on equilibrium constants, but generally not on dynamic processes.

### 1.2.1.2 Laser flash photolysis

Laser flash photolysis (lfp) experiments are based on the formation of an excited state by a laser pulse. The shortest accessible timescale is usually dependent on the pulse width of the laser. Generally, when looking at binding dynamics in supramolecular systems, nanosecond resolution is used. Most laser flash photolysis systems are capable of measuring lifetimes up to hundreds of microseconds.

Laser irradiation is orthogonal to the monitoring beam that is used to measure the absorption of the sample. Absorption is monitored before and after the laser pulse, leading to measurements of absorbance differences ($\Delta A$) with time. Usually the decays of triplet excited states are measured in lfp experiments. Triplet excited states are much longer lived than singlet excited states, and lifetimes in aqueous solution are often hundreds of nanoseconds or longer. These lifetimes are long enough for relocation of the guest between the bulk solution and the supramolecular system to occur, and dynamics occurring from tens of nanoseconds to hundreds of microseconds can be measured.

Using excited states to study dynamics in supramolecular systems adds an extra aspect to the treatment of the kinetic data since the excited state has a lifetime, which must be taken into account. The binding dynamics of an excited state guest in 1:1 host-guest systems are depicted in Figure 1.1.

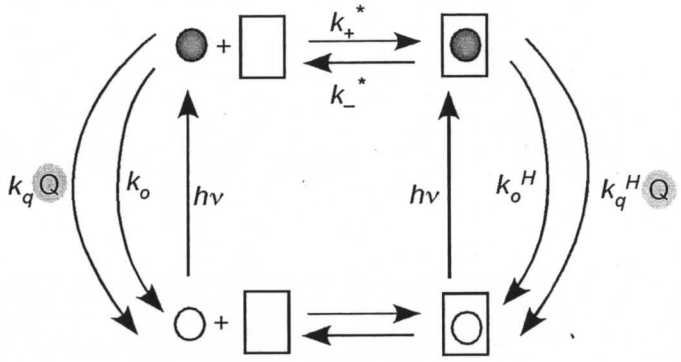


**Figure 1.1** Schematic representation of the binding dynamics of an excited state guest in the presence of quenchers. The guest is represented by the circle, the host by the rectangle, and the quencher by the circle containing a Q. The shaded circle represents the excited state guest. The parameters $k_o$ and $k_o^H$ are the decay rate constants for the guest in the absence and presence of host. The parameters $k_q$ and $k_q^H$ are the quenching rate constants in the absence and presence of the host. The parameters $k_+^*$ and $k_-^*$ are the association and dissociation rate constants for the excited state guest.

If the absorption spectra are different for the excited state guest in bulk solution and in the supramolecular system, and the equilibrium constant of the ground and excited state guest with the host are different, then the relaxation kinetics can be followed directly. However the absorption spectra of the free and bound excited state guest usually do not change enough, and a quenching methodology must be employed to obtain kinetic information (Section 2.1.3).

### 1.2.2 Temperature jump

Temperature jump experiments use a rapid change in the solvent temperature to perturb a system's equilibrium. The equilibrium being monitored must be temperature sensitive and an observable such as fluorescence, absorption, or scattering intensity must change when the equilibrium shifts. Monitoring fluorescence or absorption is most common, so the systems being studied must contain a chromophore that has different absorption or fluorescence when free or when in the supramolecular complex. A wide range of timescales can be studied using temperature jump studies, with the shortest timescale determined by the heating time. The longest accessible timescale is determined by the cooling time, which is the time it takes for the heated volume of solution to reach equilibrium with the surrounding solution. There are three different methods that have been used to achieve heating of a solution: Joule heating, microwave heating, and heating using lasers.[5]

Joule heating has been the most commonly used method for temperature jump studies. Heating is achieved when a capacitor is discharged through a solution containing electrolytes, which are responsible for the heat transfer. The typical heating time using this process is on the microsecond timescale.[5-8] Whether Joule heating can be used for temperature jump studies involving charged macromolecules, such as DNA, has been questioned, as the high electric fields applied can lead to artifacts, due to reorientation of the charged macromolecules, that interfere with the relaxation signal of interest.[6-8] However, these artifacts can be minimized in absorption measurements carried out with light polarized at the magic angle (54.7 degrees), and in fluorescence measurements when both the excitation and emission are polarized at the magic angle.[9] At the magic angle changes in the absorption or fluorescence signals due to orientation disappear.[9]

Microwave heating is carried out using a pulse of microwave energy generated within a magnetron. The only requirement for this heating method is that the solvent have a permanent dipole moment.[5] As electrolytes are not required this technique can be used for systems in non-aqueous solvents. However, this techniques is not widely used and the temperature changes are much smaller than those achieved when the other heating methods are used.[5]

Using lasers can achieve heating in pico- to nanoseconds,[10-13] and this is the best temperature jump method when fast kinetics are studied. A few different strategies have been used, and are discussed in more detail is Section 3.1.3. An early method used dyes excited by a laser in the visible region. Heating resulted from the heat release during the non-radiative decay of the dye.[14] Better methods use direct absorption of the laser light by the solvent, water. The absorption coefficient of water at the 1064 nm band of a YAG laser is too low to achieve efficient heating, so different methods, using less common laser set-ups, have been developed. Raman shifted YAG lasers[15-18] led to laser irradiation wavelengths in the 1400 – 1900 nm region. The absorption coefficient of water in this wavelength region is high, which limits the long timescales accessible, since the volumes of solution that can be heated are small. The iodine laser with emission at 1315 nm has also been used in laser temperature jump experiments.[12] The absorption coefficient of water at 1315 nm is close to the optimum value of 0.5 $cm^{-1}$.[5,12] This allows for much larger volumes to be heated, increasing the accessible time domains.

### 1.2.3 Stopped-flow

Stopped-flow experiments use a change in concentration to perturb the system being studied. Two separate solutions are driven through a mixing chamber where they are thoroughly mixed before flowing into an observation cell, where flow is stopped and further changes in the system are monitored.[19] Mixing causes perturbation of the initial equilibrium, and relaxation to the new equilibrium is monitored over time, usually by absorption or fluorescence. The use of fluorescence or absorption detection requires that either the host or guest contains a chromophore, and that the absorption or fluorescence is not the same when free in solution, or in the supramolecular complex. The time resolution of these experiments is determined by the time required to mix the solutions, and stop the flow in the observation cell, and is typically 1 – 2 ms.[19]

### 1.2.4 Ultrasonic relaxation

Ultrasonic relaxation measurements achieve perturbation of an equilibrium by passing a sound wave through a solution, which results in periodic variations in pressure and temperature.[20,21] Any system in equilibrium can be cyclically perturbed by a sound wave if it has a non-zero value of the reaction enthalpy change ($\Delta H^{o}$) or reaction volume change ($\Delta V^{o}$). When the frequency of the sound wave is of the same order of magnitude as the rate of the relaxation process in the system then energy can be absorbed from the sound wave to supply heat to the reaction. The system's relaxation rates can be determined by measuring the dependence of sound absorption on frequency of the sound wave. This technique does not require the presence of a chromophore. However, since a number of processes, such as conformational changes, can also be observed by this method, it is quite important to be able to identify the process that is being perturbed by

the sound wave.[20] Measurements need to be made at a broad range of wavelengths, and commonly lifetimes from 1 ns to 1 μs are accessible through this technique.

### 1.2.5 Surface plasmon resonance

Surface plasmon resonance measurements are made on systems where one reactant is immobilized on a metal surface and the second reactant is flowed over this surface. When the two reactants interact there are changes in the refractive index at the metal surface. Surface plasmons are oscillating surface charge density waves that propagate at the interface between a metal and a dielectric.[22] Only light at a certain angle of incidence can couple to, and resonantly excite, surface plasmons. Changes in the refractive index at the surface change the surface plasmon wave vector, and therefore change the angle of incidence required to generate surface plasmons.[22,23] Monitoring the intensity of light that strikes the interface between the metal surface and the bulk solution can therefore give information on real time changes at the surface due to host-guest complexation. The observed kinetics may not be the same as those in solution, due to conformational changes of the bound reactant or artifacts arising due to mass transport limitations.[24] Only relatively slow processes can be measured using this technique; the upper limit for detectable association rate constants had been estimated to be on the order of $10^6$ $M^{-1}$ $s^{-1}$.[24]

### 1.2.6 Fluorescence correlation spectroscopy

Fluorescence correlation spectroscopy does not require perturbation of an equilibrium, and is based on the measurement of changes in the fluorescence intensity of

individual molecules.[25,26] A very small volume of sample is continuously irradiated and fluctuations in the fluorescence intensity arise due to any event that makes the fluorophore unavailable for excitation to the singlet excited state. These events may include diffusion out of the area of detection or formation of a dark state, e.g. a triplet excited state. This technique can be used to measure binding dynamics in host-guest systems if the fluorescence quantum yields for the free and bound fluorophore are different. Data are analyzed using autocorrelation functions, which define the probability of detecting a photon from the same molecule at time zero, and at various time shifts. Various assumptions have to be made to develop appropriate models from which binding dynamics can be obtained from the autocorrelation function. Fluorescence correlation spectroscopy can be used to study a wide range of time domains, from picoseconds to seconds.[27]

### 1.2.7 Nuclear magnetic resonance (NMR)

NMR experiments can be used to obtain kinetic information on systems while they are at equilibrium.[28,29] If nuclei in either the guest or host have different chemical shifts when free in solution or in the supramolecular complex, then the line shape depends on the frequency for the species free in solution and the species bound to the host-guest complex, and the residence time in each environment. When the dynamics are slow compared to the relaxation time of the NMR experiment no exchange between the two sites occurs during the NMR experiment, and two separate peaks are observed for the species free in solution and in the complex. If the dynamics are fast compared to the experimental relaxation time then only one peak is observed. When the residence time of

the species in each environment is intermediate then broadened peaks are observed, with the broadening related to the association and dissociation processes, and kinetic information can be obtained from fitting the shape of the spectrum. Rate constants can be obtained from line-shape analysis only when relaxation processes occur over 0.1 ms to 1 second.[29]

**1.3 Relaxation kinetics**

In the simplest case a 1:1 host-guest complex is formed between a guest (G) and a host (H) molecule (Equation 1.2).

$$G + H \underset{k_-}{\overset{k_+}{\rightleftharpoons}} HG \qquad (1.2)$$

The equilibrium constant, $K$, for this system is defined as (Equation 1.3):

$$K = \frac{[HG]}{[G][H]} = \frac{k_+}{k_-} \qquad (1.3)$$

where $k_+$ is the association rate constant and $k_-$ is the dissociation rate constant.

The following rate law (Equation 1.4) defines the kinetics for this system:

$$\frac{d[HG]}{dt} = k_+ [H][G] - k_- [HG] \qquad (1.4)$$

If either the guest or host is in excess (e.g. [H] >> [G]), then this rate law is simplified to Equation 1.5:

$$\frac{d[HG]}{dt} = k_+^\circ [G] - k_- [HG] \qquad (1.5)$$

where the pseudo-first-order rate constant, $k_+^\circ$, is equal to $k_+[H]$. At equilibrium $\frac{d[HG]}{dt} = 0$, and therefore $k_+^\circ[G]_{eq} = k_-[HG]_{eq}$.

After the perturbation the concentrations deviate from their equilibrium values by a certain amount, $x$, and the rate law can be written as Equation 1.6:

$$\frac{d[HG]}{dt} = k_+^\circ([G]_{eq} - x) - k_-([HG]_{eq} + x) \qquad (1.6)$$

which simplifies to Equation 1.7:

$$\frac{d[HG]}{dt} = -(k_+^\circ + k_-)x \qquad (1.7)$$

Equation 1.7 is a first-order differential equation and the decay kinetics will therefore follow a mono-exponential function, with the observed rate constant ($k_{obs}$) given by Equation 1.8.

$$k_{obs} = k_+^\circ + k_- = k_+ [H] + k_- \qquad (1.8)$$

The concentration of free host, [H], is related to the total concentration of host, $[H]_T$, by the mass balance equation (Equation 1.9).

$$[H]_T = [H] + [HG] \quad (1.9)$$

If $[H]_T \sim [H]$, the analytical concentration of host can be used. Otherwise, a quadratic expression for the host concentration is obtained from Equations 1.3 and 1.9.

In Equation 1.8 the observed rate constant is related to the sum of the rate constants for the pseudo-first-order association process and the rate constant for the dissociation process. Changes in the host concentration can influence the association process, but the dissociation rate constant is intrinsic to the system and cannot be manipulated by external factors.

Host-guest interactions involving coupled or sequential first-order or pseudo-first-order reactions lead to decay kinetics that are a sum of exponential functions. More complex equations have to be derived if the reactions are not first-order or pseudo-first-order. In all cases, the rate law is related to both the association and dissociation processes, and these processes can never be decoupled when measuring a relaxation process.

**1.4 Biomolecules**

Biomolecules are organic molecules produced by living organisms that include large polymeric molecules such as DNA and proteins. These molecules have well-defined structures and often have a number of different binding sites for small molecules. The

biological function of most biomolecules is invariably dependent on direct, reversible interactions with other molecules. Understanding dynamic processes involving guest molecules bound to biomolecules will thus contribute to a better understanding of how biomolecules function, and how these systems can be exploited for other purposes.

### 1.4.1 DNA

#### 1.4.1.1 DNA structure

The basic nucleotide unit of DNA is composed of an aromatic base (adenine, guanine, thymine or cytosine), a sugar (2-deoxyribose), and a phosphate group. The nucleotides are joined together by a phosphodiester bond between the 3' carbon of one sugar, through the phosphate, to the 5' carbon of the adjacent sugar. The asymmetry of these bonds means that individual strands have directionality. In a DNA double helix two strands, in an antiparallel alignment, are held together by complementary hydrogen bonds between pairs of bases. The sugars and phosphate groups are on the outside of the helix and form the backbone, with the bases stacked near the centre of the helix. The double helix is quite stable, due to the hydrogen bonding interactions and the π-stacking interactions between bases. A hydration layer of water is generally associated with the DNA helix, and can be very important in stabilizing the helix structure.[30]

A number of different types of helices can be formed, but the most common is B-DNA. B-DNA is a right-handed helix that contains, on average, 10.5 base pairs per helical turn. The length per helical turn is 35.7 Å, and the distance between two adjacent base pairs is 3.4 Å. The width of the helix is about 20 Å.[31] However, the structure of the DNA helix is not uniform, and the parameters of any region depend on the actual

sequence of bases.[30] An important feature of B-DNA is the presence of two distinct grooves, a major and a minor groove. The major groove is wider than the minor groove, and different edges of the bases are accessible from the major or minor groove, resulting in distinct environments in each groove.

### 1.4.1.2 Binding of guests to DNA

The complexity of DNA structure results in a variety of ways in which small molecules can bind (Figure 1.2). Small molecules can bind through intercalation between the base pairs, groove binding in the major or minor grooves, as well as through non-specific electrostatic interactions with the negatively charged phosphate backbone.[32]

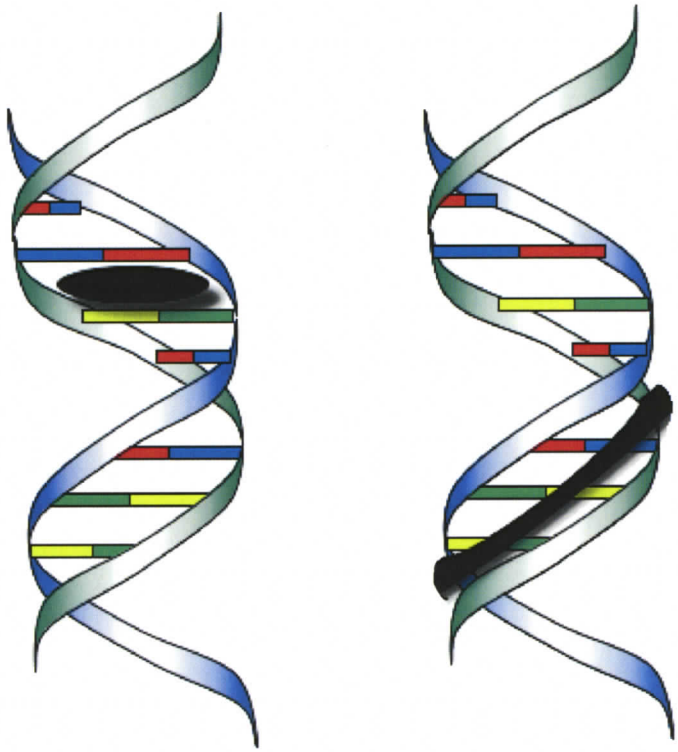

**Figure 1.2** Cartoon of intercalation and groove binding of a guest molecule with DNA.

All intercalators possess planar, electron-deficient, aromatic ring systems.[30] Typically the aromatic backbone contains three to four six-membered rings, and often incorporates heteroatoms. Often intercalators are cationic and possess flexible side chains. The equilibrium constants for organic intercalators and DNA are typically in the range of $10^4 - 10^6\ M^{-1}$.[33] The intramolecular forces involved in intercalation generally include the hydrophobic effect, electrostatic interactions, van der Waals forces, π-stacking and hydrogen bonding.[30] Intercalation significantly affects the structure of the DNA helix, because the helix must unwind so that the intercalator fits between two adjacent base pairs, leading to a lengthening of the helix.[30] When intercalators are bound to DNA binding of additional intercalators at sites immediately adjacent is inhibited. This neighbour exclusion principle means that, at most, intercalators can bind only at alternate base pair sites in DNA.

Relatively large molecules, such as proteins, bind preferentially to the major groove of DNA.[30] The smaller minor groove is the preferred binding site for smaller guest molecules.[30] Minor groove binders tend to consist of repeating aromatic rings containing heteroatoms, with the connection between rings allowing flexibility so that a shape similar to that of the DNA groove can be adopted.[30,34] Minor groove binders often also have cationic end groups. Typically equilibrium constants for groove binders are on the order of $10^5 - 10^9\ M^{-1}$.[33] Complexation is generally due to hydrogen bonding of the guest to the edges of the DNA bases, van der Waals interactions between the ligand and the walls of the DNA groove, electrostatic interactions of the charged end group with the DNA backbone and hydrophobic effects.[35] Minor groove binders typically show specificity for AT rich sequences due to specific hydrogen bonding interactions.[30,35,36]

### 1.4.2 Proteins

#### 1.4.2.1 Protein structure

All proteins are assembled from various combinations of twenty amino acids, and differ only in the specific sequence and number of amino acid residues. Amino acids are assembled in a linear chain by peptide bonds between the carboxyl and amino groups of adjacent residues. Due to interactions including hydrogen bonding, hydrophobic effects, and formation of disulfide bridges, these sequences fold into complex, but specific, three-dimensional structures. The folded structures of most proteins appear to be roughly spherical and consist of two or more structural units, or domains.[37]

Serum albumin proteins are the most abundant plasma proteins in mammals. An important function of serum albumin is its role in binding and transporting various molecules. Serum albumins consist of three highly helical domains that are homologous, but have different guest binding behaviour.[38]

#### 1.4.2.2 Binding of guests to proteins

Binding sites for guests are often sizable depressions on the protein surface. Complex formation often involves hydrogen bonding and electrostatic interactions.[37] In most cases there is a single unique binding site for a particular guest. One domain can bind more than one guest at separate binding sites, but it is unusual for there to be more than two or three such binding sites on any one domain. A protein that binds a number of different guests often binds them in separate domains.[37]

Serum albumins are known for their ability to bind many types of molecules, including long chain fatty acids and hydrophobic organic anions.[38] There are numerous sites where molecules are thought to bind to serum albumins. In human serum albumin

(HSA) an especially large number of compounds are bound in the regions termed Sudlow Site I and Sudlow Site II.[38] A wide structural variety of molecules bind to these regions, though some generalizations can be made. Molecules bound to Sudlow Site I are typically bulky heterocyclic anions with the charge centrally situated.[38] Molecules bound to Sudlow Site II are generally aromatic and may be neutral or have an anionic charge located more peripherally.[38] These sites also have the apparent ability to accommodate more than one guest at a time without significant interference.[38]

## 1.5 Example of measured dynamics in supramolecular systems

The ability to measure dynamics in supramolecular systems has developed from initial studies on relatively simple micelle systems, to more complex systems involving more than one binding site. A brief overview of work on micelles, cyclodextrins, and bile salt aggregates is given here.

### 1.5.1 Micelles

Micelles are self assemblies of surfactant molecules, which consist of alkyl chains and hydrophilic head groups. Micelles are themselves very dynamic; the whole assembly has a lifetime of milliseconds.[3] Guest molecules can be included inside the hydrophobic interior of the micelle.

Dissociation rate constants of polycyclic aromatic guests from micelles were found to decrease as the hydrophobicity of the guest was increased, with dissociation rate constants of $4.4 \times 10^6\ s^{-1}$, $0.25 \times 10^6\ s^{-1}$, $0.017 \times 10^6\ s^{-1}$ and $0.0041 \times 10^6\ s^{-1}$ obtained for the dissociation of benzene, naphthalene, anthracene, and pyrene, respectively, from SDS

micelles.[39] A similar trend was seen with a series of ketone guests, where the association rate constants were diffusion controlled, but the dissociation rate constants varied, and exit from the micelles was faster for the more polar ketones.[40,41]

### 1.5.2 Cyclodextrins

Cyclodextrin (CD) consists of 6 – 8 glucose units and are cyclic molecules with a cavity in which guests can bind. The formation of 1:1 host-guest complexes is common, but higher order complexes, such as 1:2 and 2:2 complexes, can also be formed with some guests.

The dynamics of the 1:1 complexes are fast, occurring on a nanosecond timescale.[2] For example, the association and dissociation rate constants of triplet xanthone with β-CD have been measured in lfp experiments to be $(6 \pm 1) \times 10^8$ $M^{-1}$ $s^{-1}$ and $(8.1 \pm 0.1) \times 10^6$ $s^{-1}$, respectively.[42] Comparison to ltj studies, which measured the binding dynamics of ground state xanthone, showed that the association process is largely unaffected by properties of the guest, while the dissociation processes can be greatly affected by the properties of the guest, especially by the basicity.[2] However, the size of the guest molecule can greatly affect both the association and dissociation processes, as has been shown with a series of azo dyes where the length of an alkyl substituent was varied.[43]

The increase in complexity on the formation of higher order complexes has been seen to have a significant effect on the binding dynamics. For 2:2 complexes it has been shown that the dissociation of the 2:2 complex can be up to a million times slower than

for the 1:1 complex. In the case of pyrene complexation with γ-CD a dissociation rate constant for the 2:2 complex of 73 ± 5 $s^{-1}$ has been measured.[2]

### 1.5.3 Bile salt aggregates

Bile salt aggregates form in aqueous solution from bile salts, and are an interesting system because they have been shown to have two distinct binding sites with different properties.[2] At low concentrations primary aggregates are formed which provide a hydrophobic binding site. As the concentration of bile salt is increased, further aggregation leads to the formation of secondary aggregates, which provide a relatively more polar binding site than that of the primary aggregate.

The dynamics observed for guests bound to these two distinct sites are quite different, with much longer residence times for guests in the primary binding site. For instance, the guest, 1-ethylnaphthalene is located in the primary aggregate and has a dissociation rate constant of (2.0 ± 0.4) x $10^5$ $s^{-1}$, while 1-napthyl-1-ethanol is located in the secondary aggregate and has a dissociation rate constant of (8 ± 1) x $10^6$ $s^{-1}$.[2]

## 1.6 Objectives

The objective of this work is to expand the systematic study of dynamics in supramolecular systems into more complex biomolecular systems, through the adaptation of current laser flash photolysis techniques (Chapter 2) or the development of laser temperature jump methodologies (Chapter 3) for the study of binding dynamics in DNA, and through the study of the mechanism of dynamic bimolecular reactions in proteins (Chapter 4).

# 2. PHOTOPHYSICS AND DNA BINDING DYNAMICS OF AMINOXANTHONES

The results presented in this chapter have been published in *Photochemistry and Photobiology* in 2006 in the paper 'Photophysics of Aminoxanthone Derivatives and Their Application as Binding Probes for DNA' (reference 44).

## 2.1 Introduction

### 2.1.1 Importance of binding dynamics in small molecule-DNA systems

The way in which some drugs function is thought to be related to the mode of interaction with DNA. The thermodynamics of small molecule-DNA interactions have been extensively studied, but relatively little is known about how the structure of guests affects their association and dissociation rate constants with DNA. However, there has been some suggestion that the efficacy of a small molecule as a drug is related to the residence time of the molecule within the DNA helix.[45-48] Comprehensive knowledge of how structural changes affect binding dynamics is therefore important in order to establish to what extent dynamic processes have an effect on biological function.

### 2.1.2 Binding dynamics of small molecules with DNA

The binding of various small molecules with DNA through intercalation or groove binding has been studied by stopped-flow, temperature jump experiments, surface plasmon resonance, NMR, flash photolysis, and fluorescence correlation spectroscopy.[49] The study of intercalative molecules has most commonly been carried out using stopped-flow and temperature jump experiments with dynamics in the millisecond time range

dominating. Studies on grove binding guests have more often used stopped-flow, NMR or surface plasmon resonance experiments with the majority of observed kinetic processes occurring on the millisecond to second timescales. Though systematic studies have not been carried out for very many systems, it has been observed that the dynamics in small molecule-DNA systems are complex, with most systems displaying multi-exponential relaxations.

Probably the most thoroughly studied DNA intercalator is ethidium bromide (Scheme 2.1). Description of this case gives a brief overview of the study of dynamics in these systems, and the sort of mechanistic information that can be obtained.

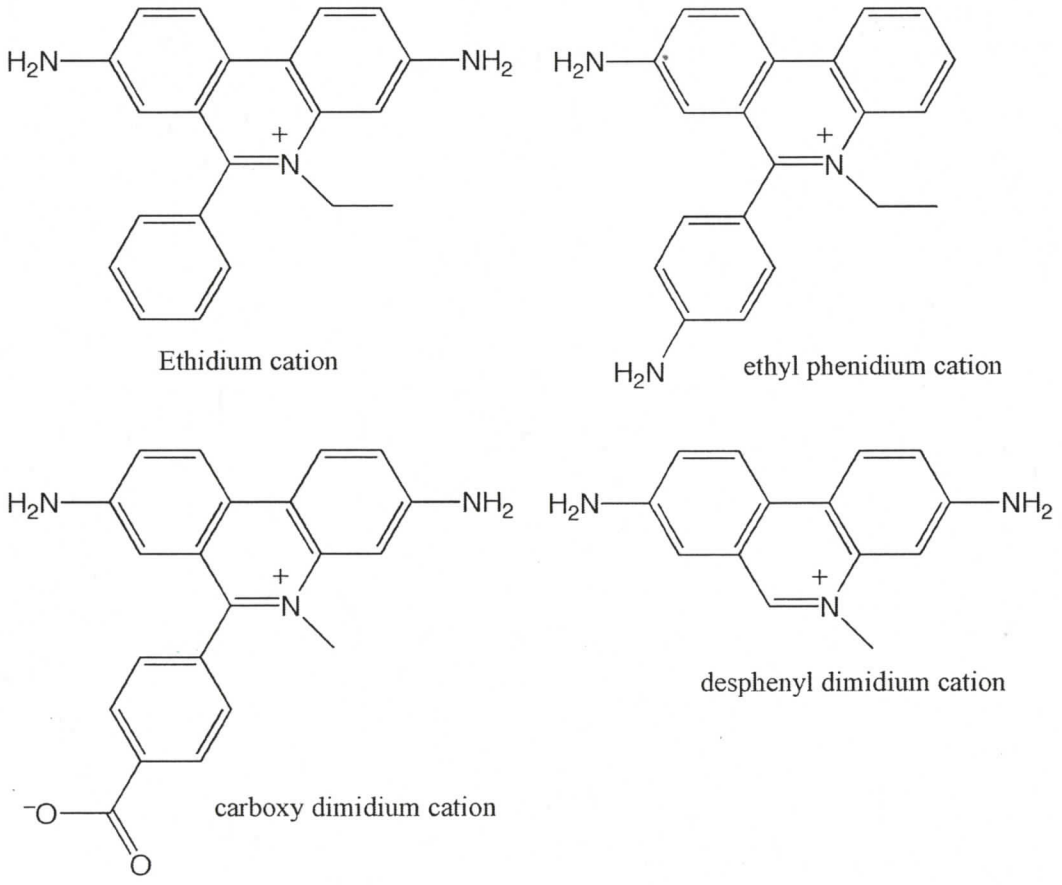


**Scheme 2.1** Ethidium bromide and derivatives.

Ethidium bromide is a widely used dye for DNA detection, because its fluorescence yield is very low in water, but increases significantly when intercalated in DNA.[50] Some studies on the ethidium bromide – DNA system assumed simple 1:1 binding when analyzing the kinetic data (Table 2.1). The binding of ethidium bromide to DNA has been investigated using fluorescence correlation spectroscopy assuming a 1:1 stoichiometry.[51] The association rate constant was determined to be more than two orders of magnitude smaller than the diffusion controlled rate, while the dissociation rate constant was found to be $0.27 \times 10^2$ $s^{-1}$.[51] An uncommon stopped-flow methodology using deuterium exchange has also been applied to the ethidium bromide – DNA system.[52] The value for the dissociation rate constant was the same as measured in fluorescence correlation spectroscopy, but the association rate constant differed greatly. Pressure jump experiments,[53] as well as temperature jump studies performed in combination with stopped-flow experiments[54] showed similar results when a 1:1 stoichiometry was assumed (Table 2.1).

**Table 2.1** Rate constants for the binding of ethidium bromide to DNA.

| Technique | $k_+^1 / 10^6$ $M^{-1} s^{-1}$ | $k_-^1 / 10^2$ $s^{-1}$ | $k_+^2 / 10^6$ $M^{-1} s^{-1}$ | $k_-^2 / 10^2$ $s^{-1}$ | $k_{12} / 10^5$ $M^{-1} s^{-1}$ | $k_{21} / 10^5$ $M^{-1} s^{-1}$ | Ref. |
|---|---|---|---|---|---|---|---|
| 1:1 binding mechanism | | | | | | | |
| Fluorescence correlation spectroscopy | 15 | 0.27 | - | - | - | - | 51 |
| Stopped-flow | 1.6 | 0.30 | - | - | - | - | 52 |
| Stopped-flow | 5.4 | 0.39 | - | - | - | - | 54 |
| Temperature jump | 6.4 | 0.16 | - | - | - | - | 54 |
| Pressure jump | 7.4 | 0.21 | - | - | - | - | 53 |
| Interconversion between two sites mechanism | | | | | | | |
| Temperature jump | | 1.6 | 0.48 | 0.35 | 21 | | 55 |
| Temperature jump | 1.4 | 1.7 | 0.26 | 0.59 | 1.3 | 2.5 | 56 |
| Stopped-flow | 7.3 | 0.39 | 1.1 | 0.14 | 6.0 | 15 | 54 |

The binding of ethidium bromide to DNA is however more complex, and a more involved binding mechanism has also been used to analyze this system. This mechanism assumes ethidium bromide binds to two distinct sites in DNA with interconversion between the two sites occurring through interaction with a second DNA molecule. This mechanism is consistent with the two coupled relaxation processes seen in subsequent stopped-flow and temperature jump experiments,[54-56] where the rate constant for each relaxation processes showed a linear dependence on the DNA concentration.[55] Both association processes ($k_+^1$ and $k_+^2$) and the interconversion rate constants ($k_{12}$ and $k_{21}$) were found to be several orders of magnitude smaller than the diffusion controlled limit, while the dissociation processes ($k_-^1$ and $k_-^2$) occurred on the millisecond timescale (Table 2.1). The dissociation rate constant from one of the sites was similar to the values determined assuming 1:1 binding.

Some insight into how structural changes affected the binding dynamics was obtained from a temperature jump experiment on ethidium bromide and several of its derivatives (Scheme 2.1).[56] This study assumed that the two binding sites were intercalation sites accessible from either the major or minor groove. The association to the site in the minor groove was slower than to the site in the major groove when amino substituents were added, indicating that steric factors are more important in binding to this site. The position of amino groups, or presence of the phenyl ring had a large effect on the dissociation rate constant of the derivatives in the major groove site, but a much smaller effect on the residence time in the minor groove site.

### 2.1.3 Laser flash photolysis methodology for determination of binding dynamics

Very little work on dynamics in small molecule – DNA systems has been carried out using laser flash photolysis studies. One study with acridine orange and proflavine (Scheme 2.2) showed that the triplet excited state lifetimes of these guests were lengthened in the presence of DNA, and the residence times for acridine orange was estimated to be roughly 1 ms.[57]

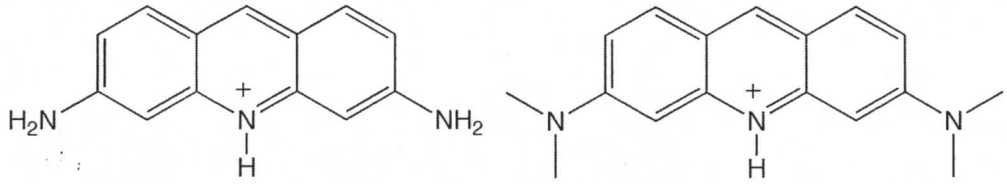


**Scheme 2.2** Proflavine and acridine orange.

However, laser flash photolysis experiments have been successfully used to study binding dynamics of guests to a number of other host systems, including micelles, cyclodextrins and bile salt aggregates.[2,3] Most commonly dynamics are obtained using a quenching methodology, where a competitive deactivation pathway for the excited state is introduced when a quencher is added to the system. Using a quencher that primarily resides in the aqueous phase the association ($k_+^*$) and dissociation rate constants ($k_-^*$) between the excited state guest and host can be measured. Guest molecules in the aqueous phase are quenched more efficiently than those bound to the host. As the concentration of quencher is increased the rate-limiting step for quenching becomes the exit of guest molecules from the host, leading to a non-linear relationship between the observed rate constant ($k_{obs}$) and the quencher concentration (Equation 2.1):

$$k_{obs} = k_o^H + k_-^* + k_q^H[\text{quencher}] - \frac{k_-^* k_+^* [\text{host}]}{k_o + k_q[\text{quencher}] + k_+^*[\text{host}]} \qquad (2.1)$$

where $k_o$ and $k_o^H$ are the lifetimes of the triplet excited state in aqueous solution and within the host, and $k_q$ and $k_q^H$ are the quenching rate constants for the triplet excited state by the quencher in water and within the host. This method assumes that quenching of the guest in the host is less efficient ($k_q > k_q^H$), and for this equation to be applicable the decay of the triplet excited state must be mono-exponential at all concentrations of quencher, since the equation is derived with the assumption that the concentration of free guest is small compared to the amount of guest bound to the host, which leads to a pseudo-first-order rate constant.

### 2.1.3 Necessary guest properties for laser flash photolysis studies with DNA

To use the laser flash photolysis quenching methodology to study the binding dynamics of guests with DNA it is important that certain conditions are met. The guest must have a long-lived triplet excited state so that during its lifetime the excited guest molecule can move between binding sites in DNA and the aqueous phase. The guest must have singlet and triplet excited states that are non-reactive towards DNA. Transients formed through reaction of a guest molecule with DNA could interfere with the investigation of the binding dynamics. The most likely reaction for guests bound to DNA is electron transfer from guanine, the most easily oxidized of the DNA bases.[58] It is also important that the singlet and triplet excited state energies of the guest molecules are lower than those of the DNA bases (Table 2.2). This will avoid deactivation of the

excited state of the guest by energy transfer from the guest to the DNA bases. It should be noted that the singlet and triplet excited state energies shown in Table 2.2 are for the free DNA bases, and that the values within the DNA helix are expected to vary due to interactions between the bases.

**Table 2.2** Singlet and triplet excited state energies of DNA bases.[59]

| DNA base | $E_s$ / kJ/mol | $E_T$ / kJ/mol |
|---|---|---|
| Adenine | 421 | 319 |
| Thymine | 408 | 315 |
| Cytosine | 403 | 334 |
| Guanine | 407 | 325 |

### 2.1.4 Xanthone

Xanthone (Scheme 2.3) was initially chosen as a suitable guest for studying binding dynamics with DNA because it has been successfully used to study binding dynamics in other host systems, and the mobility of its triplet excited state between environments of different polarity can be monitored directly.[4,60-64] The xanthone backbone is found in a variety of compounds that display potential biological action such as anti-inflammatory, anti-thrombotic, anti-malarial, antibacterial or antitumour activies,[65-71] and xanthone has a tricyclic aromatic backbone, which is one of the basic requirements for intercalation into DNA.

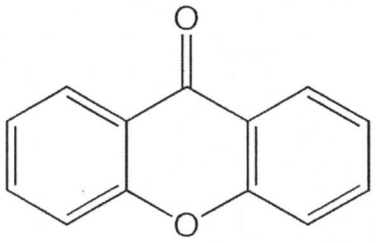

**Scheme 2.3** Xanthone.

Unfortunately preliminary laser flash photolysis experiments with xanthone in the presence of DNA showed the formation of transient species inconsistent with the triplet excited state of xanthone. It was subsequently reported that xanthone damages double-stranded DNA through a photo-induced electron transfer reaction.[72] Since xanthone reacts with DNA it was reasoned that substitution of the xanthone chromophore with electron-donating substituents, such as amino groups, would reduce the photoreactivity of the excited states towards DNA.

### 2.1.5 Objective

The objective of this chapter is to characterize the photophysics of the synthesized aminoxanthones and determine if they fulfill the conditions necessary to use laser flash photolysis for the systematic study of binding dynamics of small molecules with DNA.

## 2.2 Experimental

### 2.2.1 Synthesis and purification of aminoxanthones

Synthesis and purification of 2-aminoxanthone (MAX) and 2,7-diaminoxanthone (DAX) (Scheme 2.4) was carried out using procedures previously developed in the group.[44,73] Purity of the synthesized aminoxanthones was checked by HPLC as previously described.[44,73]

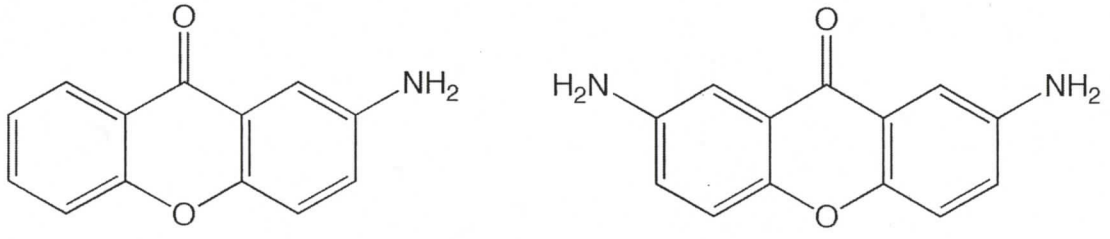


**Scheme 2.4** 2-Aminoxanthone (MAX) and 2,7-diaminoxanthone (DAX).

### 2.2.2 Materials

DNA (from calf thymus, Aldrich), guanosine (ICN Biomedicals Inc), potassium phosphate dibasic (Caledon), and potassium phosphate monobasic (BDH Chemicals) were used as received. Ferrocene (98%, Aldrich) was recrystallized from cyclohexane and sublimed, 1,3-cyclohexadiene (97%, Aldrich) was distilled, and sodium nitrite (97+%, Aldrich) was recrystallized from water before use. Deionized water (Sybron-Barnstead system) was used for all aqueous samples. Ethanol (95%, Commercial Alcohols Inc.), acetonitrile-190 (HPLC grade, Caledon), toluene (spectrograde, Caledon), and cyclohexane (spectrogradé, Caledon) were used as received.

### 2.2.3 Preparation of solutions in organic solvents

All non-aqueous solutions were prepared by dissolving MAX or DAX so that the absorbance of the sample at the excitation wavelength was approximately 0.1 in a 10 mm x 10 mm cell for fluorescence experiments, and for laser flash photolysis experiments the absorbance of the sample at the wavelength of irradiation was in the range of 0.1 – 0.3 in a 7 mm x 7 mm cell.

### 2.2.4 Preparation of aqueous and DNA solutions

Aqueous solutions were prepared by injecting small amounts of a 10 mM methanolic stock solution of the aminoxanthones into water. DNA solutions were prepared by dissolving the appropriate amount of DNA in phosphate buffer (10 mM, pH 7.0). The concentration of DNA was determined by UV spectroscopy ($\varepsilon_{260} = 6500 \pm 100$ $M^{-1}$ $cm^{-1}$ with respect to phosphate group concentration).[6] DNA solutions containing the aminoxanthones were prepared by injecting small amounts of the methanolic stock

solution into the DNA solutions. The concentration of the aminoxanthones was approximately 20 μM for fluorescence experiments and 100 μM for laser flash photolysis experiments.

It should be noted that MAX and DAX appear not to be completely solubilized in aqueous solution, even at the relatively low concentrations used here, evidenced by a small shoulder in the fluorescence spectra in water (Figure 2.1). Similar effects have previously been reported,[74] though the assignment of the emission bands is different. Unless otherwise noted this effect did not interfere with the results.

### 2.2.5 Deoxygenation procedures

Solutions for single photon counting experiments in non-aqueous solvents were deaerated by bubbling nitrogen through the solution for at least 20 minutes prior to use. All laser flash photolysis solutions were deaerated with either nitrogen or nitrous oxide for at least 20 minutes prior to use.

### 2.2.6 Quenching procedures

For quenching experiments fresh quencher solutions were prepared daily. Stock solutions of 0.5 and 1 M 1,3-cyclohexadiene in cyclohexane, ethanol and acetonitrile, 0.5 M ferrocene in ethanol and acetonitrile, and 1 M sodium nitrite in water were used. All quencher solutions were dearated by bubbling nitrogen, or nitrous oxide, through them for at least 20 minutes prior to use. The appropriate volumes of quencher were added to 2 mL aliquots of the aminoxanthone solutions using a gas-tight syringe.

**2.2.7 Binding isotherms**

Binding isotherms for MAX and DAX (20 μM) with DNA (calf thymus, 0 – 3.5 mM) were constructed using the integration of the MAX/DAX fluorescence spectra (480 - 660 nm). The data were analyzed using the treatment from McGhee and von Hippel.[75] This model assumes that the binding sites in DNA are identical and non-interacting, and the guest occupies *n* base pairs, and the probability of finding *n* unoccupied base pairs decreases as binding approaches saturation (Equation 2.2).

$$\frac{r}{L_{free}} = K(1-nr)\left[\frac{1-nr}{1-(n-1)r}\right]^{n-1} \qquad (2.2)$$

where *r* is the ratio between the concentration of bound guest ($L_{bound}$) and the concentration of DNA base pairs. $L_{free}$ is the concentration of guest free in the aqueous phase ($L_{bound} + L_{free} = [\mathrm{MAX}]_{total}$). *K* is the equilibrium constant.

$L_{bound}$ was determined from the integration of the fluorescence spectra (*I*) at various DNA concentrations, were $I_o$ is the integrated area for the fluorescence in the absence of DNA and $I_{max}$ the area when all guest is bound to DNA (Equation 2.3).

$$L_{bound} = [\mathrm{MAX}]_{total}\left(\frac{I-I_o}{I_{max}-I_o}\right) \qquad (2.3)$$

Complete saturation of the emission intensity was not achievable, and $I_{max}$ was estimated by fitting the change in the fluorescence intensity ($\Delta I$) with DNA concentration

to a hyperbolic function, where $I_{max}$ is the extrapolated asymptotic value at high DNA concentrations.

### 2.2.8 Instrumentation

Ground-state absorption spectra were measured on a Cary 1 Varian spectrophotometer.

Steady-state fluorescence spectra were obtained using a PTI QM-2 fluorimeter. The temperature was kept constant (20.0 ± 0.2 °C) using a Haake F3 water bath. The excitation and emission slits were set to optimize the emission intensity, typically with a bandpass of 3 nm. The fluorescence spectra were corrected for the baseline spectrum, using a solution containing all compounds except the aminoxanthones, ensuring that artifacts, such as Raman emission of the solvent, were subtracted from the fluorescence spectra.

Time-resolved fluorescence measurements were performed with an Edinburgh Instruments OB-920 time-correlated single photon counter with a hydrogen flash lamp excitation source. The temperature was kept constant (20.0 ± 0.2 °C) using a Lauda Super RM-6 water bath. The bandpass for the excitation and emission monochromators was ca. 16 nm. An iris was employed to ensure that the frequency of the stop pulses was less than 2% of the start pulse frequency. The number of counts collected in the channel of maximum intensity was 10000. The instrument response function (IRF) was measured using Ludox (Aldrich) to scatter light at the excitation wavelength. Fitting of the fluorescence decays, where the IRF was deconvoluted from the experimental data, was performed using the Edinburgh software. All decays were fit to mono-exponential

functions. The value of $\chi^2$ (0.9 to 1.2) and a visual inspection of the residuals and the autocorrelation function were used to determine the quality of the fit.[76]

The laser flash photolysis system used for transient absorption measurements has been described previously.[63] MAX and DAX were excited at 308 nm with an excimer laser from Lumonics (EX-510) or at 355 nm using a Spectra Physics GCR-12 Nd:YAG laser. Transient decays and spectra were measured using a xenon arc lamp as the monitoring beam. Ten kinetic traces were averaged for each measurement. Experiments were performed at 20 ± 2 °C.

## 2.3 Results

### 2.3.1 Steady-state fluorescence

Steady-state fluorescence spectra were obtained for MAX in a number of solvents ($\lambda_{ex}$ = 380 nm for toluene, acetonitrile, cyclohexane, ethanol and water) and DAX in water ($\lambda_{ex}$ = 400 nm). The absorption spectra of MAX showed a band around 370 – 390 nm that did not change significantly with different solvents (Table 2.3). However, the fluorescence maximum showed a clear dependence on solvent polarity (Figure 2.1, Table 2.3), with the maximum red-shifted in polar solvents. This indicates that the singlet excited state energy of the aminoxanthones decreases as solvent polarity is increased. The fluorescence emission spectra of MAX and DAX were also significantly red-shifted when compared to the parent xanthone (in water $\lambda_{max}$ = 590 ± 5 nm (MAX), 592 ± 4 nm (DAX) and 396 nm (xanthone)[4,77,78]).

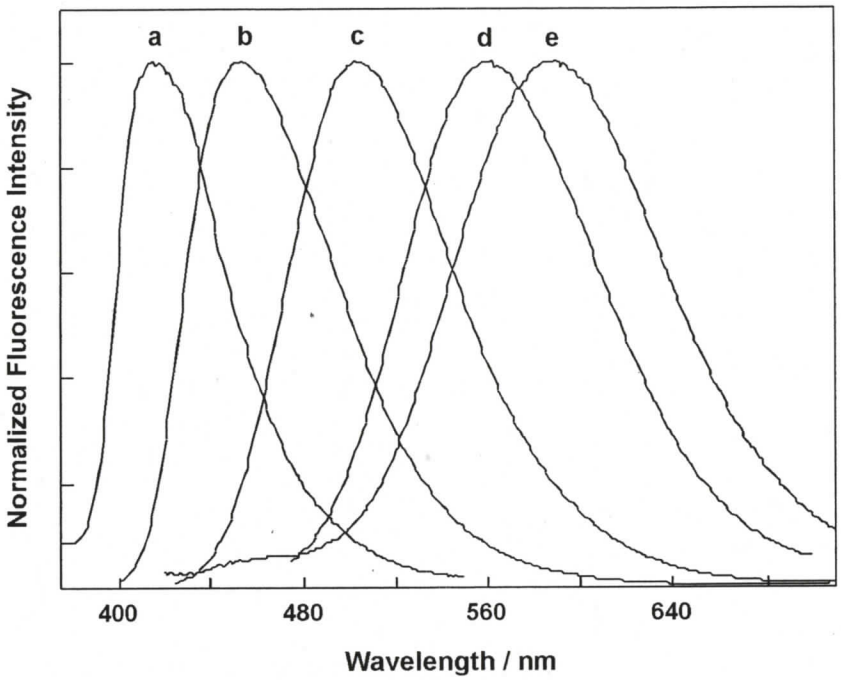


**Figure 2.1** Normalized fluorescence spectra of MAX ($\lambda_{ex}$ = 380 nm) in (a) cyclohexane, (b) toluene, (c) acetonitrile, (d) ethanol and (e) water. Reproduced with permission from reference 44, copyright 2006 Wiley-Blackwell.

In each solvent studied, there was a significant shift between the absorption and emission spectra for the aminoxanthones, so the energy of the singlet excited state was calculated by averaging the wavelengths for the absorption maximum and the maximum of the fluorescence spectra (Table 2.3). When these values were calculated, where possible, from the intersection point of the normalized absorption and fluorescence spectra the same values were obtained within 5 kJ/mol.

**Table 2.3** Absorption and fluorescence maxima, singlet excited state energies and relative fluorescence intensities for MAX in various solvents and DAX in water.

| Solvent | $\lambda_{max}$ (Abs) / nm | $\lambda_{max}$ (Flu) / nm | $E_s$ / kJ/mol | Relative fluorescence intensity |
|---|---|---|---|---|
| MAX | | | | |
| Cyclohexane | 371 | 415 | 305 | - |
| Toluene | 382 | 455 | 286 | 210 |
| Acetonitrile | 387 | 503 | 268 | 130 |
| Ethanol | 389 | 562 | 251 | 9 |
| Water | 381 | 590 | 247 | 1 |
| DAX | | | | |
| Water | 402 | 592 | 241 | - |

The singlet excited state energies for the aminoxanthones are much lower than the singlet excited state energy for xanthone, which varies from 334 kJ/mol in hexane to 329 kJ/mol in acetonitrile.[79]

The relative emission intensities in different solvents, compared to emission in water, were estimated from the integration of the fluorescence spectra, taking into account the fraction of absorbed photons ($1 - 10^{-A}$, where A is the absorbance) when solutions had different absorbance values at the excitation wavelength. The large changes in the relative emission intensities of MAX (Table 2.3) show that the fluorescence quantum yield is very dependent on the solvent. The fluorescence quantum yields for MAX and DAX in water have been previously measured ($(0.9 \pm 0.1) \times 10^{-3}$ and $(1.0 \pm 0.1) \times 10^{-3}$, respectively) and are much lower than the fluorescence quantum yield of xanthone ($(17 \pm 2) \times 10^{-3}$).[44,73]

The addition of DNA to buffered aqueous solutions of MAX or DAX resulted in a blue-shift of the emission maxima to approximately 550 nm, and an increase in the fluorescence intensity (Figure 2.2).

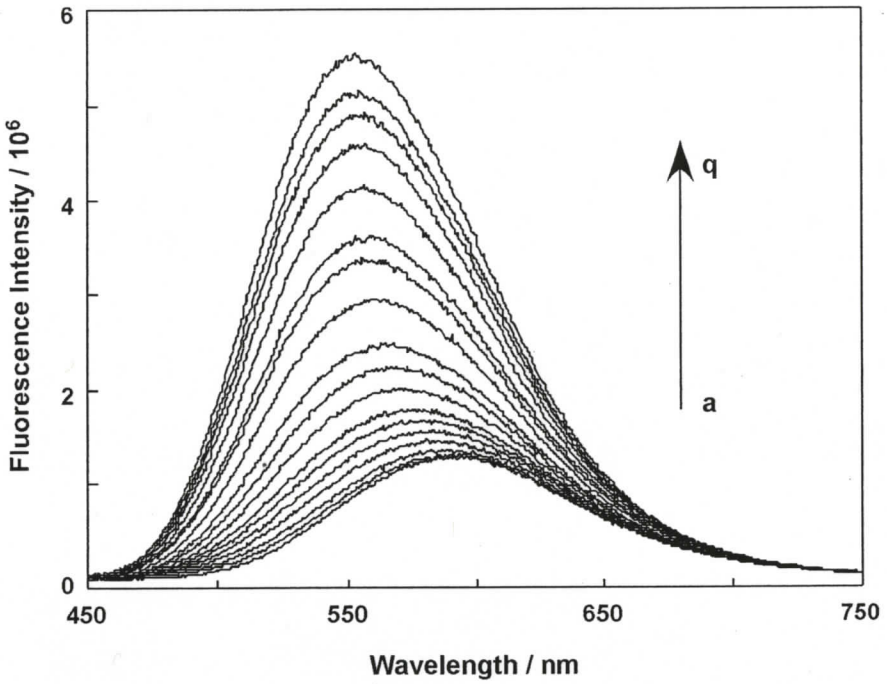


**Figure 2.2** Fluorescence spectra of MAX ($\lambda_{ex}$ = 380 nm) in the presence of increasing concentrations of *ct*-DNA (a) 0 mM – (q) 3.7 mM. Reproduced with permission from reference 44, copyright 2006 Wiley-Blackwell.

The integrated area of the fluorescence spectra of the aminoxanthones in the presence of DNA corresponds to the sum of the emission from the guest free in the aqueous solution and from the guest bound to DNA. The equilibrium constants were calculated using the McGhee and von Hippel approach[75] (Figure 2.3). The obtained $K$ values were $(6.6 \pm 0.5) \times 10^3$ $M^{-1}$ for MAX and $(3.8 \pm 0.1) \times 10^3$ $M^{-1}$ for DAX. The number of base pairs per binding site, $n$, was $9 \pm 1$ for MAX and $12 \pm 1$ for DAX. These values are much larger than usual for the binding of small molecules to DNA. This is most likely due to the large uncertainty in the data at high $r$ values.

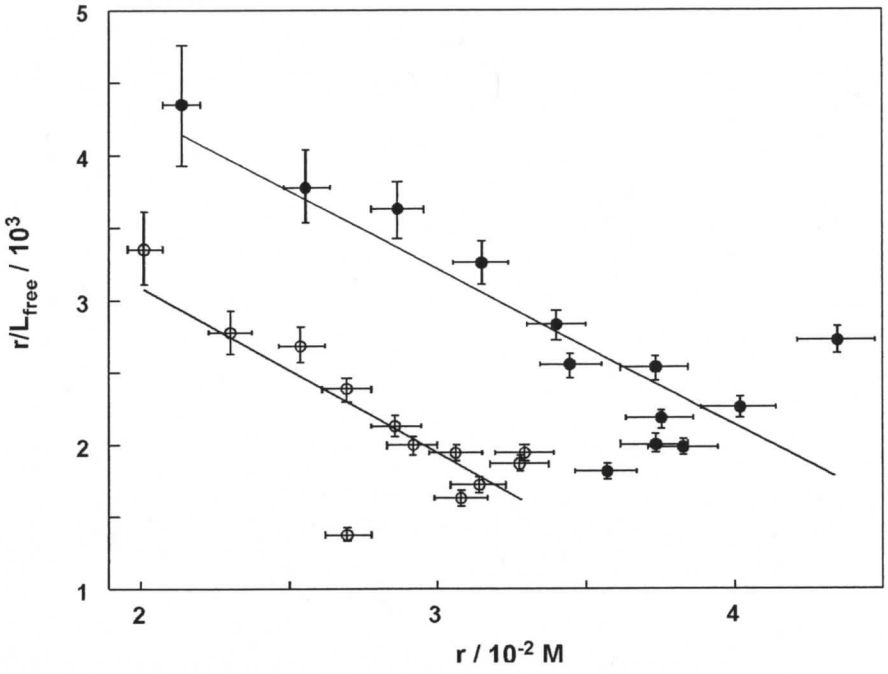


**Figure 2.3** McGhee – von Hippel plots for the binding of MAX (closed circles) and DAX (open circles) to *ct*-DNA. Reproduced with permission from reference 44, copyright 2006 Wiley-Blackwell.

### 2.3.2 Time-resolved fluorescence

The lifetimes obtained for the decay of the singlet excited states of MAX and DAX in acetonitrile were 22.3 ± 0.3 ns and 17.5 ± 0.1 ns, respectively (Figure 2.4a). In water the decay profile for both MAX and DAX was very close to the profile for the instrument response function (Figure 2.4b), indicating that the lifetimes of MAX and DAX in water are shorter than 1 ns, the time resolution of the single photon counter. This observed difference in lifetimes is consistent with the large differences observed in the relative intensities of the steady-state fluorescence above.

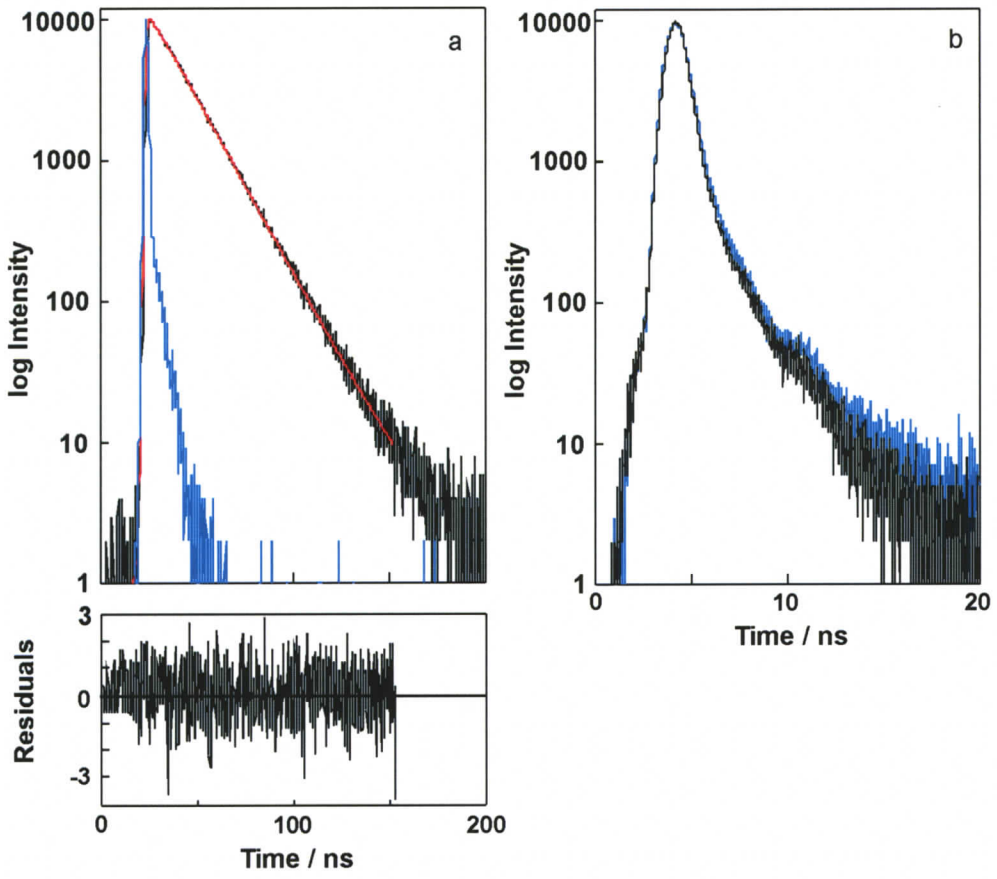


**Figure 2.4** Time-resolved fluorescence decay (black) with IRF (blue) for DAX (a) in acetonitrile, fit to a mono-exponential function (red) ($\lambda_{ex}$ = 350 nm, $\lambda_{em}$ = 500 nm), and (b) in water ($\lambda_{ex}$ = 280 nm, $\lambda_{em}$ = 575 nm).

In the presence of DNA the decay profiles of MAX and DAX were also very close to the profile for the instrument response function. The increase in the fluorescence intensity seen in the steady-state fluorescence experiments on the addition of DNA suggests the lifetimes of MAX and DAX increase when bound to DNA. However, the lifetimes cannot be measured with the time resolution of our equipment, and the lifetimes of the aminoxanthones bound to DNA are still shorter than 1 ns.

**2.3.3 Transient spectroscopy**

MAX and DAX were excited at either 308 or 355 nm, and the observed transient kinetics were independent of the laser wavelength. In polar solvents the absorption of solvated electrons was detected above 600 nm, indicating that MAX and DAX are photoionized. Photoionization of ketones and aromatic hydrocarbons is commonly seen in polar solvents.[80-82] Prior to measurement solutions were bubbled with nitrous oxide ($N_2O$), which is known to trap solvated electrons.[83]

In cyclohexane a transient absorption for MAX with a maximum around 600 nm was observed, while bleaching of the precursor was seen in the 350 - 400 nm region (Figure 2.5a). At long delays a residual absorption with a maximum at 440 nm was observed. The transient spectra for MAX were seen to broaden in polar nonprotic solvents such as acetonitrile (Figure 2.5a). In phosphate buffer (Figure 2.5b) and ethanol the maximum of the transient absorption spectra for MAX were shifted to 440 – 460 nm. The signals were much weaker in water compared to ethanol or cyclohexane for solutions with similar absorptions at the excitation wavelength. The transient absorption spectra of DAX were red-shifted compared to those of MAX, but displayed similar features. The transient decays were measured at the transient absorption maximum and the kinetics followed a mono-exponential decay for MAX and DAX in cyclohexane, acetonitrile and ethanol, with lifetimes in excess of 4 μs in acetonitrile and ethanol, and 0.6 μs in cyclohexane. For the transient decay in water, a small component with a short lifetime was observed, along with the predominant long-lived component with a lifetime in excess of 60 μs. The transient spectra of the fast component and the long-lived component were very similar. MAX and DAX are not completely solubilized in aqueous solution (see

above) and the fast component was assigned to the decay of the transient in aggregated MAX and DAX.

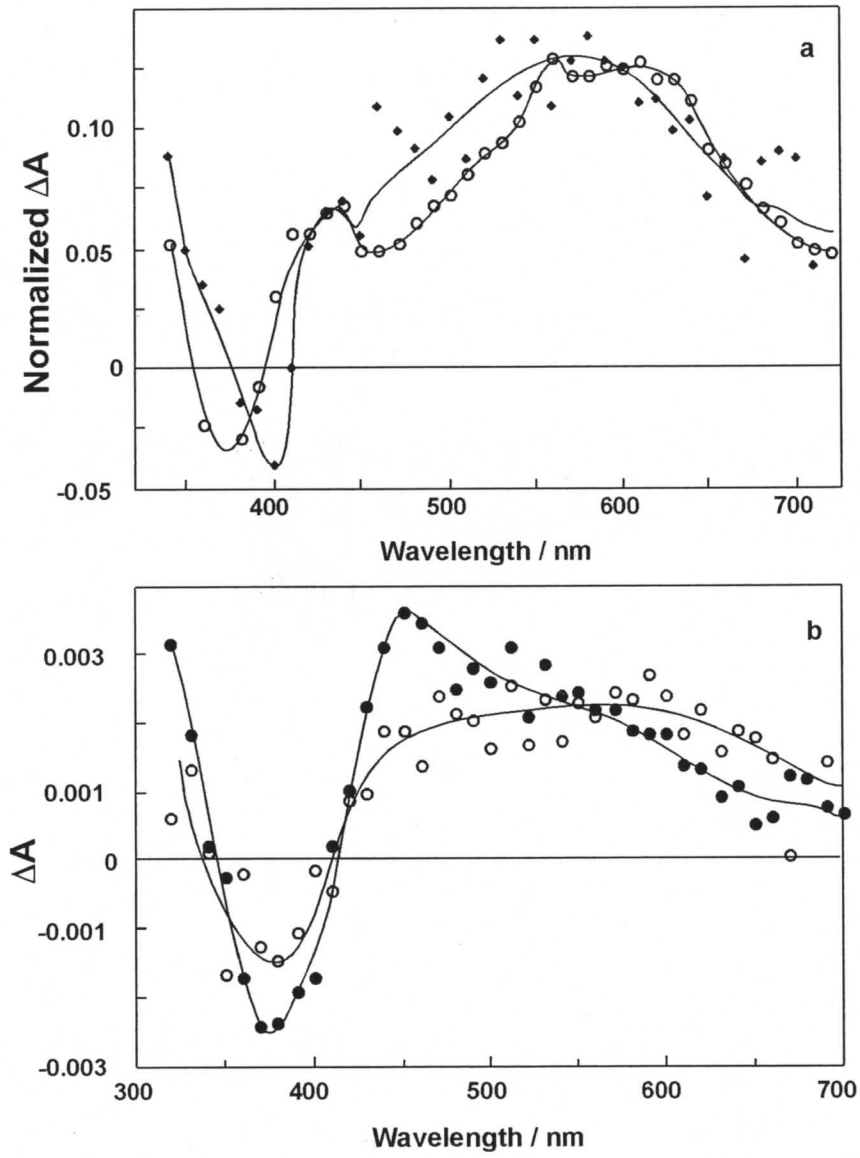


**Figure 2.5** (a) Transient absorption spectra for MAX in cyclohexane 240 ns after the laser pulse (open circles) and in acetonitrile 830 ns after the laser pulse (diamonds) (b) Transient absorption spectra 10 μs after the laser pulse for MAX in 10 mM phosphate buffer (pH 7.0) in the absence (solid circles) and presence (open circles) of 4 mM *ct*-DNA (open circles). Reproduced with permission from reference 44, copyright 2006 Wiley-Blackwell.

The transient absorption spectra of MAX (Figure 2.5b) and DAX in the presence of DNA are broad and featureless, similar to the transient spectra observed in aqueous solution in the absence of DNA. Because transient absorption are difference spectra of the absorption of the transient and the ground state, the transient absorption for MAX is smaller in the presence of DNA in the 450 nm region due to a slight broadening and red shift of the ground state absorption spectrum.

Quenching experiments were performed to assign the observed transients. The quenching rate constants ($k_q$) were obtained from plots of the dependence of the observed rate constant ($k_{obs}$) on the quencher concentration (Equation 2.4):

$$k_{obs} = k_o + k_q[\text{quencher}] \qquad (2.4)$$

In all solvents the transients were efficiently quenched by oxygen in a diffusion controlled process (Table 2.4). The transient for MAX in cyclohexane was quenched by 1,3-cyclohexadiene ($E_T$ = 218 kJ/mol)[84] but no quenching was observed for 1,4-cyclohexandiene.

The effect of solvent on the observed rate constants for quenching with 1,3-cyclohexadiene was significant (Table 2.4), indicating that the energy of the triplet excited state decreases as the solvent polarity is increased. The $k_q$ value for MAX in cyclohexane was close to the rate constant for a diffusional controlled process ($6.7 \times 10^9$ $M^{-1}$ $s^{-1}$),[59] and was decreased in other solvents. Ferrocene has a lower triplet excited state energy (159 kJ/mol)[59] than 1,3-cyclohexadiene, and the quenching rate constants obtained with ferrocene were much higher.

**Table 2.4** Quenching rate constants for the triplet excited states of MAX and DAX by oxygen, 1,3-cyclohexadiene and ferrocene in various solvents.

| Solvent | $k_q$ / $10^8$ $M^{-1}$ $s^{-1}$ | | |
|---|---|---|---|
| | $O_2$ | 1,3- cyclohexadiene | ferrocene |
| MAX | | | |
| Cyclohexane | a | 55 ± 3 | a |
| Acetonitrile | a | 2.4 ± 0.6 | 11 ± 2 |
| Ethanol | 23 ± 1 | 0.0056 ± 0.0002 | 25 ± 7 |
| DAX | | | |
| Cyclohexane | a | a | a |
| Acetonitrile | a | 2.7 ± 0.5 | 11 ± 1 |
| Ethanol | 33 ±1 | < 0.001 | 2.7 ± 0.1 |

[a] not measured

Quenching of the triplet excited state of MAX by guanosine was investigated. In a 1:1 ethanol/water solution no quenching of triplet excited state MAX was observed for the highest guanosine concentration of 4 mM. The highest concentration was limited by the solubility of guanosine in aqueous solution.

Nitrite ions are frequently used as a triplet quencher in aqueous solutions. Nitrite has a triplet excited state energy of 222 kJ/mol and quenches triplet states through an energy transfer process.[85] The quenching rate constant of triplet MAX by nitrite in phosphate buffer solution (pH 7.0) was (2.2 ± 0.1) x $10^6$ $M^{-1}$ $s^{-1}$, and the quenching rate constant for DAX was at least one order of magnitude lower than observed for MAX. These quenching rate constants are much lower than the value for the quenching of the parent xanthone (5.9 x $10^9$ $M^{-1}$ $s^{-1}$)[86].

The quenching plot for MAX in the presence of DNA was linear and the quenching efficiency was much lower than observed for the quenching of triplet MAX in aqueous solution (Figure 2.6). The fact that the quenching plot does not curve in the presence of DNA precluded the determination of values for $k_+$, $k_-$, and $k_q^{DNA}$.

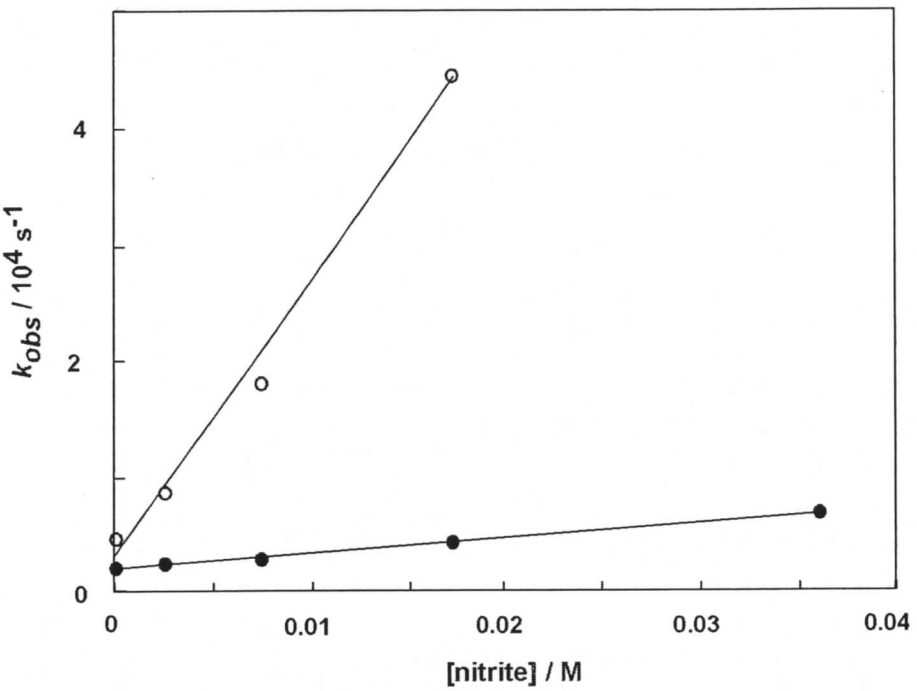


**Figure 2.6** Nitrite quenching plot for triplet excited state MAX in phosphate buffer in the absence (open circles) and presence (closed circles) of *ct*-DNA. Reproduced with permission from reference 44, copyright 2006 Wiley-Blackwell.

## 2.4 Discussion

### 2.4.1 Singlet excited state character of aminoxanthones

The aminoxanthones showed a marked solvatochromic effect on their photophysics when compared to xanthone. The singlet excited state energies for MAX and DAX (Table 2.3) are significantly lower than observed for the singlet excited state of xanthone. There was a much larger decrease in the excited state energy in polar solvents for the aminoxanthones, suggesting that the lowest excited state of the aminoxanthones has significant charge transfer character. Similar results have been previously reported with amino-substituted aromatic ketones, such as fluorenones and anthraquinones.[87,88] The shortening of the observed singlet excited state lifetimes in water compared to acetonitrile can also be attributed to the charge transfer character of the singlet excited

state. Previous reports show that the hydrogen bonding of solvent to the carbonyl moiety of amino-substituted fluorenones and anthraquinones increases the internal conversion rate constant, introducing an efficient alternative deactivation pathway for the excited state, and thus shortening the singlet excited state lifetime.[87-91]

### 2.4.2 Triplet excited state character of aminoxanthones

Triplet excited states are quenched by 1,3-cyclohexadiene through energy transfer, where the triplet excited state energy of the quencher is 218 kJ/mol,[84] while 1,4-cyclohexadiene quenches triplet excited states through hydrogen atom transfer. The aminoxanthones were quenched by the former, but not by the latter. These results are consistent with the formation of a triplet excited state that cannot undergo hydrogen abstraction reactions. The transients observed for MAX and DAX were therefore assigned to be the triplet $\pi$-$\pi^*$ excited state. Sensitization experiments performed previously using naphthalene as a triplet sensitizer confirmed that the transient observed in protic solvents is also the triplet excited state of MAX and DAX.[44,73]

In the transient decays a smaller signal was observed after the laser pulse for MAX and DAX in water than the signal in other solvents, suggesting that the intersystem crossing yield in water was lower. This result is consistent with the observation of singlet excited state lifetimes that were shorter in water than in acetonitrile. A solvatochromic effect was observed for the triplet excited states of MAX and DAX (Figure 2.5). In protic solvents the triplet-triplet absorption spectra were shifted and the spectra were broadened (Figure 2.5b), suggesting that hydrogen bonding of the solvent to the fluorophore also

occurs for the triplet excited state. Unlike the singlet excited state this solvent interaction does not significantly decrease the triplet excited state lifetime.

The effect of solvent polarity on the triplet excited state energy can be evaluated by looking at the quenching rate constants (Table 2.4). As the polarity of the solvent was increased, the quenching rate constants decreased, indicating a considerable decrease in the triplet excited state energies. This trend is consistent with an excited state with charge transfer character as an increase in solvent polarity stabilizes the excited state with respect to the ground state.

If quenching occurs through energy transfer, as is the case for 1,3-cyclohexadiene, ferrocene and nitrite anions, the triplet excited state energies can be estimated from the quenching rate constants. Quenching rate constants are close to the diffusional controlled limit when the triplet excited state energy of the quencher is much lower than the triplet excited state energy of the probe molecule. If the triplet excited state energy of the quencher is higher than that of the probe molecule then the quenching rate constant will be decreased by several orders of magnitude. The quenching rate constant for quenching of MAX by 1,3-cyclohexadiene was diffusion controlled in cyclohexane, an order of magnitude smaller in acetonitrile and several orders of magnitude smaller in ethanol, while the quenching rate constants for quenching of MAX by ferrocene were diffusion controlled in both acetonitrile and ethanol. These results indicate that the triplet excited state energy of MAX in cyclohexane is higher than that of 1,3-cyclohexadiene (218 kJ/mol), is close to 218 kJ/mol in acetonitrile, and in ethanol is further decreased but still higher than the triplet excited state energy of ferrocene (159 kJ/mol). The results with DAX are very similar, with the exception of the quenching rate constant for quenching by

ferrocene in ethanol, which is an order of magnitude smaller than that for MAX, indicating that the triplet excited state energy of DAX is lower than that of MAX.

In water the triplet excited state energies of the aminoxanthones are also low. The quenching rate constants for quenching by nitrite, which has a triplet excited state energy of 222 kJ/mol, were three orders of magnitude smaller than the diffusion controlled limit. The triplet excited state energy of the aminoxathones is lower than the parent xanthone, and much lower than the triplet state energies of the DNA bases. This is an important property, so that energy transfer from the excited guest to the DNA bases is avoided.

### 2.4.3 Binding of aminoxanthones to DNA

Both aminoxanthones were seen to form complexes with DNA with a reasonable binding affinity, though the binding mode was not established. On binding to DNA the fluorescence maximum shifted to shorter wavelengths, indicating the environment experienced by the aminoxanthones was less polar than water. Any lengthening of the singlet excited state lifetimes for MAX and DAX on binding to DNA could not be measured with the time resolution of the equipment used. In the presence of DNA the singlet excited state lifetimes were less than 1 ns, much shorter than the lifetimes in acetonitrile, which suggests that in the binding site there is still some hydrogen bonding to the carbonyl group of the aminoxanthones, either from the solvent or from DNA itself.

### 2.4.4 Reactivity of aminoxanthones towards DNA

It was important to check if the aminoxanthones were reactive towards DNA from their excited states. No quenching was observed for the triplet excited state of MAX by

guanosine, indicating that the triplet excited state energy of MAX is less than that of guanosine, consistent with the quenching results above, and more importantly that there was no quenching through electron transfer. Guanosine was used to investigate electron transfer as it is the most easily oxidized of the nucleotides.[58] Furthermore no new transients were observed in the presence of DNA, confirming that the triplet excited states of the aminoxanthones are non-reactive towards DNA. This decrease in photoreactivity towards DNA compared to xanthone could either be due to the decreased triplet excited state energies being insufficient to drive electron transfer, or due to the destabilization, by the electon-donating amino groups, of the radical anion formed through an electron transfer process.

### 2.4.5 Binding dynamics of aminoxanthones with DNA

The association and dissociation rate constants of a guest with a host system is studied by measuring the kinetics of the triplet excited state of the guest, since its long lifetime means that the triplet guest can relocate between the binding site and the aqueous phase during its lifetime. The triplet excited state lifetime for MAX or DAX in the presence of DNA was tens of microseconds long, and was equal to or longer than the lifetime in water. This long-lived triplet excited state of MAX or DAX observed in the presence of DNA corresponds to the triplet states of the aminoxanthones bound to the DNA, and not free in the bulk solution. This was established by the lower quenching rate constant for nitrite in the presence of DNA when compared to the quenching rate constant in water (Figure 2.6). Nitrite anions are an appropriate quencher, as the quencher will

remain primarily in the aqueous phase, because of the negative charge on the phosphate backbone of DNA.

Unfortunately the quenching plots in the presence of DNA were not curved. This linearity precludes the determination of the association and dissociation rate constants of MAX and DAX with DNA, as the plateau region, where quenching in water is limited by the exit of the guest from the host, was not reached. The quenching of triplet excited states of the aminoxanthones by nitrite in water is quite inefficient, with quenching rate constants more than three orders of magnitude lower than the observed rate constants with other guests, such as the parent xanthone. With quenching so inefficient it is possible that the association process of the aminoxanthones with DNA is faster than quenching in water ($k_+$[DNA] > $k_q$[Q]). In this case, quenching does not occur in the aqueous phase and the decay of the triplet excited state is determined solely by its intrinsic lifetime in the host and the quenching efficiency for the guest in the host.[92]

The lowest possible value for the dissociation rate constant can be estimated by assuming that the last point in the quenching plot is the lowest value for the observed rate constant at which the quenching plot could have leveled off. For MAX this point is 0.7 x $10^4$ $s^{-1}$, and $k_-$ has to be equal to, or larger than, this value. The highest value for the dissociation rate constant will occur when association is diffusion controlled (6.5 x $10^9$ $M^{-1}$ $s^{-1}$)[59]. The value of the dissociation rate constant can be estimated from the equilibrium constant ($K = k_+/k_-$), and is estimated to be 2 x $10^6$ $s^{-1}$. This range of dissociation rate constants means that the residence time for MAX in DNA is estimated to be between 1.0 and 140 μs.

## 2.5 Conclusions

The aminoxanthones bind to DNA, and the singlet and triplet excited states of MAX or DAX are not quenched by DNA when bound. The triplet excited state of the aminoxanthones is long-lived, and amino-substitution eliminated the reactivity of the xanthone backbone towards DNA. Unfortunately the extent of stabilization required to prevent reaction also lowered the triplet excited state energy to a point where quenching by nitrite anions became inefficient, and the laser flash photolysis quenching methodology could not be used to extract association and dissociation rate constants. This connection between reactivity and triplet excited state energies is likely to be a wide spread issue, making laser flash photolysis unsuitable for extensive studies on the binding dynamics of small molecules with DNA. However, it was shown that the residence time of the aminoxanthones within DNA is short, with exit occurring in microseconds. The dynamics in the aminoxanthone DNA system occur on a faster timescale than those seen for the binding of guests such as ethidium bromide or proflavine. This difference in dynamic processes seen for different guests with DNA highlights the need for access to a wide range of timescales. Systematic studies on the binding dynamics will only be possible when a kinetic technique is available to perform real-time kinetic studies across a wide time range, including the microsecond time domain.

# 3. DEVELOPMENT OF LASER TEMPERATURE JUMP EXPERIMENTS

## 3.1 Introduction

### 3.1.1 Temperature jump experiments

The basic premise and methods of temperature jump experiments were described is Section 1.2.2. A rapid change in the solvent temperature is used to perturb a temperature sensitive equilibrium. At the new higher temperature the system is no longer at equilibrium, and the relaxation to the new equilibrium state can be monitored to obtain dynamic information. Because the perturbation of the system is achieved by a change in the solvent, and not by directly exciting the molecules involved in the equilibrium being studied, temperature jump experiments will avoid the excited state reactivity problems encountered using laser flash photolysis experiments (Chapter 2).

### 3.1.2 Theoretical temperature jump

The theoretical temperature jump achievable is determined by the following equation (Equation 3.1):

$$\Delta T = \frac{\Delta U}{C_V m} \qquad (3.1)$$

where $\Delta T$ is the change in temperature, $\Delta U$ is the change in internal energy, $C_V$ is the heat capacity of the solvent, and m is the mass of solvent being heated. This equation shows

that, experimentally, the temperature jump achieved is determined by the amount of energy transferred to the solvent, and the volume of solvent heated.

### 3.1.3 Laser temperature jump

Of the three different methods that can be used to achieve a temperature jump (Section 1.2.2) laser temperature jump (ltj) is the most attractive for studying dynamic processes in supramolecular systems. The absorption of laser light by the solvent can achieve heating in pico- to nanoseconds,[10-13] making much shorter timescales accessible when compared to the more commonly used Joule-heating method, which achieves heating in microseconds.[5] The use of laser light to heat the solution also avoids the potential artifacts seen in Joule heating experiments, and eliminates the need for high electrolyte concentrations. However, this technique has not been widely used, and a major challenge in the development of laser temperature jump experiments has been finding methods that can efficiently transfer the laser energy into thermal energy.

One early ltj method used dyes that were excited by a laser in the visible region. The dye was excited by the absorption of the laser light, and then decayed back to the ground state. The decay was a non-radiative process which released heat, resulting in heating of the solution.[14] The excited dye has a finite lifetime, which limits the rate and efficiency of energy conversion. Efficient heating was achievable only when the laser was used in non-Q-switched mode, allowing the dye molecules to be excited multiple times, achieving a temperature jump of 5 °C in 300 μs.[14] Further, precautions have to be taken to ensure that the dye does not interact with the reaction being studied. This

experimental setup monitored changes in the solution by absorption, with the monitoring beam perpendicular to the laser beam.[14]

Much faster heating times, on the order of the laser pulse width, can be obtained if the laser light is directly absorbed by the solvent. However, the useful range for absorption for most solvents, including water, is very narrow, and finding suitable lasers that emit in this range has been difficult. The optimum value for the absorption coefficient of water is around 0.5 $cm^{-1}$.[5,12] If the absorption coefficient is too low, heating is inefficient, as only a small proportion of the energy from the laser is transferred to the solution. If the absorption coefficient is too high, the laser light cannot penetrate far into a sample, which results in a steep temperature gradient, unless the sample volume is exceedingly small. Water is transparent in the visible region and opaque in the infrared region, and there is only a narrow region around 1300 – 1400 nm where the absorption coefficient of water is suitable for efficient, homogeneous heating.[5]

The absorption coefficient of water at the 1064 nm band of a YAG laser is too low to achieve efficient heating, so different methods, using less common laser set-ups, have been developed. Raman shifted YAG lasers using $H_2$,[15] $D_2$,[18] $CH_4$,[17] or liquid $N_2$[16] led to laser irradiation wavelengths of 1890, 1560, 1540 and 1410 nm respectively. The absorption coefficient of water in this wavelength region is high, which limits the volume of sample that can be heated, as the irradiation path length has to be short to avoid non-homogeneous heating. At 1540 nm temperature jumps of 1 to 2 °C were achieved when sample volumes on the order of 20 μL were heated.[17] At 1560 nm cooling occurred after ca. 10 ms.[18] Relaxation processes in these systems were monitored by absorption, most commonly with the monitoring beam nearly collinear to the laser beam.[16,17] It is also

possible to modulate the absorption coefficient of the solutions by working in $H_2O/D_2O$ mixtures, since the $D_2O$ absorption coefficient at these wavelengths is significantly lower than the absorption coefficient of water.[16]

Laser temperature jump experiments have also been performed using an iodine laser with emission at 1315 nm.[12] Though this is a high maintenance chemical laser, it has many attractive characteristics for use in laser temperature jump experiments. The absorption coefficient of water at 1315 nm is 0.76 $cm^{-1}$,[12] close to the optimum value 0.5 $cm^{-1}$. At this wavelength a dual pass of the laser beam through a 2 mm cell allows 50% of the laser light to be absorbed, and leads to less than 10% inhomogeneity in heating through the cell.[12] Temperature jumps of 1 °C were obtained when heating 150 μL of sample.[93] This experimental setup allows for much larger volumes to be heated (up to 500 μL) than were attainable with the Raman shifted YAG lasers described above, leading to longer cooling times, often in excess of a second. This increase in cooling time gives access to measurement of an additional three orders of magnitude in the dynamic range. Relaxation signals were monitored by absorption with a monitoring beam perpendicular to the laser beam, or by fluorescence with the excitation beam coaxial to the laser beam, and detectors perpendicular to the excitation beam.[93]

### 3.1.4 Objective

The objective of this work is to implement a laser temperature jump system adapted from systems described in the literature. Ideally the system will consist of a laser, suitable for heavy use, which emits at a wavelength near 1315 nm. The system should achieve temperature jumps in excess of 1 °C, for large enough volumes of solution

that cooling rates are in excess of seconds, thus allowing access to a wide dynamic range. Ideally the system would extend from the nanosecond and microsecond timescales accessible in laser flash photolysis experiments, up to the millisecond and second timescales accessible by stopped-flow. The system should also incorporate the ability to monitor relaxation processes using both absorption and fluorescence detection.

## 3.2 Experimental

This section includes all the background chemistry necessary for testing the laser temperature jump system.

### 3.2.1 Materials

F127 (Sigma), proflavine (3,6-diaminoacridine hemisulfate, Acros Organics) DNA (from calf thymus, Aldrich), sodium chloride (ACP Chemicals), potassium phosphate dibasic (Caledon), and potassium phosphate monobasic (BDH Chemicals) were used as received. Deionized water (Sybron-Barnstead system) was used for all aqueous samples.

### 3.2.2 Solution preparation

Aqueous solutions of 2.6% F127 (w/v) were prepared by weighing out the appropriate amount of F127 into a volumetric flask and dissolving it in water.

Aqueous solutions of proflavine were prepared by injecting small amounts of a 1 mM methanolic stock solution of proflavine into water. DNA solutions were prepared by dissolving the appropriate amount of DNA in phosphate buffer (10 mM, pH 7.0). The

concentration of DNA was determined by UV spectroscopy ($\varepsilon_{260} = 6500 \pm 100\ M^{-1}\ cm^{-1}$ with respect to phosphate group concentration).[6] DNA solutions containing proflavine were prepared by injecting small amounts of the methanolic stock solution into the DNA solutions.

### 3.2.3 Instrumentation

Ground-state absorption spectra were measured on a Cary 1 or Cary 5 Varian spectrophotometer.

Steady-state fluorescence spectra and steady-state light scattering intensities were obtained using a PTI QM-2 fluorimeter. The temperature was varied using a Haake F3 water bath. The excitation and emission slits were typically set with a bandpass of 1 nm for light scattering experiments, and 2 nm for fluorescence experiments. For light scattering experiments the excitation and emission wavelengths were the same. The fluorescence spectra were corrected for the baseline spectrum, using a solution containing all compounds except proflavine, ensuring that artifacts, such as Raman emission of the solvent, were subtracted from the fluorescence spectra.

### 3.2.3 Temperature dependence of F127 light scattering

F127 is a poly(ethylene oxide)-poly(propylene oxide)-poly(ethylene oxide) block copolymer that forms micelles in aqueous solutions. The solution dynamics of these types of polymers have been previously studied using ltj by Holzwarth et al.[94,95] In general the dynamic processes observed for these polymers include incorporation of unimers into micelles, size redistribution of the micelles, and clustering of micelles into larger

aggregates. These processes result in changes in particle size with temperature. Since the amount of light scattered by a particle is related to its size, the change in temperature of these solutions can be monitored using light scattering. The steady-state light scattering intensity of a 2.6% F127 solution was measured at various temperatures (Figure 3.1). F127 exhibits a large change in scattering intensity around 26 °C.

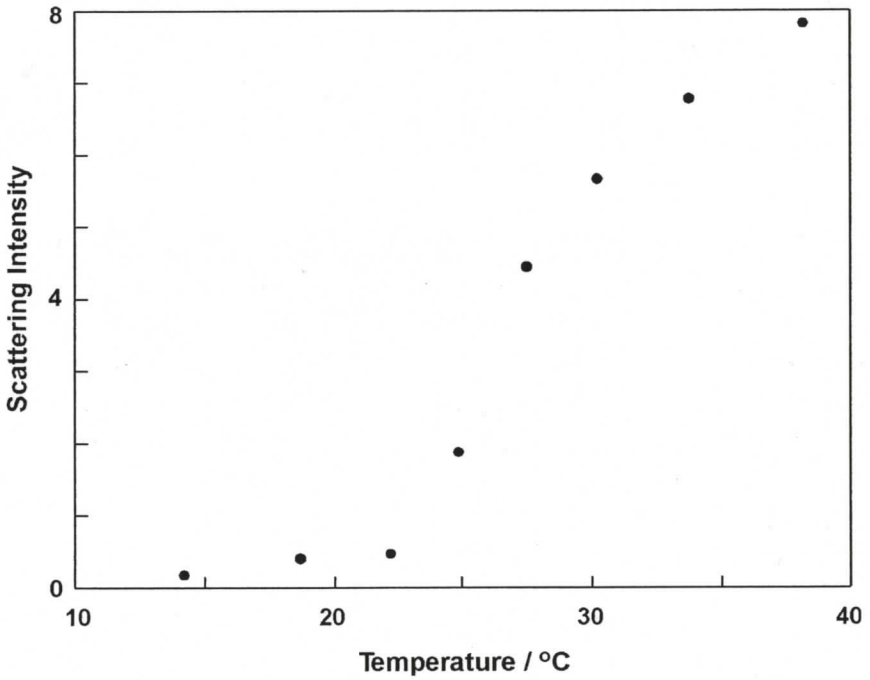


**Figure 3.1** Temperature dependence of the steady-state light scattering intensity for a 2.6% aqueous solution of F127 ($\lambda = 360$ nm).

### 3.2.4 Proflavine/DNA steady-state fluorescence

Steady-state fluorescence spectra were collected for proflavine (4 μM) in the presence of varying concentrations of DNA (0 – 150 μM) (Figure 3.2). As the DNA/dye ratio was increased the fluorescence intensity was seen to decrease, with no change in the position of the fluorescence maximum. The decrease in intensity is due to quenching of

proflavine by the DNA bases. At the highest DNA concentration this trend changed, and the fluorescence maximum was blue-shifted, and the intensity was somewhat increased.

This change in spectra is most likely due to a change in the predominate binding mode. Proflavine is known to interact with DNA through both intercalation and electrostatic interactions.[96] The observation of a blue shift in the fluorescence maximum is consistent with an environment with a different polarity than water. This would be expected for molecules bound through intercalation, indicating that at the high DNA/dye ratio the dominant binding mode is intercalation. At the lower DNA/dye ratios the position of the fluorescence maximum is the same as that for proflavine free in water, indicating that the polarity of the binding environment is similar to that of water. This is consistent with non-specific binding through electrostatic interactions with the DNA backbone.

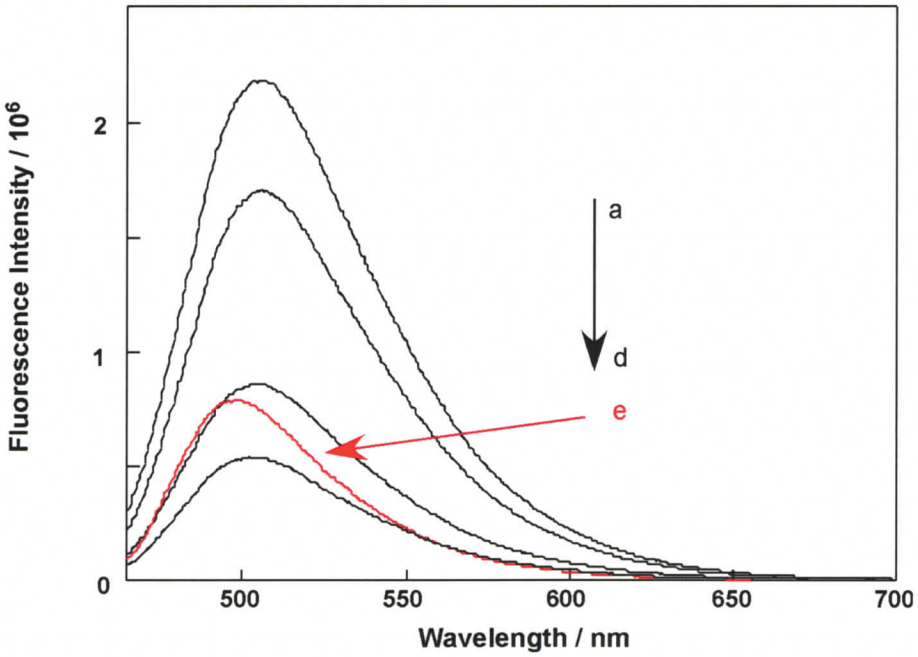


**Figure 3.2** Fluorescence spectra of proflavine (4 μM, $\lambda_{ex}$ = 450 nm) in the presence of *ct*-DNA (a) 0 μM, (b) 1.5 μM, (c) 7.5 μM, (d) 15 μM and (e) 150 μM (red curve).

### 3.2.4.1 Temperature dependence of proflavine/DNA fluorescence

The temperature dependence of proflavine fluorescence was measured for solutions of DNA/dye ratios of 4 and 38 (Figure 3.3). At the high DNA/dye ratio very little change in fluorescence intensity was observed with temperature. At the lower DNA/dye ratio the fluorescence intensity was seen to increase with temperature, showing a change of ca. 1.5% / degree. It will only be possible to monitor changes in proflavine/DNA solutions by fluorescence at low DNA/dye ratios. This experiment establishes that the signal-to-noise ratio obtained on the ltj system has to be such that changes of this magnitude can be measured.

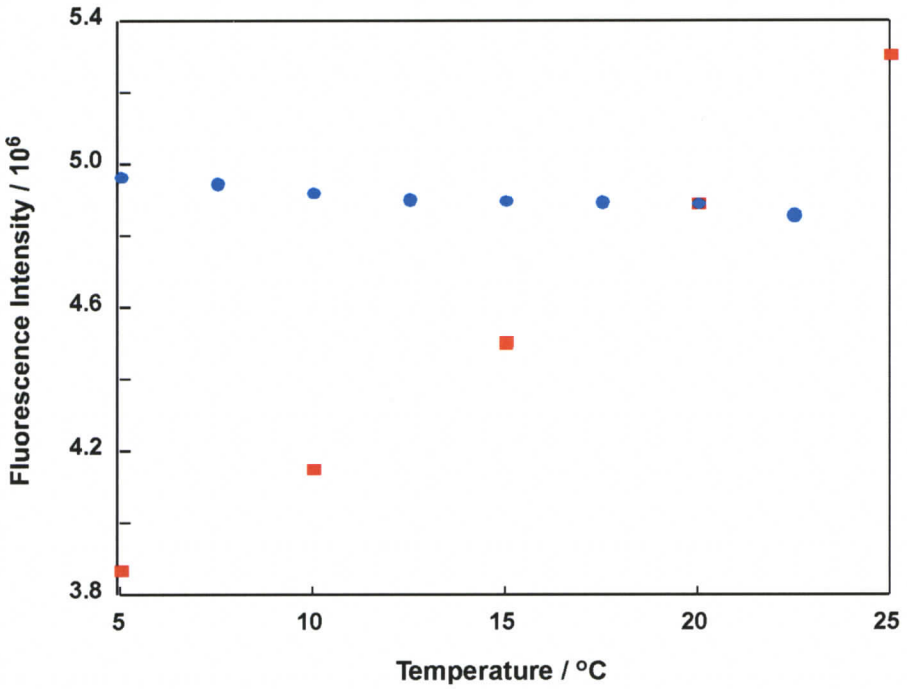


**Figure 3.3** Temperature dependence of the fluorescence intensity of 4 μM proflavine in DNA (red squares: [DNA] = 15 μM (DNA/dye = 4); blue circles: [DNA] = 150 μM (DNA/dye = 38)).

The temperature dependence of the fluorescence of proflavine in water was also measured, and no significant changes were seen in the fluorescence intensity with

temperature. This indicates that the changes seen above are entirely due to a change in the proflavine/DNA equilibrium.

### 3.2.5 Proflavine/DNA absorption

Absorption spectra were collected for proflavine (4 μM) in the presence of varying concentrations of DNA (0 – 150 μM). As the DNA/dye ratio was increased the absorption maximum was red-shifted.

#### 3.2.5.1 Temperature dependence of proflavine/DNA absorption

The temperature dependence of the absorbance was measured for solutions of 15 μM proflavine with 400 μM *ct*-DNA in the presence of 0.5 M NaCl (DNA/dye = 27) (Figure 3.4).

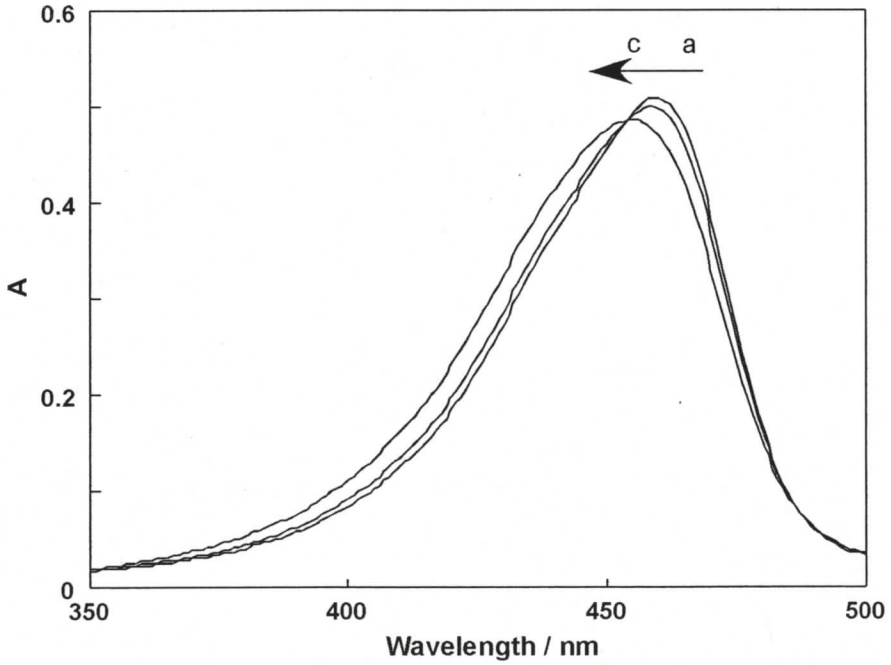


**Figure 3.4** Temperature dependence of the absorption spectrum of 15 μM proflavine in the presence of 400 μM *ct*-DNA and 0.5 M NaCl (DNA/dye = 27), (a) 10 °C, (b) 20 °C, and (c) 40 °C.

As the temperature was increased the absorption maximum was blue-shifted indicating the amount of bound proflavine was decreased. Monitoring at 430 nm a change in intensity of ca. 0.5% / degree was observed.

## 3.3 Results

### 3.3.1 Description of laser temperature jump system

The basic setup of the laser temperature jump system is shown in Figure 3.5. A laser emitting at 1319 nm is used to heat the sample by making a double pass through the solution. A xenon arc lamp equipped with a shutter and a monochromator is used as the monitoring beam, with a fibre optic carrying the light to the sample holder. Two fibre optics at 90 and 180 degrees to the monitoring beam carry light to detectors for fluorescence and absorbance, respectively. The delay generator is used to control the timing of the laser firing, and data acquisition, on the oscilloscope. The program used to run the system and analyze data was written in LabView by L. Netter.

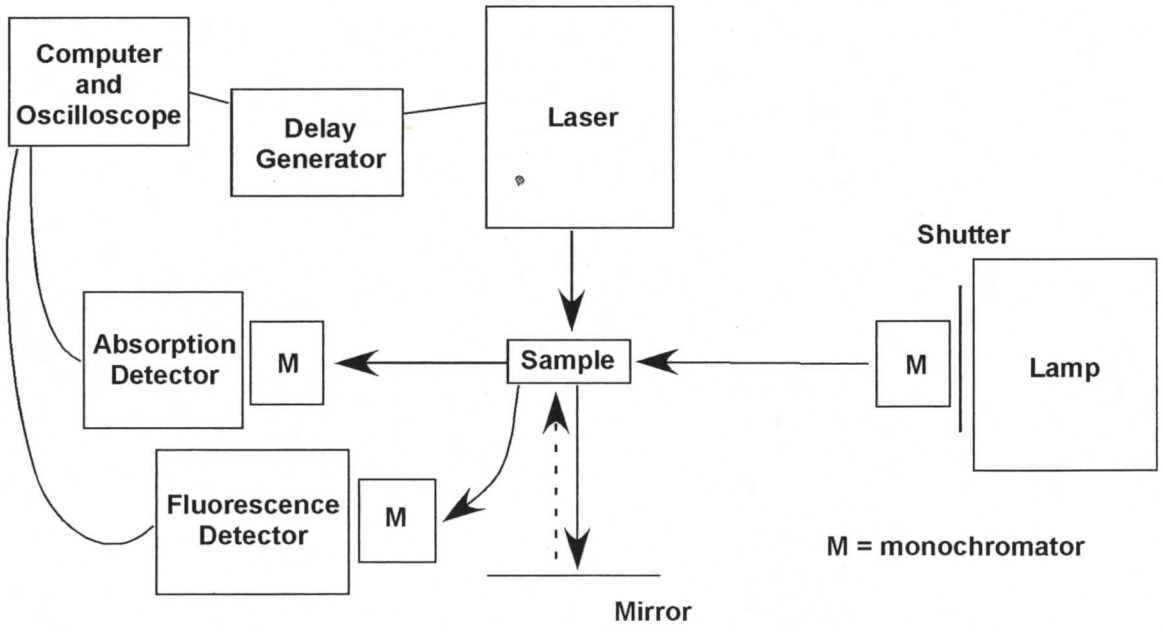


**Figure 3.5** Schematic of laser temperature jump system.

### 3.3.2 Laser

The laser used to achieve emission at 1319 nm is a custom built laser from Positive Light, and a schematic of the laser is shown in Figure 3.6. The 1319 nm peak is a side band of the Nd:YAG emission, and all optics in the system are coated at 1319 nm, to prevent lasing at the peak Nd:YAG wavelength of 1064 nm. The laser operates at 5 Hz and has a pulse width of 40 ns. The shortest accessible timescale is defined by the width of the laser pulse. With the 40 ns pulse width of the laser, kinetic processes can be measured on timescales as short as ca. 100 ns.

The laser consists of an oscillator providing a maximum energy of 8 mJ/pulse. The beam is first amplified through a double pass amplifier, achieving 40 mJ/pulse. Further amplification through two double pass amplifiers achieves a final energy of 400 mJ/pulse or higher. This is the minimum laser power required to achieve the desired temperature jump (see below), below this power routine experiments will not be possible. The laser power is routinely checked after the oscillator and after each amplification stage to ensure that there are no problems with the laser power or alignment. Prior to exit from the laser cavity the beam passes through a vacuum spatial filter (VSF), which avoids air breakdown at the focal point of the laser.

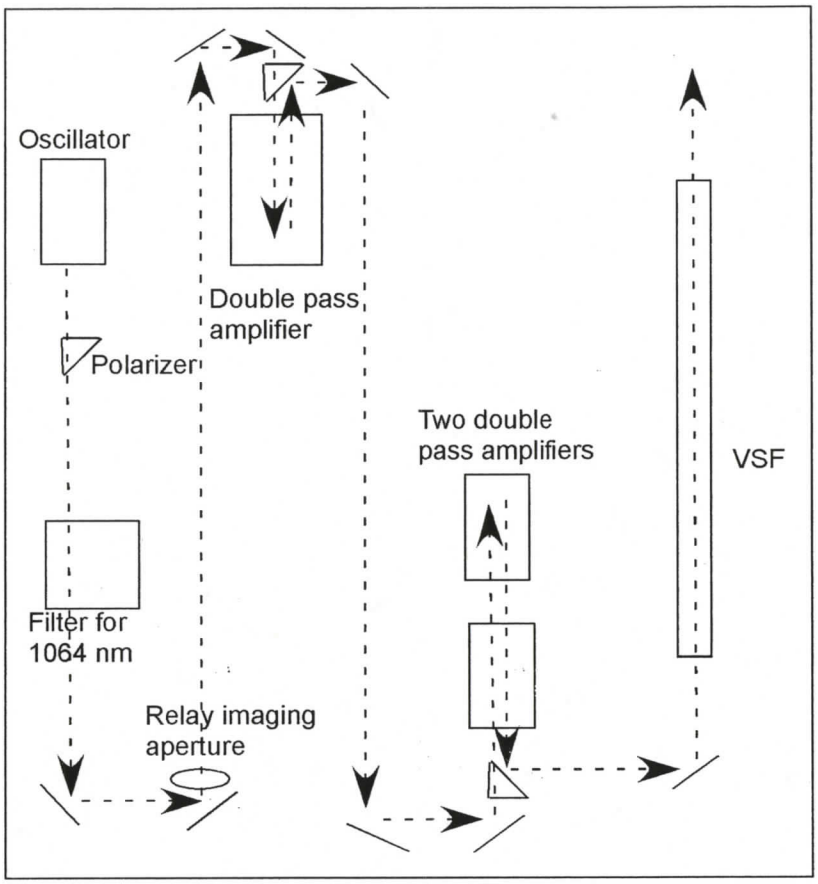


**Figure 3.6** Schematic of 1319 nm laser.

### 3.3.2.1 Absorption of water at 1319 nm

At 1319 nm the absorption coefficient of water is between 0.8 and 1.0 $cm^{-1}$.[5,97] The lower value will be used in subsequent calculations. The beam is passed through the sample (2 mm) and reflected back through the sample with a mirror (Figure 3.8). The transmittance of light through the solution can be calculated using Equation 3.2:

$$\begin{aligned} T &= 10^{-A} = 10^{-\varepsilon l} \\ &= 10^{-(0.8\ cm^{-1})(0.4\ cm)} \\ &= 0.48 \end{aligned} \qquad (3.2)$$

where T is the transmittance of the solution, A is the absorbance of the solution, ε is the absorption coefficient of water, and l is the path length.

Thus, this setup leads to 52% absorption of the laser light. The double pass of the laser beam through the sample minimizes the temperature gradient across the cell (Figure 3.7). The back mirror is slightly misaligned to avoid back reflection into the laser cavity.

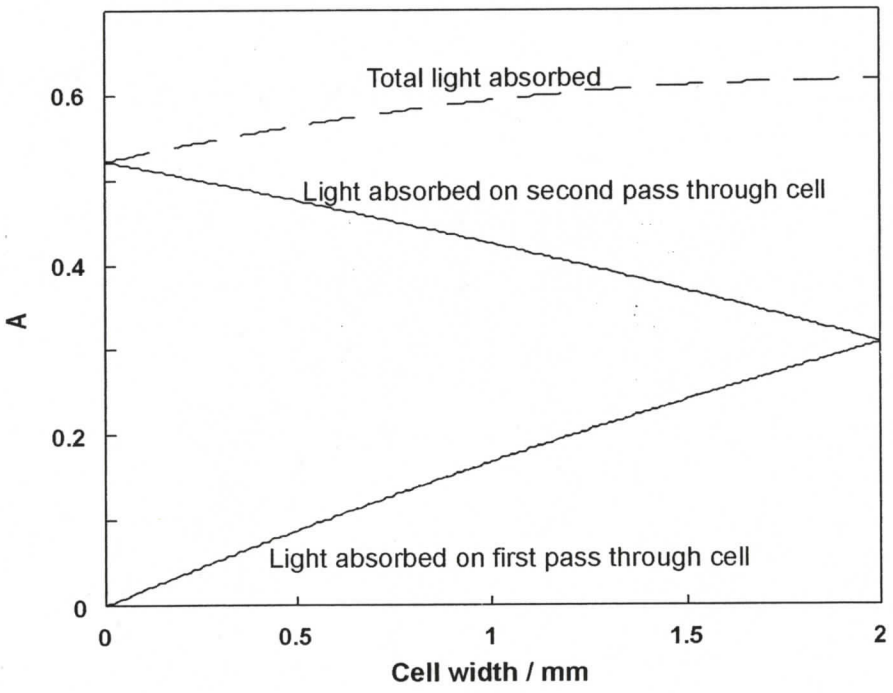


**Figure 3.7** Light absorbed over the cell width during the first and second pass of the laser beam (solid lines), and total light absorbed over the cell width (dotted line).

### 3.3.2.2 Shaping of laser beam

On exit from the laser cavity the beam is passed through a series of optics in order to achieve a rectangular beam profile (Figure 3.8). This beam shape allows heating of the entire length of the cuvette (10 mm) and a section of sample about 2 mm high. The volume of sample heated is therefore ca. 40 μL (2 x 2 x 10 mm).

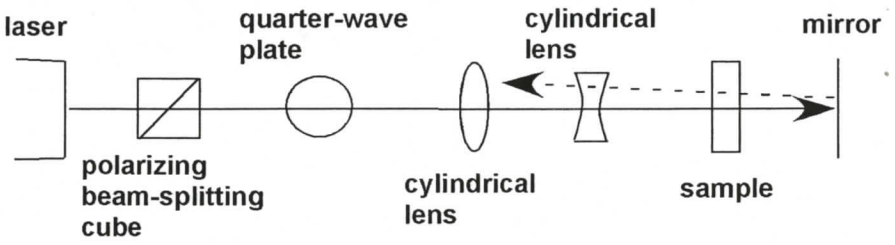


**Figure 3.8** Optical set-up following laser cavity.

### 3.3.2.3 Temperature jump

The theoretical temperature jump for this ltj system can be calculated using Equation 3.1. The change in internal energy is the amount of energy absorbed by the sample from the laser (52% of the 400 mJ laser pulse), the heat capacity of water is 4 J $K^{-1}$ $g^{-1}$, and the mass of water being heated is ca. 0.040 g (40 μL). The calculated temperature jump is thus 1.3 °C. In theory a higher temperature jump can be achieved by heating a smaller volume, and this can be achieved by shaping the laser beam to heat a smaller portion of the sample. However, heating a smaller volume will result in faster cooling rates (Section 3.3.2.4) and restrict access to longer timescales.

The actual temperature jump achieved was examined using the F127 solution. The change in light scattering for this solution was measured, and following the laser pulse an increase in the light scattering intensity of 4.3 % was seen (Figure 3.9). This corresponds to a 0.7 °C jump in temperature, and greater than 50% efficiency of the calculated temperature jump was obtained. Losses likely occur through the beam shaping optics, and because of a non-ideal beam shape incident on the sample holder.

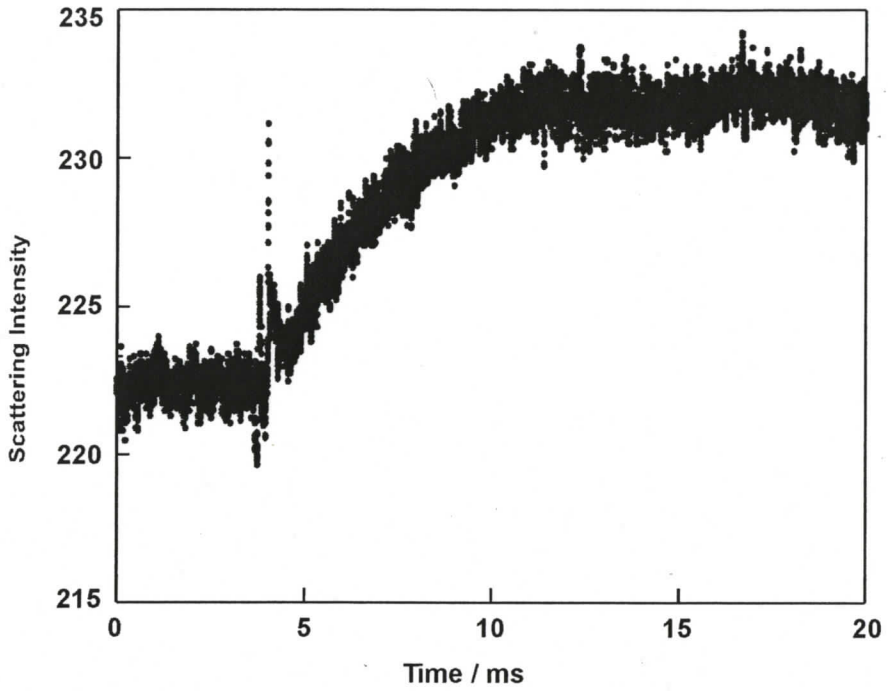


**Figure 3.9** Changes, on a 20 ms timescale, in light scattering intensity of a 2.6% F127 solution ($\lambda$ = 360 nm, $T_i$ = 26 °C) following excitation by a 1319 nm laser.

### 3.3.2.4 Cooling rates

The longest accessible timescale is defined by the cooling rate of the system, that is, how long it takes the heated portion of the sample to equilibrate with the surrounding solution. The cooling rate of the ltj system was measured using the F127 solution. The light scattering of the F127 solution was measured on longer timescales, as it returned to the intensity seen before the laser pulse (Figure 3.10). This intensity decay corresponds to the cooling of the solution to its original temperature. The half-life for the cooling was 1.3 s. The upper limit for the measurement of kinetics with this system will therefore be on the order of one second.

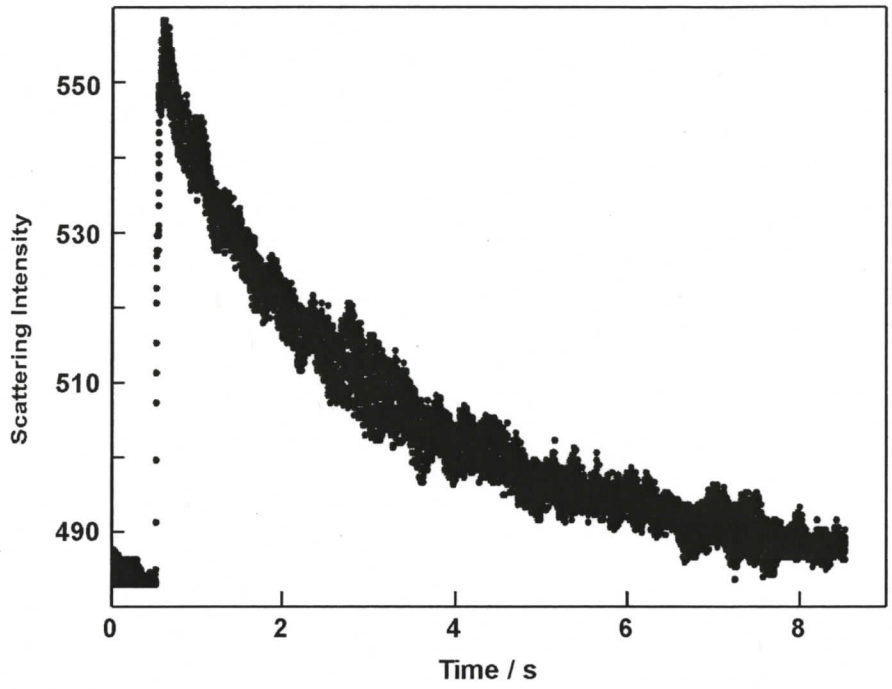


**Figure 3.10** Changes, on a 10 second timescale, in light scattering of a 2.6% F127 solution ($\lambda$ = 360 nm, $T_i$ = 26 °C) following excitation by a 1319 nm laser.

### 3.3.3 Sample holder

The sample holder functions both to hold the cuvette, and to maintain a constant sample temperature. The sample holder consists of two pieces: a cell holder made of copper, and an aluminum block through which water is flowed (Figure 3.11). There is a large opening in the centre of both the cell holder and the aluminum block through which the laser light passes. The hole in the aluminum block is tapered, with a larger opening facing the mirror that reflects the laser beam back through the sample. This minimizes the likelihood of the reflected beam hitting the aluminum block.

The copper block holds a 2 x 10 mm cuvette that has five polished surfaces, with enough room for a thin metal slit to be inserted when necessary (Section 3.3.4.5.1). There are connections for fibre optics on the two sides and bottom of the copper block.

The monitoring beam is brought into one side of the cell through a fibre optic. The height of the entire sample holder can be adjusted to assure that the monitoring beam is aligned to the same height as the laser beam. The fibre optic on the opposite side of the cell to the monitoring beam is used to transmit light to the detector for absorption experiments. The fibre optic on the bottom of the cell, at 90 degrees to the monitoring beam, transmits light to the detector for fluorescence or light scattering experiments. Fibre optics are employed to make implementation and alignment of the components possible in a relatively small area.

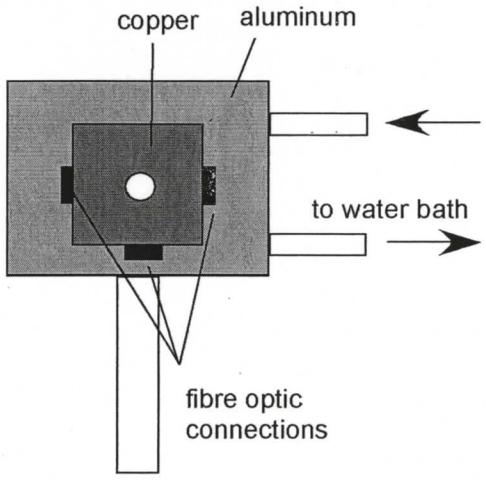


**Figure 3.11** Schematic of the sample holder design for the laser temperature jump system.

### 3.3.3.1 Temperature control

Maintenance of the sample at a constant temperature is important, as different systems will have differing behaviour depending on the initial temperature of the system. Temperature control also ensures that the system returns to the same initial temperature before each individual laser shot. If the system does not return to the initial temperature after each shot a gradual shift in the entire signal for each subsequent laser shot will be

observed. Experiments were carried out with different delays between laser shots to see if the signal was returning to the original baseline between each shot. The signal was found to drift over the course of the experiment when there was less than 90 seconds between laser shots.

Initially temperature control was carried out using a Peltier cooler placed between the cell holder and a heat sink. Unfortunately, there were problems reaching and maintaining a constant temperature, especially around ambient temperatures. Temperature control is currently carried out using a water bath. Water is flowed from the water bath through an aluminum block, to which the cell holder is attached. Monitoring the temperature of the solution in the cell has shown that a constant temperature is maintained using this approach.

### 3.3.4 Detection of signals

#### 3.3.4.1 Lamp

A PTI xenon arc lamp is used as the monitoring source. A broadband lamp provides high intensity light across the visible region, and thus puts no wavelength restrictions on the systems that can be studied. Initially the sample was continuously irradiated during the experiment, including the re-equilibration time between laser shots. This resulted in unwanted heating of the sample, and some degradation of the sample during the time frame of an experiment was seen. A shutter was introduced, so that the sample was only irradiated during collection of data, and the irradiation time of the sample was decreased. No further heating or degradation was observed.

The lamp appears to be a major source of random background noise in the observed signals. Typically on a 100 mV signal, there is 4 mV of noise on one shot, and 1

mV noise on an average of 10 shots. A xenon lamp from a different source was tested, and the power supply of the lamp was run on a line conditioner, but there were no significant improvements in the signal-to-noise ratio.

The possibility of decreasing lamp noise by baseline subtraction in absorption mode was explored. A fibre optic bundle, which after the lamp and monochromator splits into two random bundles, was used. This is the fibre optic equivalent of a beam splitter. The use of randomly split fibre bundles is necessary to diminish effects of any inhomogeneity in the lamp profile. One fibre delivered the monitoring beam through the sample, while the second was sent directly to a second detector (Figure 3.12). Combination of these signals did not improve the random noise on any timescale. This may in part be due to the fact that the detectors were not exactly matched, though it is not likely, even with matched detectors, that the random noise at each detector would be precisely the same. However, this approach would prove useful for any systematic drift in the lamp, which could be especially important for measurements made on longer timescales.

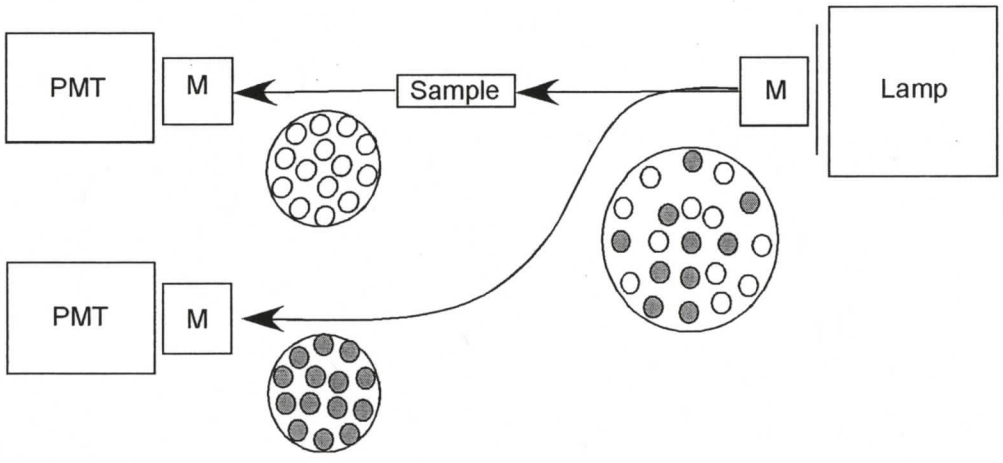


**Figure 3.12** Schematic of the set-up used for baseline subtraction with a split fibre optic bundle.

### 3.3.4.2 Monochromators

A monochromator allows for selection of a specific wavelength of light, while a cut-off filter allows transmission of all wavelengths longer than the selected wavelength. A monochromator was employed after the lamp for the selection of the excitation wavelength. On the detection side the light was passed through a monochromator for absorption experiments. For fluorescence experiments the signal is inherently small compared to absorption experiments and the light lost through the monochromator may be disadvantageous, and the use of the appropriate cut-off filter may result in a stronger signal, and thus a better signal-to-noise ratio. However, depending on how the fluorescence spectrum changes with temperature, and the available cut-off filters, the magnitude of the amplitude change of the observed signal may actually be larger when using a monochromator. The use of a monochromator also decreases the contribution from the main artifact in the system observed in fluorescence experiments (Section 3.3.4.6.2). Consequently most fluorescence experiments have been carried out using a monochromator on the detection side.

### 3.3.4.3 Detectors

Two types of detectors have been tested: photomultiplier tubes (PMT) and large-area avalanche photodiodes (LAAPD). The dark noise for the detectors was measured. For the PMT 0.5 mV noise was measured for one shot, and 0.1 mV noise was measured for an average of 10 shots. The dark noise from the LAAPD was about twice that measured for the PMT.

The LAAPD was shown to be much less sensitive than the PMT. Fluorescence signals were not detected at all by the LAAPD, but were detected by the PMT.

Absorption signals were detected by the LAAPD when the slits of the lamp were fully open, while absorption signals were detected by the PMT even when the slits were nearly closed. For these reasons, fluorescence detection has been carried out using the PMT, and absorption experiments have been carried out with the both types of detectors.

#### 3.3.4.4 Termination

Termination is important for the time resolution of experiments, since the termination itself has a finite rise time. Lower resistance terminators are needed for fast timescales because they have faster rise times, however, as the detected signal is proportional to the resistance, the magnitude of the measured signal is smaller.

For implementation of the system 1 MΩ termination was used, so that initial development and testing could be carried out with strong signals. For experiments on nanosecond timescales it will be necessary to use 50 kΩ termination, which is an additional motivation for improvement of the signal-to-noise ratio.

#### 3.3.4.5 Absorption

##### 3.3.4.5.1 Comparison of ltj to UV-Vis

Absorption experiments on the ltj actually measure intensity of light transmitted through the sample. Control experiments were carried out to ensure that what was being measured on the ltj system corresponded to the absorption. The intensity of the transmitted light for a 4 μM solution of proflavine in water was measured (I) at 450 nm, and the intensity of transmitted light for a cell containing water was measured ($I_o$) with the same optical setup. The absorbance was calculated from its definition (Equation 3.3):

$$A = \log \frac{I_o}{I} \qquad (3.3)$$

The calculated absorbance from ltj measurements was then compared to the value obtained by UV-Vis. In initial experiments the absorbance calculated from ltj measurements was always lower than that obtained from UV-Vis. For example, at 450 nm an absorption of 0.097 was measured on the absorption spectrometer, while an absorption of 0.062 was calculated from the ltj experiment.

It was found that due to the narrow width of the cell (2 mm) some of the incident light was being transmitted through the cell walls (Figure 3.13). Since more light is absorbed by the sample than by the cell walls, I is larger than it should be, and the calculated absorbance value is low.

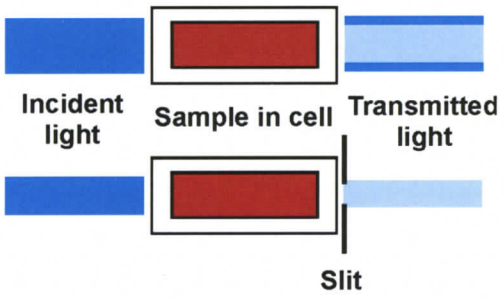


**Figure 3.13** Cartoon representation of transmission of light through the cell in the absence and presence of a slit.

The amount of light transmitted through the cell walls was diminished by using a smaller diameter fibre optic from the lamp. Collection of any light still transmitted through the cell walls was prevented by the introduction of a 1 mm slit. The slit is

smaller than the width of the cell, and though some light transmitted through the cell was also lost, the signals for absorption experiments are intense enough that this is of no concern. When the slit was placed on the side of the cell closest to the monitoring beam the calculated absorbance was closer to that from UV-Vis, but still low. The monitoring beam is most likely slightly divergent and some light was still transmitted through the cell walls. When the slit was placed on the side of the cell closest to the detector the calculated absorbance values from the ltj measurements were in agreement with those from UV-Vis measurements. All subsequent absorption experiments were carried out with the 1 mm slit in place.

This artifact would have had no effect on the observed kinetics. It would however cause the observed amplitude changes to be smaller, thus deteriorating the signal-to-noise ratio.

**3.3.4.5.2 Proflavine/DNA ltj absorbance signal**

Control experiments were carried out to see if the change in intensity with temperature detected in the ltj setup was the same as seen with UV-Vis above. Intensity of light transmitted through a solution of 15 μM proflavine with 420 μM DNA was collected at 25 °C and at 35 °C (Figure 3.14). The signal at 435 nm decreased with temperature, indicating an increase in absorption, and a 5% change in the signal intensity was observed, consistent with the 0.5% / degree change observed in UV-Vis experiments.

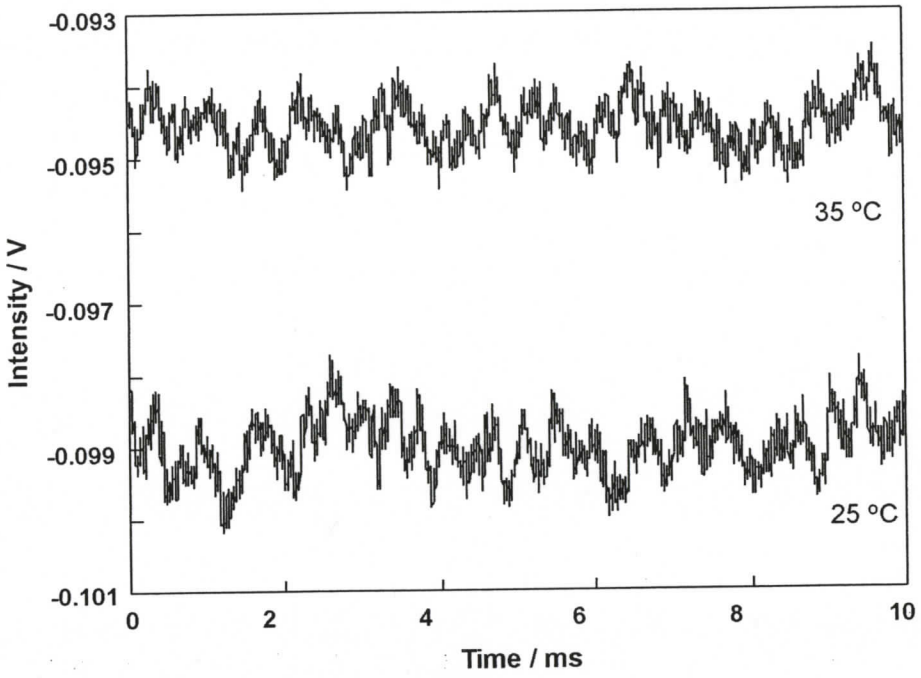


**Figure 3.14** Intensity of transmitted light through a solution of 15 μM proflavine with 420 μM DNA in the presence of 0.5 M NaCl at 25 °C and 35 °C detected by the absorbance setup of the ltj system (λ = 435 nm, PMT, average of 10 shots). A more negative intensity indicates a higher intensity of transmitted light, and therefore a lower absorbance value.

Laser temperature jump experiments using absorption detection were carried out with a solution of 15 μM proflavine in the presence of 430 μM DNA and 0.5 M NaCl in 10 mM phosphate buffer (Figure 3.15a). A change in intensity was observed after heating by the laser. The relaxation process observed occurred on the millisecond timescale, consistent with what has been previously reported for the proflavine/DNA system.[6,93,98-103] The same experiment was performed for a solution of proflavine in the absence of DNA, and no change in intensity was observed following the laser pulse (Figure 3.15b). These experiments show that the system works in principle. However, improvements in the signal-to-noise ratio are needed before useful kinetic data can be extracted.

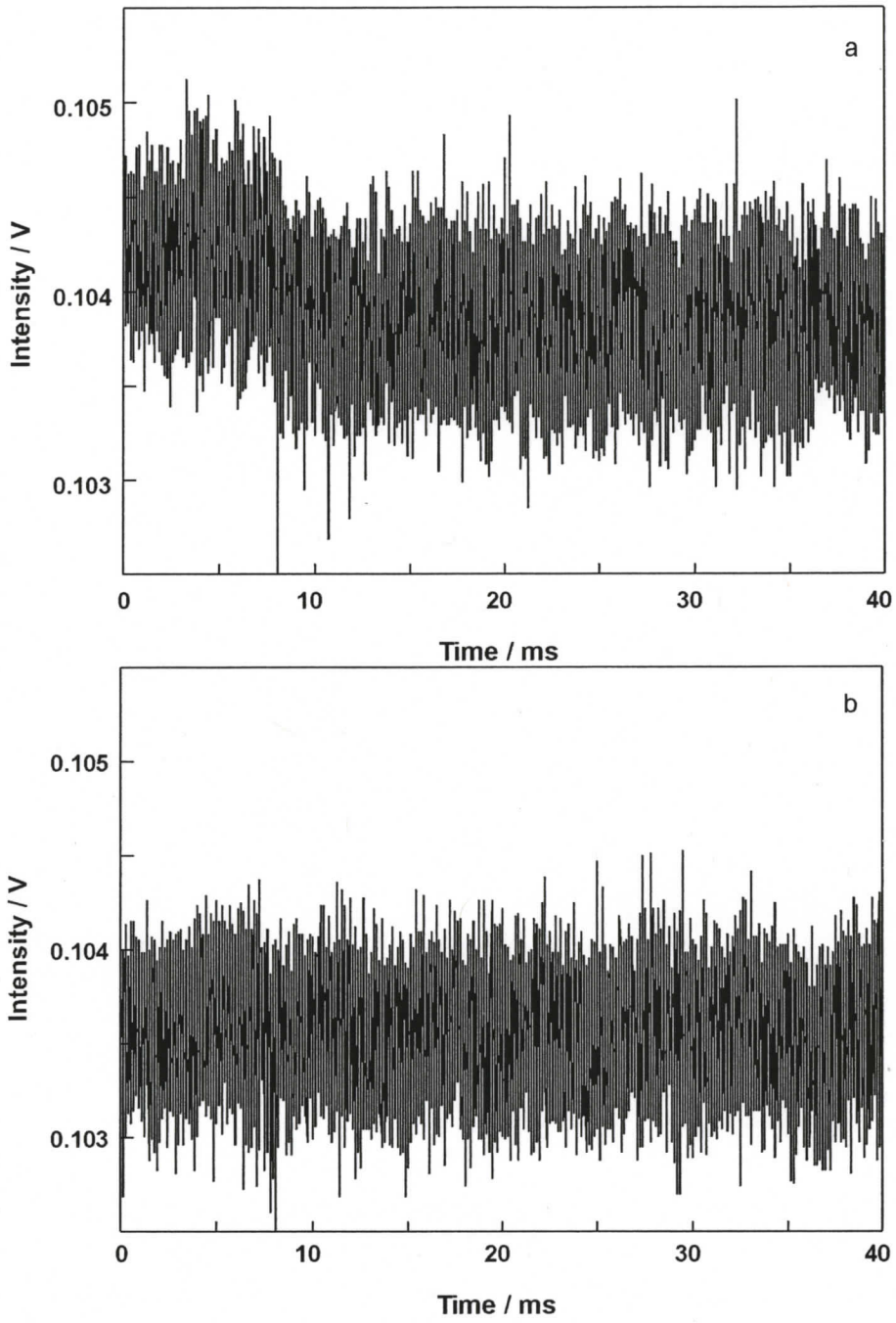


**Figure 3.15** Laser temperature jump absorption experiment for a) 15 μM proflavine/420 μM DNA/0.5 M NaCl in 10 mM phosphate buffer and b) 15 μM proflavine/0.5 M NaCl in 10 mM phosphate buffer ($T_i$ = 26 °C, LAAPD, λ = 435 nm, average of 10 shots). A more positive intensity indicates a higher intensity of transmitted light, and therefore a lower absorbance value.

### 3.3.4.6 Fluorescence

#### 3.3.4.6.1 Proflavine/DNA ltj fluorescence signal

Control experiments were carried out to determine if the change in intensity with temperature detected in the ltj setup was the same as seen in steady-state fluorescence experiments above. The fluorescence intensity of a solution of 5 μM proflavine with 30 μM DNA was collected at 25 °C and at 35 °C (Figure 3.16). The emission intensity at 500 nm increased with temperature and a 13% change in the signal intensity was observed, consistent with the 1.5% / degree change observed in the steady-state fluorescence experiments.

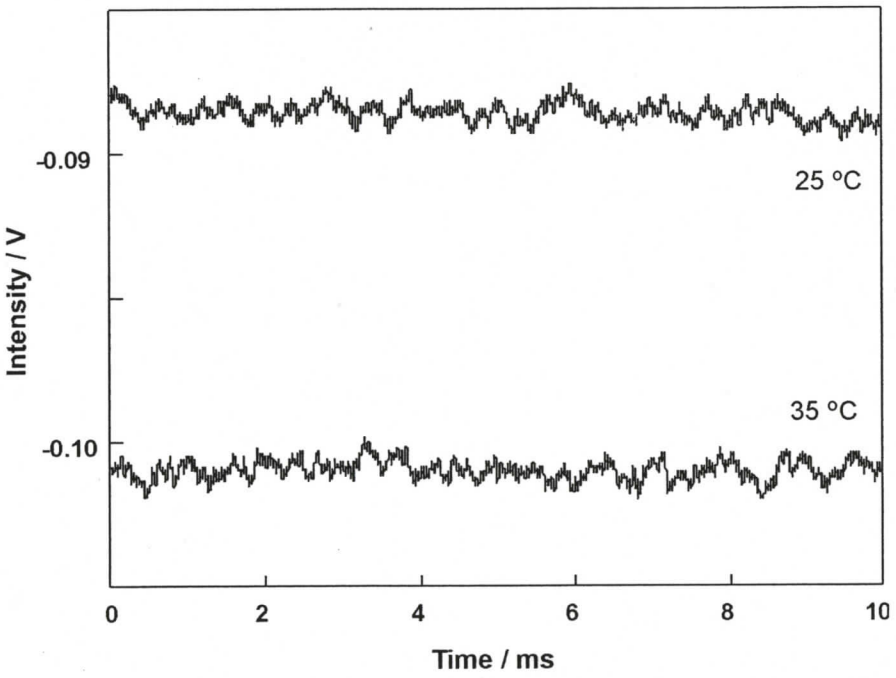


**Figure 3.16** Fluorescence intensity of 5 μM proflavine with 30 μM DNA in 10 mM phosphate buffer at 25 °C and 35 °C detected by the fluorescence setup of the ltj system ($\lambda_{ex}$ = 450 nm, $\lambda_{em}$ = 500 nm, PMT, average of 10 shots). A more negative intensity indicates higher fluorescence intensity.

Laser temperature jump experiments using fluorescence detection were carried out with a solution of 5 μM proflavine in the presence of 30 μM DNA in 10 mM phosphate buffer (Figure 3.17). A change in intensity was observed after the laser pulse, with the relaxation process occurring on the millisecond timescale. Signals can be obtained using fluorescence detection, but improvements in the signal-to-noise ratio are needed before any reasonable kinetics can be extracted.

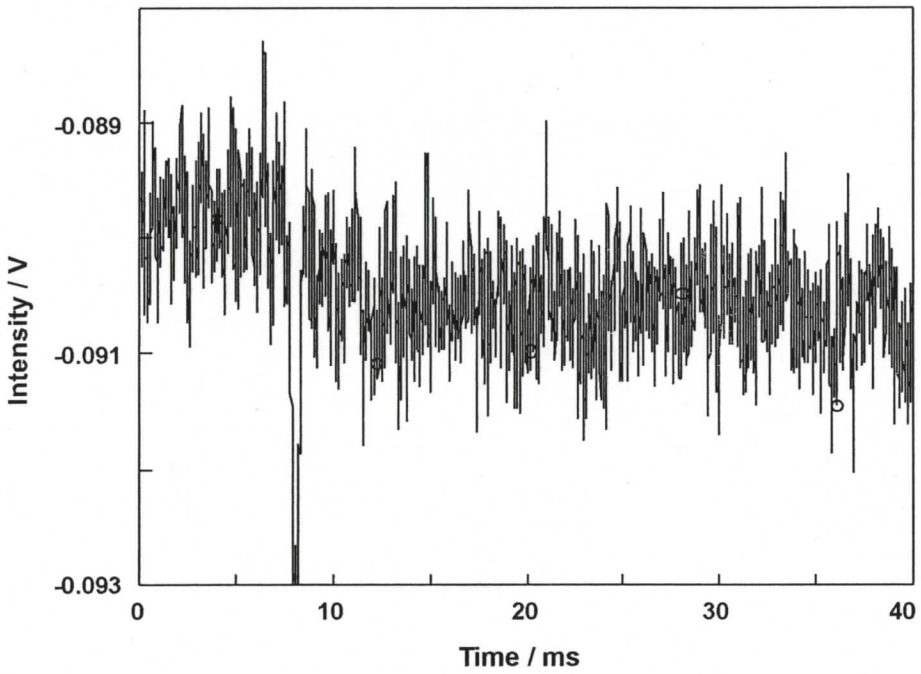


**Figure 3.17** Laser temperature jump fluorescence experiment for 5 μM proflavine/30 μM DNA in 10 mM phosphate buffer ($T_i$ = 26 °C, PMT, $\lambda_{ex}$ = 450 nm, $\lambda_{em}$ = 500 nm, average of 20 shots). A more negative intensity indicates higher fluorescence intensity.

### 3.3.4.6.2 Artifact in fluorescence experiments

There is an artifact present in fluorescence experiments that can be seen as the sharp peak coinciding with the time of laser pulse in Figure 3.17 and in Figure 3.18. This artifact overlays important kinetic data and it is imperative that it be eliminated.

The artifact was found to be present at all wavelengths between 300 and 700 nm, and was particularly intense between 400 and 500 nm. The artifact was only detected when the laser flash lamps were flashing, whether the laser was lasing or not. It was concluded that the artifact is light from the laser flash lamps that is emitted coincident to the laser beam. The optics outside the laser cavity (Figure 3.8) were removed one by one to see if they contributed to focusing this light on top of the laser beam, but the optics were found to have no effect on the position of the light.

The artifact is greatly diminished if a monochromator is used instead of cut-off filters at the detector, since a much smaller portion of the spectrum from the flash lamps is collected through the monochromator (Figure 3.18). The intensity of fluorescence detected is reduced by half when the monochromator is in place, but the reduction in the artifact is greater. Since the artifact signal is smaller, the recovery of the PMT is faster, and the width of the peak decreased. However, the intensity of the artifact when using a monochromator is still significant compared to the intensity of the signal of interest, and impedes fluorescence measurements on microsecond timescales.

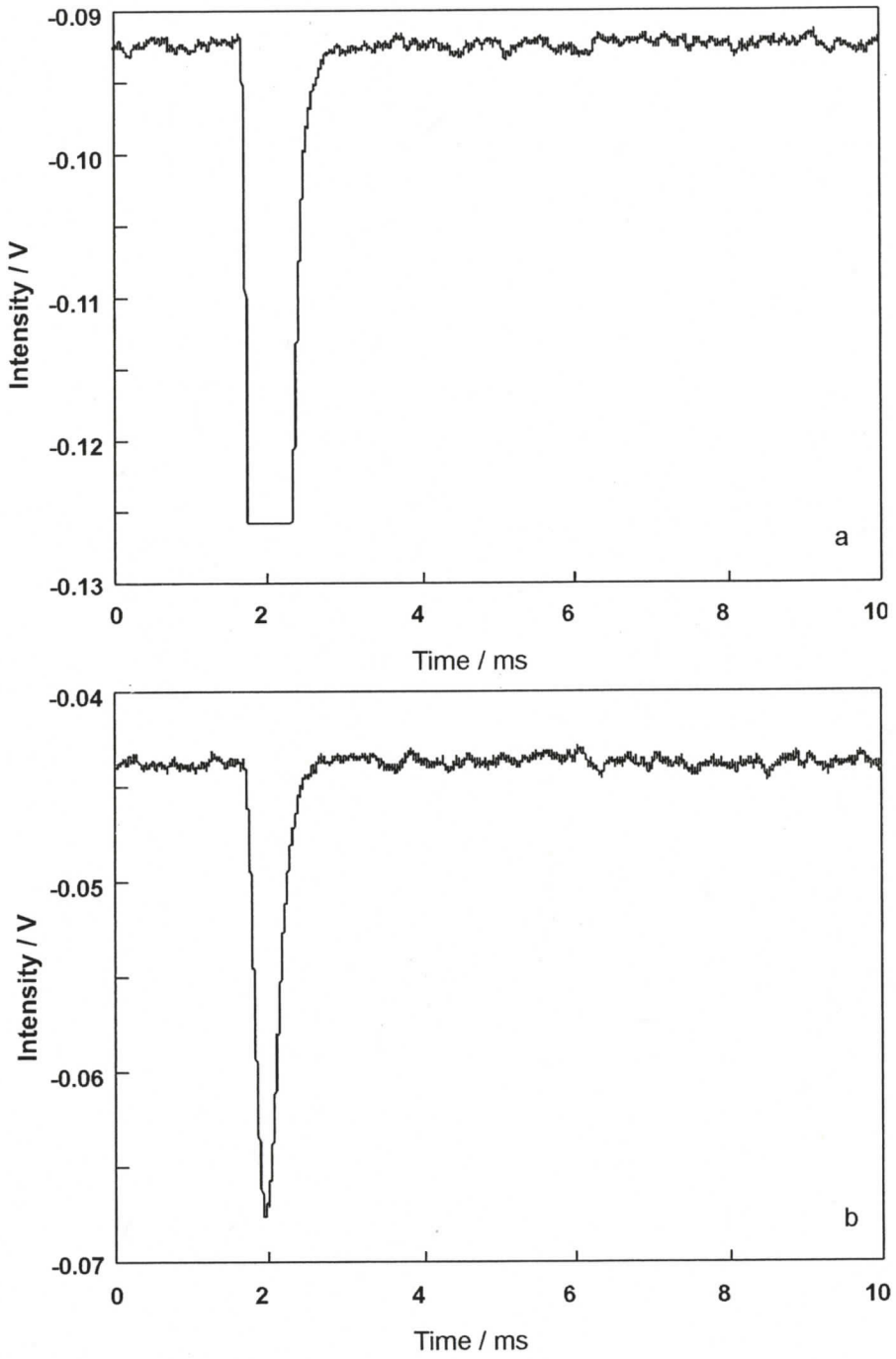


**Figure 3.18** Artifact in ltj fluorescence detection for a solution of 5 μM proflavine (a) $\lambda_{ex}$ = 450 nm, $\lambda_{em}$ > 495 nm (cut-off filter), (b) $\lambda_{ex}$ = 450 nm, $\lambda_{em}$ = 500 nm (monochromator). A more negative intensity indicates a higher intensity of detected light.

This artifact is not seen, for the most part, in absorption experiments. The artifact is only seen in absorption experiments around 500 nm as a very small peak if a

monochromator is not used. This is most likely because the area from which light is collected in absorption experiments is very small compared to the fluorescence experiments.

### 3.4 Recommendations

Due to unforeseen circumstances in the lab completing the implementation of the laser temperature jump system was not possible.

Further improvement of signal-to-noise ratios needs to be achieved. Decreasing the noise level of the monitoring lamp will likely have the largest effect on the signal-to-noise ratio. It may be possible to achieve lower noise levels from alternate light sources, such as diode lasers.

Implementation of the ltj system was carried out so that a wide dynamic range would be accessible. It may be worthwhile for studying fast kinetics to explore the possibility of heating smaller volumes of sample. Heating a smaller volume will increase the cooling rate, and therefore shorten the accessible timescales, but if a smaller volume of solution is heated larger temperature jumps, and thus larger signals and improved signal-to-noise ratios, will be obtained.

In order to extract kinetic data from fluorescence data at short timescales, the artifact needs to be eliminated. A similar artifact has also hampered the performance of fluorescence detection in previous ltj systems. Holzwarth et al. saw a signal due to white light from the laser that was of one order of magnitude larger than the signal of interest.[104] They eliminated this signal by not recording fluorescence data for the first 20 μs following the laser pulse.[104] We hope to completely eliminate the fluorescence artifact

seen in our system with the use of a prism between the laser and the sample holder, which should allow the 1319 nm light to reach the cell, while scattering the shorter wavelengths emitted by the flash lamps.

### 3.5 Conclusions

The custom-built laser temperature jump system is an adaptation of systems described in the literature, with the main difference being the 1319 nm laser optimized for excitation of water, providing the ability to access kinetics across a wide time range. The laser and detection systems for absorbance and fluorescence were successfully implemented, and a number of artifacts have been identified and eliminated. The expected temperature jump has been obtained and signals have been detected by both fluorescence and absorption, though the signal-to-noise ratio still needs to be improved for DNA work.

The changes in fluorescence or absorbance with temperature are inherently small with DNA systems, and there may be some systems for which dynamics will not be measurable using the ltj system. At times the sample volume heated may need to be decreased in order to achieve a larger temperature jump, and therefore a larger signal. This approach will always have the disadvantage of increasing the cooling rate of the system, thus decreasing the long timescale resolution of the system. However, continuing improvements in the current setup should allow the system to become operational for routine experiments.

# 4. DIFFERENTIATION OF AC BINDING SITES IN HSA

The work carried out in this chapter is part of a collaboration between the Bohne group and the Inoue group at Osaka University, Japan. Unless otherwise indicated the results presented were carried out by the author at Osaka University. These results have been submitted to the Journal of Physical Chemistry B as a manuscript titled 'Photophysical Studies of the Supramolecular Photochirogenesis for the Photocyclodimerization of 2-Anthacenecarboxylate within Human Serum Albumin'.

## 4.1 Introduction

### 4.1.1 Use of proteins as a host system in enantioselective reactions

The use of a number of chiral supramolecular systems to influence the outcome of enantioselective reactions has been explored. Systems including cyclodextrins,[105-115] modified zeolites,[116-118] and hydrogen bonding templates[119-123] have been used to affect the chirality of products achieved in reactions such as photocyclizations, photoisomerizations, photodimerizations, and photoadditions. Proteins are potentially useful supramolecular systems in which to achieve photochirogenesis because they have well-defined structures with chiral binding sites where reaction can take place. However, proteins have not yet been widely used in such applications.

Zandomeneghi et al. have shown that, for molecules such as 1,1'-bi-2-naphthol and ketoprofen, photodecomposition of one enantiomer occurs preferentially when bound to bovine serum albumin (BSA).[124-126] Thus enantiomeric excess (ee) is achieved for racemic mixtures as one enantiomer is more readily destroyed. The ee obtained increased

as the sample was destroyed; for the photolysis of a racemic mixture of ketoprofen in BSA ee's of ca. 20% were obtained when more than 80% of the mixture was destroyed.[126] The photolysis of racemic 1,1'-bi-2-naphthol in BSA was a special case, involving the combined effects of preferential destruction of one enantiomer, and preferential photoinversion of the same enantiomer, resulting in ee's of up to 99% when more than 77% of the mixture was destroyed.[125]

The ability of proteins to stereodifferentiate between enantiomers has been further shown by Miranda et al,[127-129] and Monti et al.[130] The enantiomers of carprofen,[128] flurbiprofen methyl ester,[127] and ketoprofen[130] have different triplet excited state lifetimes when bound to human serum albumin (HSA). When bound to Site I of HSA the (*S*)-enantiomer of carprofen has a triplet lifetime of 2.3 μs, while the (*R*)-enantiomer has a lifetime of 8.9 μs.[128] In Site II of HSA the (*S*)-enantiomer of carprofen has a triplet lifetime of 24 μs, while the (*R*)-enantiomer has a lifetime of 40 μs.[128] The shortening of lifetimes in Site I compared to Site II was explained to be due to quenching by the tryptophan residue located in Site I.[128]

These examples involve unimolecular processes, and though neither of these examples involves the creation of a chiral centre, they do show that the chiral environment of the protein affects the binding, photophysics and photochemistry of guest molecules. These factors make serum albumin proteins a good potential system to study the ability of proteins to act as a host for photochirogenic reactions.

### 4.1.2 AC dimerization reaction

The photodimerization of 2-anthracenecarboxylate (AC) is used as a model bimolecular reaction to study photochirogenesis. AC undergoes [4 + 4]

photocycloaddition to form four regio-isomers (Scheme 4.1), of which products **2** and **3** have enantiomers. In solution the head-to-tail (HT) products, **1** and **2**, are formed preferentially, and no ee is observed.

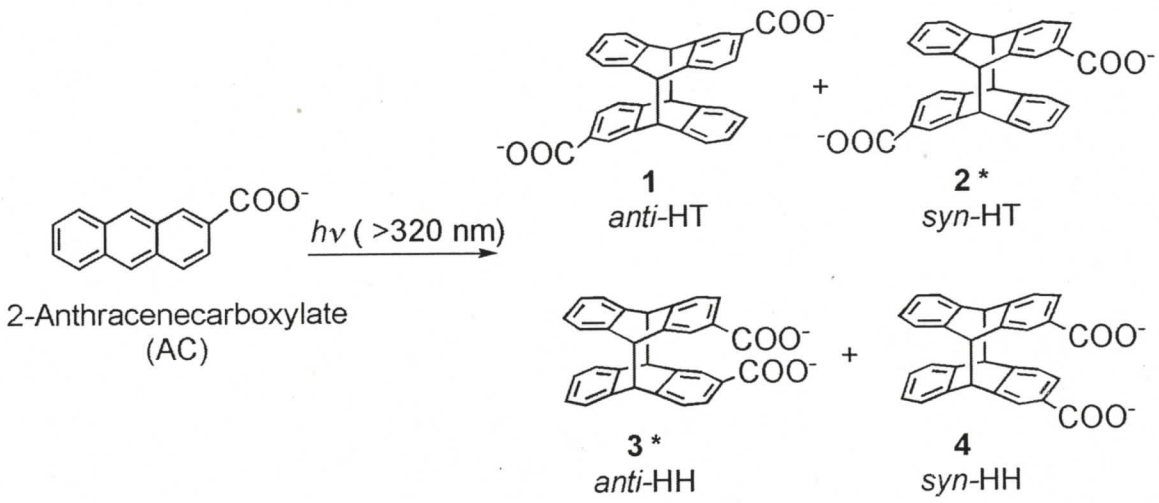


**Scheme 4.1** Photocyclodimerization of AC.

In general, mechanistic evidence has supported a singlet excited state pathway for the dimerization of anthracene and its derivatives, and in a number of examples the formation of an excimer has been shown to be an intermediate in the dimerization reaction.[131] In general the triplet excited state of anthracene does not lead to photodimerization. It has been shown that the self-quenching of triplet anthracene with ground state anthracene leads exclusively to the anthracene monomer.[131] However, triplet-triplet annihilation can generate a singlet excimer, which then forms the photodimer.[131] We assume that the photocyclodimerization of AC in our system is a singlet excited state reaction, though this has not been directly shown.

### 4.1.3 AC dimerization reaction in cyclodextrins

The photodimerization reaction of AC has been studied in a number of different cyclodextrins.[108,109,112-115] Reaction occurs between two AC molecules bound in close proximity to each other in the cyclodextrin. The reaction is static, i.e. it occurs immediately upon excitation, and the products formed are defined by the orientation of the molecules bound to the cyclodextrin. In γ-cyclodextrin product **2** is produced in up to 41% ee,[108] and through the use of chemical modification of the cyclodextrin interior or rims some control is obtained over which product shows enhanced ee. The ee's obtained were always modest, and either the ee of product **2** or product **3** was enhanced, but not both simultaneously.

### 4.1.4 AC dimerization reaction in bovine serum albumin

The binding of AC to bovine serum albumin, and its photoreaction has been studied by Inoue et al.[132,133] We began collaborating on the AC/serum albumin projects to look at the mechanistic aspects of the reaction, and the photophysics of AC when bound to the proteins.

#### 4.1.4.1 Binding of AC to BSA

AC is proposed to have four binding sites in BSA. Modeling of binding data from absorption, fluorescence and circular dichroism experiments showed that the four sites bind 1, 3, 2 and 3 molecules with binding constants of $5.3 \times 10^7\ M^{-1}$, $1.3 \times 10^5\ M^{-1}$, $1.4 \times 10^4\ M^{-1}$ and $3 \times 10^3\ M^{-1}$.[133] The sites are numbered according to their decreasing binding affinity. For the sites that bind multiple AC molecules there was evidence from CD experiments that the molecules are not in close proximity to each other; each site could

be a single site that binds multiple AC molecules, or multiple sites that all have very similar binding constants.

#### 4.1.4.2 Photoreaction of AC complexed to BSA

Both product distribution and ee of the AC dimerization reaction were affected by complexation to BSA. At the lowest AC/BSA ratios studied, where AC is bound only to site 1, no products were observed, indicating that AC in site 1 is not reactive. At low AC/BSA ratios, where AC is bound only to the higher affinity sites (sites 1 and 2), the amount of HH products were increased, and moderate ee's were obtained for both **2** and **3**, up to -22% and 58% , respectively.[132] As the AC/BSA ratio was increased the ratio of HT and HH products changed, and the ee's obtained decreased, though the behaviour seen for the ee of **2** and **3** was different. This indicated that the enantiomers and products formed preferentially are not the same in each binding site.

#### 4.1.4.3 Photophysical studies of AC in the presence of BSA

Photophysical studies were carried out, and the steady-state and time-resolved fluorescence were studied at various AC/BSA ratios.[132] The steady-state spectra decreased in intensity in the presence of BSA, and fluorescence decays revealed different lifetimes for AC in site 1 and AC in site 2, shorter than that for AC in bulk solution, while AC in site 3 and 4 could be not be distinguished from AC in bulk solution.

A comparison was made between the steady-state fluorescence intensities and the average lifetimes at different AC/BSA ratios. The average lifetime, $<\tau>$, corresponds to the integral of the decay curve, and is calculated using Equation 4.1:

$$\langle \tau \rangle = \sum_{1}^{i} A_i \tau_i \qquad (4.1)$$

where $\sum_{1}^{i} A_i = 1$

The shorter lifetimes observed in the presence of BSA were consistent with the decrease in the steady-state emission intensity (Figure 4.1). This agreement implies that there was no static quenching of AC molecules. Static quenching occurs when a fluorophore is deactivated directly after excitation, which leads to a decrease in the fluorescence intensity, but no shortening of fluorescence lifetimes. This result showed that the AC molecules in BSA are not located in close enough proximity to undergo photodimerization as a result of a static process, which is different from what was seen for the reaction in cyclodextrins, as described above.

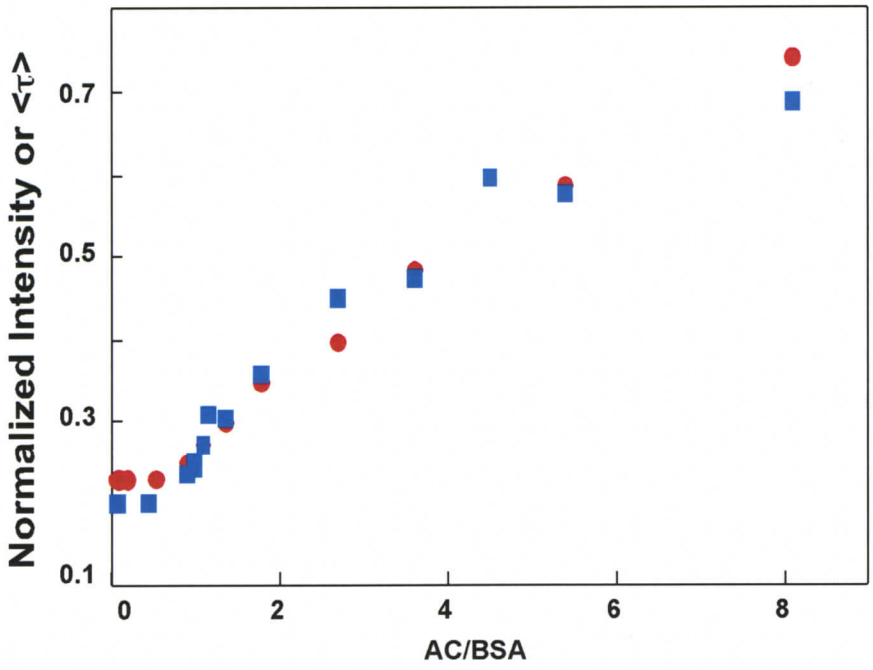


**Figure 4.1** Dependence of fluorescence emission intensity (square, blue) and average lifetime (circle, red) on AC/BSA ratio. Data are normalized to unity for AC in buffer (normalized point not shown). Reproduced with permission from reference 132, copyright 2007 American Chemical Society.

Quenching experiments with nitromethane were carried out to determine how protected the different AC species were. Nitromethane has been shown to quench AC with a rate constant of $(5.8 \pm 0.2) \times 10^9$ $M^{-1}$ $s^{-1}$,[132] which is close to the diffusion controlled rate constant in water ($6.5 \times 10^9$ $M^{-1}$ $s^{-1}$).[59]

Nitromethane quenching experiments in the presence of BSA revealed that AC in site 1 was very protected from the bulk solution ($k_q < 2 \times 10^8$ $M^{-1}$ $s^{-1}$).[132] AC in site 2 was found to be less protected than AC in the first site, but the quenching rate constant of AC in site 2 was still one order of magnitude smaller than for AC in bulk solution.[132] AC in sites 3 and 4 were completely exposed to the bulk solution.

#### 4.1.4.4 AC/BSA product studies in the presence of nitromethane

Further AC/BSA product studies were carried out in the presence of nitromethane to take advantage of the different quenching efficiencies for AC in site 2 and AC in site 3, revealed in the photophysical studies. These studies indicated that the dimerization reaction is more efficient in site 3. The ee for product **2** from site 2 was of opposite sign to that from site 3, while the ee for product **3** was of the same sign in each site, but much higher ee values were obtained from the reaction in site 3.[132]

#### 4.1.4.5 Conclusions from AC/BSA work

The AC/BSA work showed that the ee is not due to a static reaction in a high affinity binding site. Instead the dimerization reaction is a dynamic process, and the highest ee's are obtained from reaction in moderate binding sites.

### 4.1.5 AC dimerization reaction in human serum albumin

The AC dimerization was subsequently studied in HSA.[134] The product distribution and ee's obtained were markedly different from the reaction in the presence of BSA (see below).

#### 4.1.5.1 Differences between HSA and BSA

HSA and BSA are similar structurally, differing by only 26 amino acid residues.[135] They are however known to differ significantly in how they bind molecules, and in the photophysical and photochemical behaviour of the bound guests.[38,126,129,135-137] For example, a comparison of the binding of flurbiprofen methyl ester to HSA and BSA showed that under conditions where binding to the protein was well below saturation all the guest was bound to HSA, while more than 20% of the guest was free in bulk solution under the same conditions with BSA.[129] Additionally, while strikingly different triplet lifetimes were seen for the (*R*)- and (*S*)-enantiomers when bound to HSA, the triplet lifetimes were very similar for both enantiomers when bound to BSA.[129] Another example is the binding of camptothecin, an anticancer agent, to serum albumins. Though very active in animals, camptothecin shows only modest activity against human cancers.[136] Camptothecin contains a δ-lactone ring, which can hydrolyze to a carboxylate form, which is biologically inactive.[136] The difference in activities is mainly attributed to different binding affinities of the inactive form of the drug with the serum albumin proteins. HSA has a strong preference for binding the carboxylate form over the lactone form, while animal serum albumins, including BSA, do not bind the carboxylate form so strongly.[136]

In addition to the differences described above, the crystal structures for HSA, and its complexes with various molecules have been solved,[138,139] while such data is not available for BSA. Figure 4.2 shows a summary of guest binding to HSA from crystallographic studies.[138]

See Figure 7 from reference 138

**Figure 4.2** Location of guests bound to HSA from crystallographic studies including binding to Sudlow Site I (Drug site 1) and Sudlow Site II (Drug site 2). Reprinted from reference 138, Copyright (2005), with permission from Elsevier.

#### 4.1.5.2 Binding of AC to HSA

Binding of AC to HSA was investigated by fluorescence and circular dichroism. The changes in the CD signals at different wavelengths with AC/HSA ratio had a number of inflection points and turning points, which indicated binding sites in HSA that bind 1, 1, 3, 5 and more than 10 AC molecules.[134] These sites are referred to as sites 1 through 5,

according to their decreasing binding affinity. The binding constant for AC to site 1 was determined, by fitting of fluorescence titration data, to be 3.0 x $10^8$ $M^{-1}$.[134] Unfortunately, determination of binding constants for AC to the other sites has not been possible. This makes interpretation of photoreaction and photophysical data more complicated than in BSA, since it is unknown exactly where AC is bound at each AC/HSA ratio studied.

Warfarin (Scheme 4.2) binds to Sudlow Site I in HSA with a binding constant of 3.3 x $10^5$ $M^{-1}$,[38] while 4-iodobenzoate (Scheme 4.2) binds to the Sudlow Site II in HSA with a binding constant of 1.8 x $10^6$ $M^{-1}$.[140] Site 1 and site 2 for AC binding to HSA have been shown to correspond to the Sudlow Site II and Site I, respectively, through circular dichroism experiments in the presence of warfarin and 4-iodobenzoate.[141] Sites 3 – 5 are likely to be less well-defined binding sites on the protein surface. Knowledge of guests that competitively bind to sites in HSA occupied by AC provides an additional tool to study the AC dimerization reaction in HSA, that was not available with BSA.

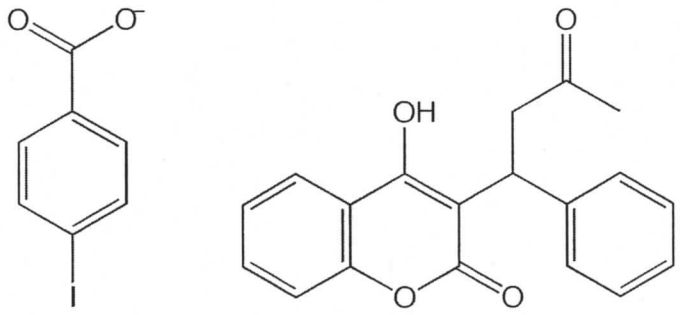


**Scheme 4.2** 4-Iodobenzoate (4-IB) and warfarin.

### 4.1.5.3 Photoreaction of AC complexed to HSA

The product distribution for the AC photodimerization reaction in HSA was similar to that in bulk solution at all AC/HSA ratios, unlike BSA where an enhancement

of head-to-head products was observed. The ee obtained for products **2** and **3** were remarkably high, up to 79% and 88%, respectively (Table 4.1).[134] At AC/HSA ratios below 2 no products were seen, indicating that AC bound to site 1 and site 2 are not reactive, and all the ee results from reaction in sites 3 - 5. At higher ratios the ee's obtained decreased, but were still markedly high.

**Table 4.1** Enantiomeric excess obtained for the AC photodimerization reaction at various AC/HSA ratios.[a,b]

| AC/HSA | ee / % | |
|---|---|---|
| | **2** | **3** |
| 3 | 79 | 88 |
| 5 | 59 | 42 |
| 10 | 61 | 33 |
| 25 | 50 | 14 |

[a] Irradiated at $\lambda > 320$ nm for 1 hr under Ar; [AC] = 0.6 mM, errors for ee < 5%
[b] Data from reference 134

### 4.1.6 Objective

The objective of this work with the AC/HSA system is to develop experimental strategies using fluorescence techniques to differentiate between the binding of AC to sites 3, 4 and 5 in HSA where all the photoreaction occurs, and to determine conditions under which product studies could be carried out to isolate ee produced from reaction in the different sites, in order to gain further mechanistic insight on the photochirogenic dimerization of AC in the presence of serum albumin proteins.

## 4.2 Experimental

### 4.2.1 Materials

2-Anthracene carboxylic acid (Tokyo Chemical Industry), human serum albumin (fat-free grade, lot # 120K76031 and # 085K7541, Sigma), nitromethane ($CH_3NO_2$, Aldrich), sodium hydroxide (NaOH, Wako), potassium phosphate monobasic ($KH_2PO_4$, Wako), sodium phosphate dibasic ($Na_2HPO_4$, Wako), 4-iodobenzoate (Wako), warfarin (Aldrich), and acetonitrile (HPLC grade, Wako) were used as received. Deionized water (Millipore system) was used for all aqueous solutions.

### 4.2.2 Preparation of solutions

A 5.0 mM AC stock solution was prepared by dissolving the appropriate amount of AC in an aqueous solution of 10 mM NaOH. A 10 mM warfarin stock solution was prepared by dissolving the appropriate amount of warfarin in 10 mM aqueous NaOH. A 10 mM aqueous 4-iodobenzoate stock solution was prepared by dissolving the appropriate amount of 4-iodobenzoate in 10 mM NaOH. The warfarin and 4-iodobenzoate stock solutions were sonicated to achieve solubilization.

All AC/HSA solutions were buffered at pH 7.0 with a 33 mM phosphate solution. The buffer was prepared by mixing 33 mM $Na_2HPO_4$ and 33 mM $KH_2PO_4$ in a 2:1 ratio, and then adjusting the pH of the resulting solution to pH 7.0 by further addition of the $KH_2PO_4$ solution.

AC/HSA solutions were prepared by weighing the appropriate amount of HSA into a volumetric flask, then adding a few mLs of buffer. The solution was set aside until the HSA had completely dissolved. The appropriate amount of AC stock solution was injected into the solution (30 μM final AC concentration for photophysical studies, 0.6

mM final AC concentration for photolysis studies), and the flask was filled to the mark with buffer.

For photolysis experiments in the presence of inhibitors, the appropriate amount of inhibitor stock solution was added at the same time as the AC stock solution. For photophysical experiments in the presence of inhibitors, the inhibitor stock solution was added later, by injection into the 3 mL aliquot of solution used for experiments, since the added volume was small (< 3%).

### 4.2.3 Quenching procedures

Quenching was carried out using neat nitromethane, or the stock solutions of 4-iodobenzoate or warfarin. The appropriate amount of quencher was injected into 3 mL aliquots of AC or AC/HSA solutions.

### 4.2.4 Deoxygenation procedures

All photophysical experiments were carried out on aerated solutions. Solutions for photolysis experiments were deaerated using three freeze-pump-thaw cycles, and then put under an argon atmosphere.

### 4.2.5 Photolysis procedures

Photolysis was carried out at 25 °C in a temperature-controlled water bath. A 3 mL aliquot of solution was irradiated for one hour at wavelengths > 320 nm, using a high pressure mercury lamp (300 W) fitted with a uranium filter. A 400 μL portion of the irradiated solution was added to 400 μL of acetonitrile, and was permitted to stand

overnight. The resultant solution was filtered by ultrafiltration, and used for the HPLC analysis.

### 4.2.6 Instrumentation

Absorption spectra were collected on a JASCO V-550 spectrophotometer.

Steady-state fluorescence spectra were recorded on a JASCO FP6500 instrument. The excitation and emission slits were set to optimize the emission intensity, typically with a bandpass of 1 and 3 nm, respectively. The excitation wavelength was 394 nm, and spectra were collected between 405 and 600 nm. Fluorescence intensities were determined by integration of the spectra between 410 and 480 nm.

Time-resolved fluorescence measurements were performed with an Edinburgh Instruments FL 920S time-correlated single photon counter with a hydrogen flash lamp excitation source. The bandpass for the excitation and emission monochromators was 10 nm. The number of counts collected in the channel of maximum intensity was 2000. The excitation wavelength was 394 nm, and the emission wavelength was 420 nm. The instrument response function (IRF) was measured using Ludox (Aldrich) to scatter light at the excitation wavelength. All decays in the presence of HSA were multi-exponential functions, and fitting of the fluorescence decays, where the IRF was deconvoluted from the experimental data, was performed using the accompanying software from Edinburgh, or the Edinburgh FAST software. Both programs fit the decays to the sum of exponentials (Equation 1.1). The FAST software has an additional feature, which allows pre-exponential factors to be fixed during fitting. The value of $\chi^2$ (0.9 to 1.2) and a visual

inspection of the residuals and the autocorrelation function were used to determine the quality of the fit.[76]

HPLC analysis was performed on a JASCO system equipped with tandem columns of Mightysil RP-18 (Kanto) and Chiralcel OJ-R (Daicel). The columns were kept at 35 °C. A mixture of acetonitrile containing 0.1 % trifluoroacetic acid and water (36:64 by volume) was used as the eluent. The relative yield and ee values were determined by peak area on the HPLC chromatogram detected by fluorescence ($\lambda_{ex}$ = 254 nm, $\lambda_{em}$ = 420 nm). The fluorescence method detects AC monomers that are produced in the detection cuvette by photodecomposition of the photodimers by the excitation light. This method produces the same results as the more conventional absorption detection of the dimers, but is much more sensitive.

## 4.3 Results

### 4.3.1 AC/HSA steady-state fluorescence

Steady-state fluorescence spectra were obtained at AC/HSA ratios from 0.1 to 20 (Figure 4.3). AC in buffer at pH 7.0 is deprotonated and its emission spectrum is broad. The spectra at high AC/HSA ratios were similar in shape to the spectrum of AC in buffer, while at lower ratios a more structured spectrum was obtained, similar to that for AC in pentane.[132] A decrease in fluorescence intensity was seen from the lowest AC/HSA ratio until a ratio of 2; at higher ratios the fluorescence intensity then increased. This initial decrease results from AC in site 2 being silent in fluorescence experiments, due to static quenching by a tryptophan residue of HSA in close proximity to the binding site.

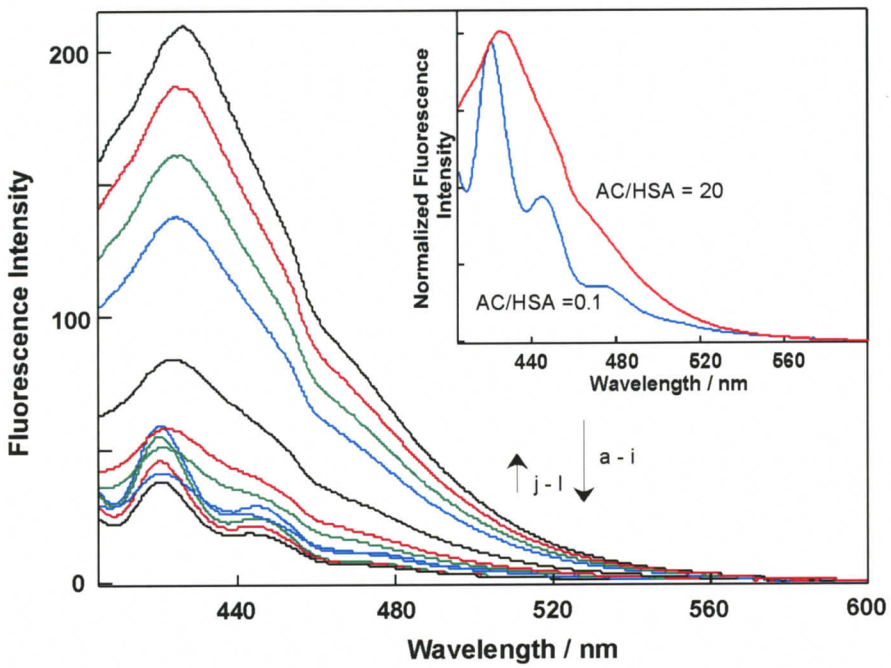


**Figure 4.3** Fluorescence emission spectrum of (a) AC (30 μM) in buffer and spectra at AC/HSA ratios of (b) 20, (c) 15, (d) 10, (e) 5, (f) 4, (g) 3, (h) 2.5, (i) 2 (j) 1.5, (k) 1 and (l) 0.1($\lambda_{ex}$ = 394 nm). Inset: Fluorescence emission spectra at AC/HSA ratios of 20 (red) and 0.1 (blue) normalized at 420 nm. Reproduced with permission from the Journal of Physical Chemistry B, submitted for publication, unpublished work copyright 2009 American Chemical Society.

### 4.3.2 AC/HSA time-resolved fluorescence

The fluorescence decay of AC in buffer is mono-exponential, with a lifetime of 15.8 ± 0.6 ns.[132] In AC/HSA the fluorescence decay did not follow a mono-exponential function at any AC/HSA ratio studied. Even at low ratios, where AC is bound only to site 1 the decay was fit to a sum of two exponentials (Figure 4.4), with the values for the lifetimes and pre-exponential factors the same for all ratios below 0.1. The average values for these two lifetimes were 4.0 ± 0.2 ns and 1.8 ± 0.1 ns, with pre-exponential factors of 0.24 ± 0.04 and 0.76 ± 0.04, respectively. This result is similar to the two lifetimes seen for AC bound to site 1 in BSA.[132] The dual lifetimes are an inherent characteristic of these systems, since the ratios of the pre-exponential factors for these

lifetimes do not change with the AC/HSA ratio at low AC/HSA ratios. The origin of the two lifetimes has not been explained, though they are likely due to different alignments of AC in the binding site.

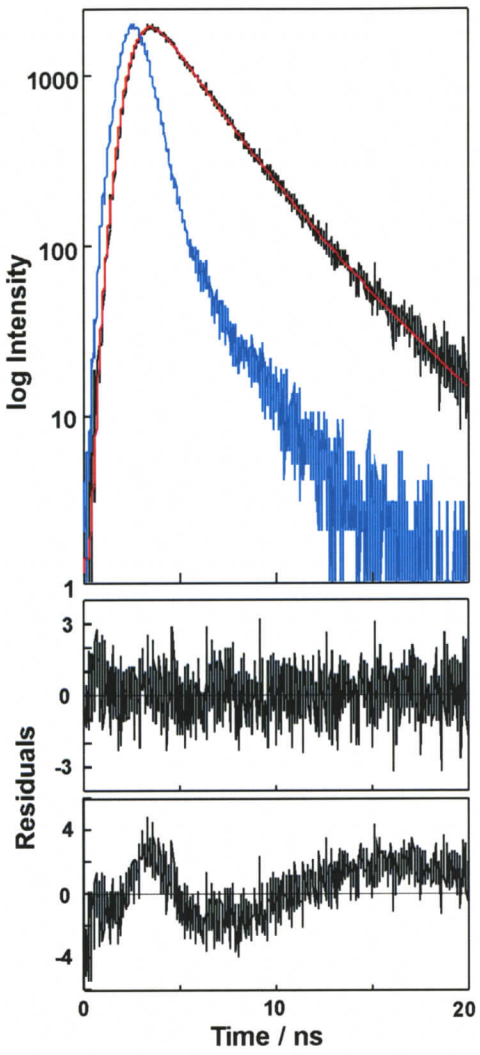


**Figure 4.4** Time-resolved fluorescence decay for an AC/HSA ratio of 0.1 (black), showing the IRF (blue), and fit to a sum of two exponentials (red). The residuals for the fit to a sum of two exponentials are shown in the middle panel, and the residuals for a mono-exponential fit are shown in the bottom panel. Reproduced with permission from the Journal of Physical Chemistry B, submitted for publication, unpublished work copyright 2009 American Chemical Society.

The variability between HSA lots was tested by measuring the lifetimes at an AC/HSA ratio of 0.1. Comparable results were obtained for all lots used, indicating that there is little variability between lots of HSA.

Fluorescence decays were obtained for various AC/HSA ratios (Table 4.2). Because some AC will be bound to site 1 at all AC/HSA ratios, two lifetimes were fixed to the values of 4.0 and 1.8 ns, and the fluorescence decays at higher AC/HSA ratios were adequately fit to the sum of three exponentials (Figure 4.5). The third component had a longer lifetime than the two components observed at low AC/HSA ratios. At an AC/HSA ratio of 1 a third longer component appeared with a lifetime of 13.9 ns with a very small pre-exponential factor. No further change was seen until AC/HSA ratios over 2 were reached, where an increase in the pre-exponential factor for the third component was seen, along with a lengthening of the long lifetime. While the pre-exponential factor for the long-lived component increased, the pre-exponential factor for the 1.8 ns component decreased, but the pre-exponential factor for the 4.0 ns component changed very little. If the only AC species contributing to the two short components is AC in site 1, then the ratio of the pre-exponential factors for the two short components ($A_1/A_2$) would not be expected to change. This is not the case, which indicates that there is another AC species with a lifetime close to 4 ns. However, it was not possible to resolve a fourth component when fitting these data.

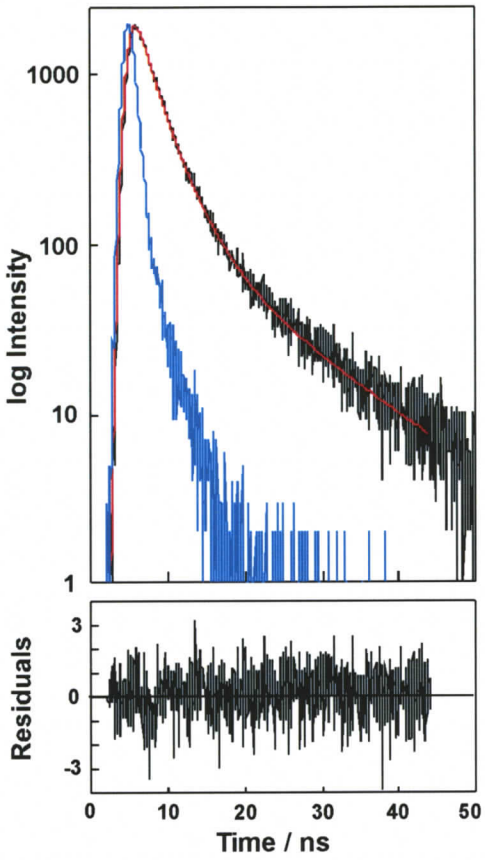


**Figure 4.5** Time-resolved fluorescence decay for an AC/HSA ratio of 2 (black), showing the IRF (blue), and fit to a sum of three exponentials (red). The residuals are shown in the bottom panel.

**Table 4.2** Fluorescence lifetimes of AC in the presence of HSA at various AC/HSA ratios ($\lambda_{ex}$ = 394 nm, $\lambda_{em}$ = 420 nm).

| AC/HSA | $\tau_1$ / ns [a] | $A_1$ | $\tau_2$ / ns [a] | $A_2$ | $\tau_3$ / ns | $A_3$ |
|---|---|---|---|---|---|---|
| 0.1 | 1.8 | 0.76 | 4.0 | 0.24 | - | - |
| 1 | 1.8 | 0.79 | 4.0 | 0.20 | 13.9 | 0.01 |
| 2 | 1.8 | 0.78 | 4.0 | 0.19 | 13.3 | 0.03 |
| 2.5 | 1.8 | 0.66 | 4.0 | 0.20 | 15.1 | 0.14 |
| 3 | 1.8 | 0.58 | 4.0 | 0.20 | 15.2 | 0.22 |
| 5 | 1.8 | 0.36 | 4.0 | 0.15 | 15.3 | 0.49 |
| 10 | 1.8 | 0.13 | 4.0 | 0.18 | 15.6 | 0.69 |
| 15 | 1.8 | 0.07 | 4.0 | 0.14 | 15.5 | 0.79 |
| 20 | 1.8 | 0.02 | 4 | 0.13 | 15.6 | 0.85 |

[a] fixed to values for low AC/HSA ratios

### 4.3.3 Relationship between fluorescence intensity and average lifetime

In order to compare changes in fluorescence intensities in the steady-state spectra to changes in the lifetimes, average lifetimes were calculated (Equation 4.1). The dependence of the fluorescence intensity and average lifetime on AC/HSA ratio are plotted in Figure 4.6. Overall, the shorter lifetimes for AC in the presence of HSA are consistent with the decreased intensity seen in the steady-state fluorescence spectra. The initial decrease seen in the fluorescence intensity with increasing AC/HSA ratio is not seen in the average lifetimes, consistent with static quenching of AC bound to site 2 in HSA. Aside from this, the changes in the average lifetimes and the integrated fluorescence intensities are similar.

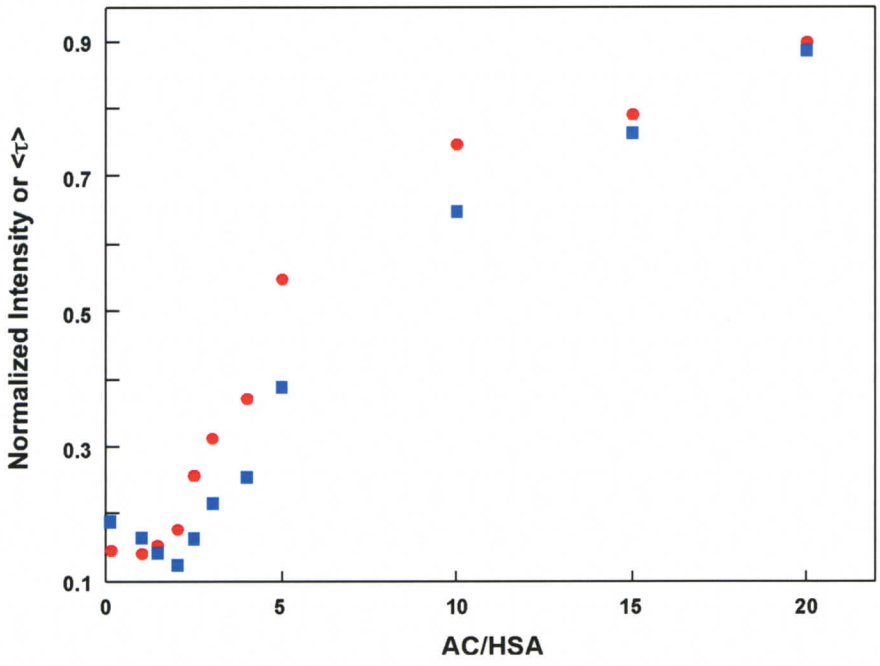


**Figure 4.6** Dependence of fluorescence emission intensity (square, blue) and average lifetime (circle, red) on AC/HSA ratio. Data are normalized to unity for AC in buffer (normalized point not shown). Reproduced with permission from the Journal of Physical Chemistry B, submitted for publication, unpublished work copyright 2009 American Chemical Society.

### 4.3.4 AC fluorescence quenching by nitromethane

Quenching experiments were preformed with nitromethane to determine how protected the various AC species bound to HSA were from the bulk solution. Steady-state quenching plots for quenching of AC by nitromethane in the presence of HSA showed that the quenching efficiency of AC by nitromethane was decreased as the AC/HSA ratio was decreased (Figure 4.7). A very low quenching efficiency was observed at the AC/HSA ratio of 0.1, indicating that AC is very well protected from nitromethane quenching when bound to site 1 of HSA. At low ratios the quenching plot was linear, but at ratios larger than 2 the quenching plot curved downward, suggesting that multiple AC species were present. At low quencher concentrations the species exposed to the bulk solution is efficiently quenched, while at higher quencher concentrations, all the exposed species have been quenched, and less efficient quenching of the more protected species occurs, resulting in the downward curvature in the quenching plot.

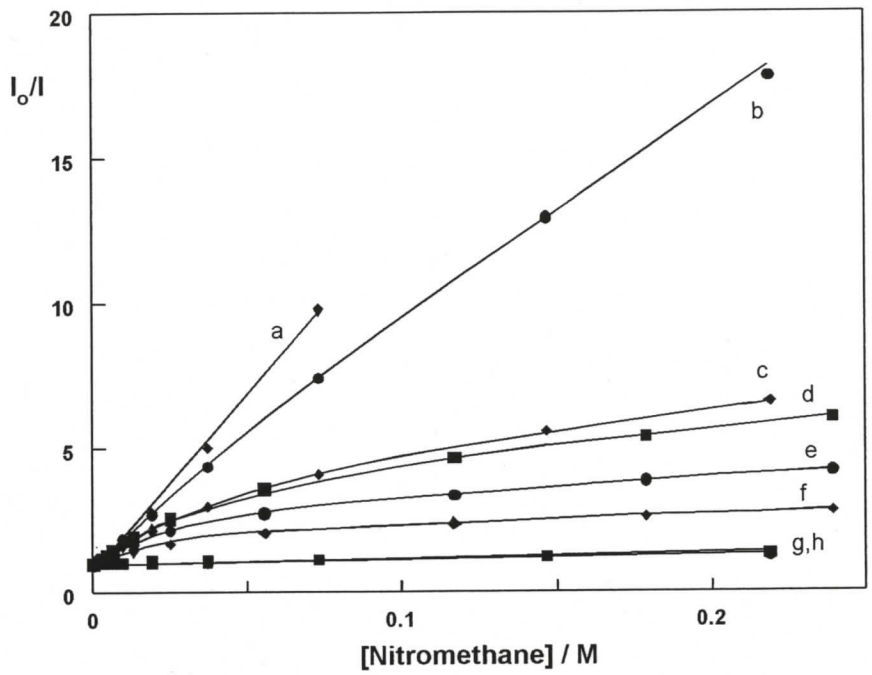


**Figure 4.7** Stern-Volmer plots for the quenching of AC by nitromethane in the absence (a)[a] and presence of HSA ((b)[a] AC/HSA = 10, (c)[a] AC/HSA = 5, (d) AC/HSA = 4, (e) AC/HSA = 3, (f) AC/HSA = 2.5, (g)[a] AC/HSA = 2 and (h)[a] AC/HSA = 0.1). Fits for AC/HSA = 0.1 and AC in buffer are linear, while all other data are fit to Equation 4.3.

[a] data obtained at University of Victoria by M. Nishijima of Osaka University

Fluorescence spectra are composites of the spectra of all species present, with a greater contribution from the species with longer lifetimes. The shape of the fluorescence spectra for AC/HSA ratios smaller than 2 did not change with increasing concentrations of nitromethane (Figure 4.8a), indicating all AC bound to HSA is exposed to the same environment. The spectra for intermediate AC/HSA ratios sharpened with addition of nitromethane, changing from that for AC exposed to water, to that for AC bound to protected sites in HSA as the quencher was increased (Figure 4.8b). This change in the shape of the spectra indicated that AC was located in more than one environment, and that AC in sites exposed to the bulk solution were preferentially quenched.

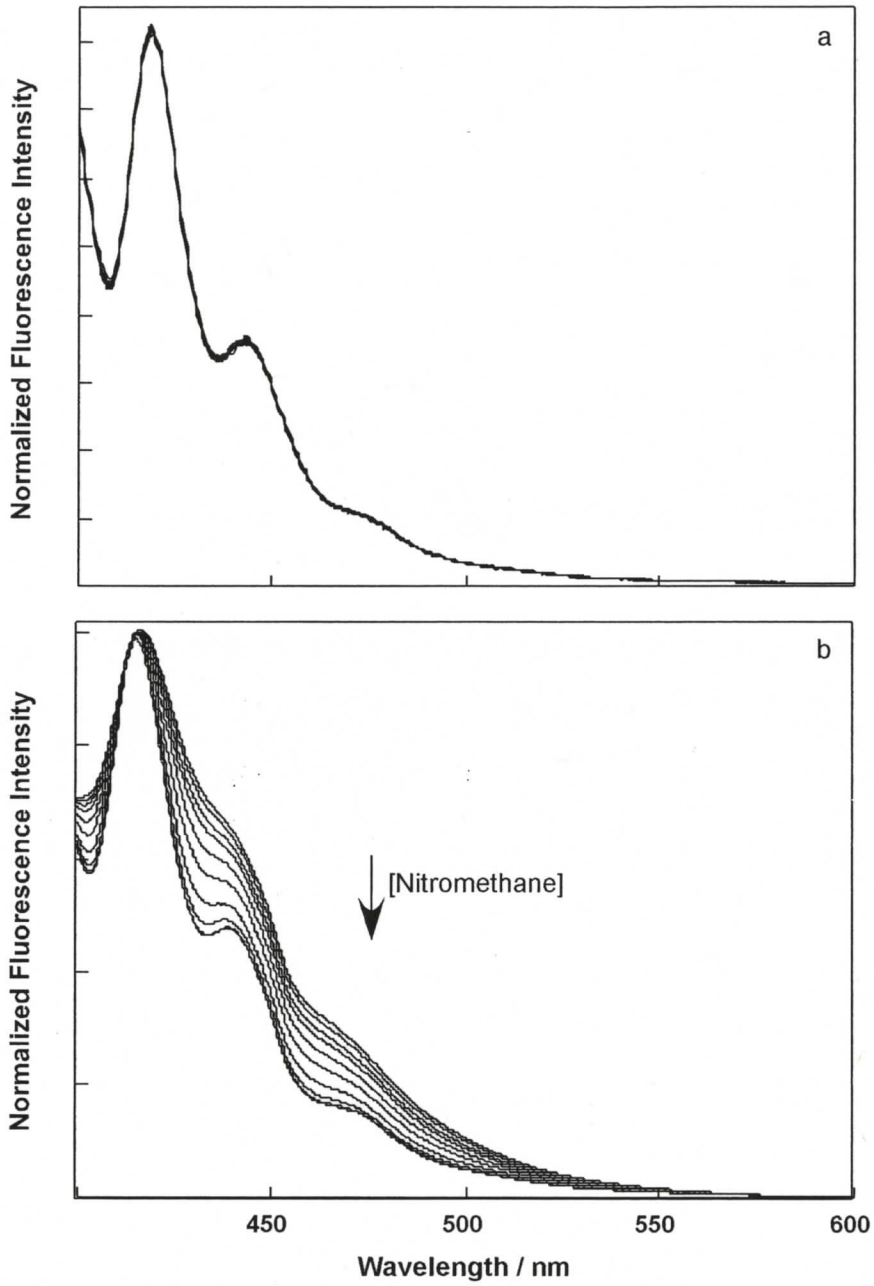


**Figure 4.8** (a)[a] Steady-state spectra for an AC/HSA ratio of 1 in the presence of increasing concentrations of nitromethane (normalized at 420 nm), (b) Steady-state spectra for an AC/HSA ratio of 3 in the presence of increasing concentrations of nitromethane (normalized at 420 nm).

[a] data obtained at University of Victoria by M. Nishijima of Osaka University

The quenching plots were fit to Equation 4.2,[142] where $K_{SV,i}$ is the Stern-Volmer constant of species $i$, and $F_i$ is the fraction of the integrated fluorescence spectrum corresponding to species $i$.

$$\frac{I_o}{I} = \frac{1}{\sum_1^i \frac{F_i}{1 + K_{SV,i}[Q]}} \qquad (4.2)$$

The quenching plots for AC in buffer, and at low AC/HSA ratios are linear, giving $K_{SV}$ values of 119 $M^{-1}$ and 1.2 $M^{-1}$, respectively (Table 4.3). The Stern-Volmer constant is the product of the quenching rate constant and the fluorescence lifetime ($K_{SV} = k_q \tau_o$), and indicates the accessibility of nitromethane to AC. Because the AC species have different lifetimes the relevant comparison should be that for the quenching rate constants. Using the lifetime of AC in buffer and the average lifetime of AC in site 1 in HSA, the quenching rate constants are respectively 7.5 x $10^9$ $M^{-1}$ $s^{-1}$ and < 4 x $10^8$ $M^{-1}$ $s^{-1}$ (see below).

The Stern-Volmer constants are shown in Table 4.3. Curved quenching plots were obtained for AC/HSA ratios above 2, and two components were recovered from the fits at these ratios. The Stern-Volmer constants were on the order of 1 $M^{-1}$ and 100 $M^{-1}$, with the contribution from the smaller $K_{SV}$ values decreasing as the AC/HSA ratio was increased. These two components are consistent with a well-protected species in binding site 1 of HSA, and an AC species exposed to the bulk solution. A number of different fits were tried for the curved quenching plots; the only successful fits had two components, and no further AC species could be resolved from this data.

**Table 4.3** Stern-Volmer constants for various AC/HSA ratios.

| AC/HSA | $K_{SV,1}$ / $M^{-1}$ | $F_1$ | $K_{SV,2}$ / $M^{-1}$ | $F_2$ |
|---|---|---|---|---|
| 0.1[a] | 1.2 ± 0.1 | 1 | - | - |
| 1[a] | 1.3 ± 0.1 | 1 | - | - |
| 2[a] | 1.3 ± 0.1 | 1 | - | - |
| 2.5 | 1.2 ± 0.2 | 0.43 ± 0.02 | 100 ± 14 | 0.56 ± 0.02 |
| 3 | 1.5 ± 0.1 | 0.28 ± 0.01 | 107 ± 5 | 0.71 ± 0.01 |
| 4 | 1.3 ± 0.2 | 0.18 ± 0.01 | 116 ± 7 | 0.85 ± 0.01 |
| 5 [a] | 1.4 ± 0.1 | 0.15 ± 0.02 | 95 ± 2 | 0.87 ± 0.01 |
| 20[a] | 118 ± 3 | 1 | - | - |
| buffer[a] | 119 ± 2 | 1 | - | - |

[a] data obtained at University of Victoria by M. Nishijima of Osaka University

Results from time-resolved quenching experiments were similar. At an AC/HSA ratio of 0.1 there was no change observed in the 1.8 ns and 4 ns lifetimes, even at the highest quencher concentration employed (239 mM). A small decrease in lifetimes might have been expected based on the $K_{SV,1}$ value determined from the steady-state experiments. This difference indicates that the quenching rate constant of AC in site 1, calculated from $K_{SV,1}$ is an upper limit. Since the site 1 lifetimes didn't change with quencher concentration, they could be fixed when fitting the quenching data at higher AC/HSA ratios.

The lifetimes for AC/HSA ratios of 2.5, 3 and 4 at various nitromethane concentrations are shown in Table 4.4. At the first quencher concentration (6.2 mM) the lifetime of the long-lived component decreases, and there is no change in the pre-exponential values. This decrease is consistent with what would be expected for AC in buffer ($k_q = 5.8 \times 10^9$ $M^{-1}$ $s^{-1}$, so for [Q] = 6.2 mM, $\tau_w$ = 10 ns; [Q] = 56 mM, $\tau_w$ = 2.6 ns). At the second quencher concentration the lifetime of the long-lived species has decreased to the point that it is combined with the 1.8 ns component of AC in site 1, supported by the changes in the pre-exponential factors. Unexpectedly there is still a small long-lived

component that was not quenched by nitromethane, which may indicate an additional AC species that is longer lived than AC in site 1, and protected from the bulk solution.

**Table 4.4** AC lifetimes at various AC/HSA ratios and various nitromethane concentrations.

| AC/HSA | $[CH_3NO_2]$ / mM | $\tau_1$ / ns [a] | $A_1$ | $\tau_2$ / ns [a] | $A_2$ | $\tau_3$ / ns | $A_3$ |
|---|---|---|---|---|---|---|---|
| 2.5 | 0 | 1.8 | 0.65 | 4.0 | 0.21 | 15.1 | 0.14 |
| 2.5 | 6.2 | 1.8 | 0.67 | 4.0 | 0.20 | 9.60 | 0.13 |
| 2.5 | 56 | 1.8 | 0.80 | 4.0 | 0.20 | 13.5 | 0.004 |
| 3 | 0 | 1.8 | 0.58 | 4.0 | 0.20 | 15.3 | 0.22 |
| 3 | 6.2 | 1.8 | 0.59 | 4.0 | 0.19 | 9.45 | 0.22 |
| 3 | 56 | 1.8 | 0.81 | 4.0 | 0.19 | 14.1 | 0.003 |
| 4 | 0 | 1.8 | 0.47 | 4.0 | 0.22 | 15.8 | 0.31 |
| 4 | 6.2 | 1.8 | 0.51 | 4.0 | 0.18 | 10.3 | 0.31 |
| 4 | 56 | 1.8 | 0.77 | 4.0 | 0.22 | 13.9 | 0.003 |

[a] fixed for values at low AC/HSA ratios

### 4.3.5 Quenching of AC by inhibitors

The quenching of AC by the site 1 and site 2 inhibitors, 4-iodobenzoate and warfarin, was examined. Experiments were carried out in 10 mM aqueous NaOH solution in order to solubilize the inhibitors. Both 4-iodobenzoate ($k_q = 2.8 \times 10^9$ $M^{-1}$ $s^{-1}$) and warfarin ($k_q = 2.5 \times 10^9$ $M^{-1}$ $s^{-1}$) are efficient quenchers of AC in bulk solution. This will be important to consider in the interpretation of data obtained in the presence of the inhibitors.

### 4.3.6 AC/HSA steady-state fluorescence in the presence of inhibitors

Steady-state spectra were obtained for AC/HSA ratios of 0.1, 1, 2 and 3 for various AC/inhibitor ratios. The steady-state spectra of AC/HSA in the presence of 4-iodobenzoate are consistent with binding of 4-iodobenzoate to site 1 in HSA (Figure 4.9).

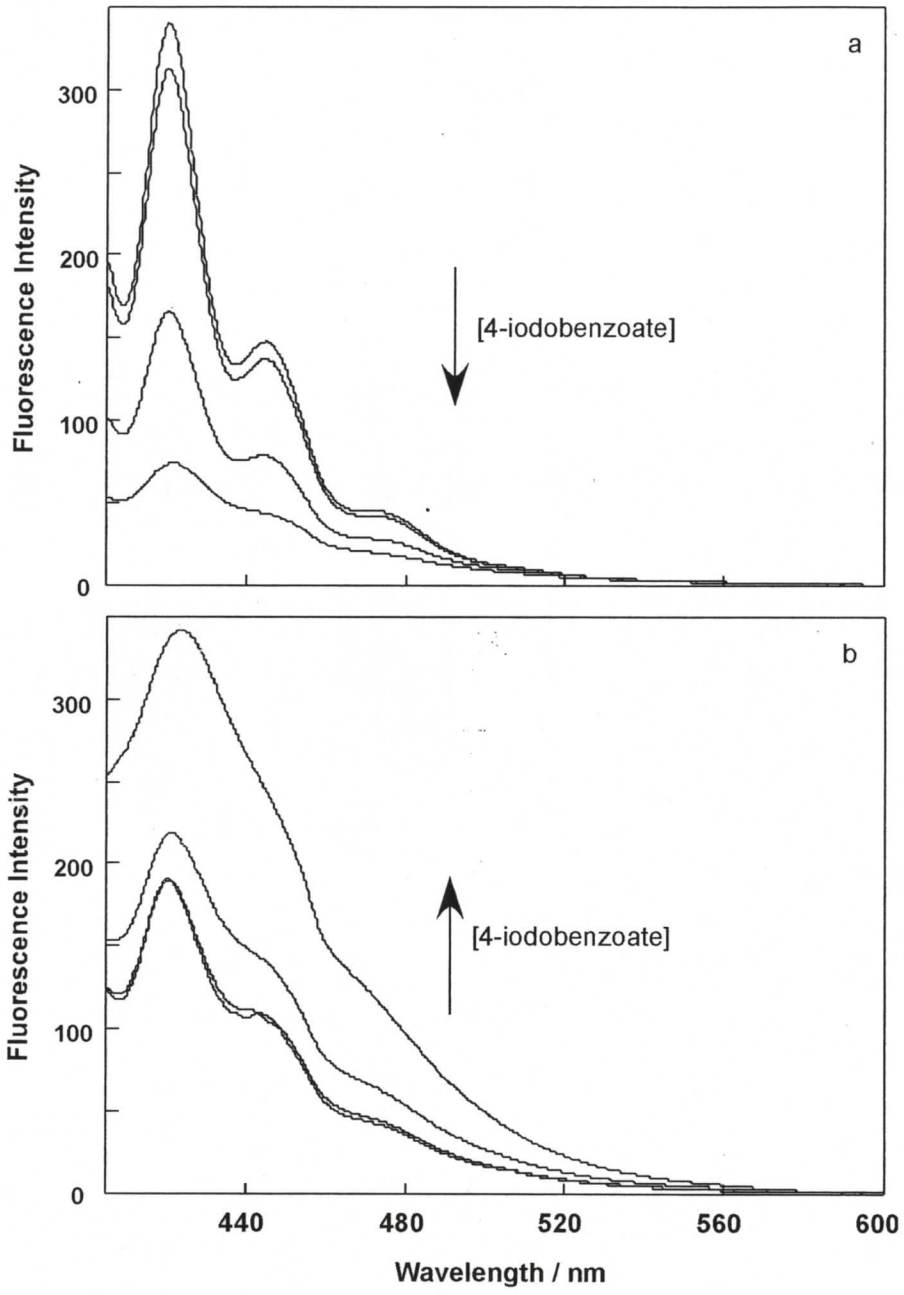


**Figure 4.9** Steady-state fluorescence spectra of (a) AC/HSA = 1 and (b) AC/HSA = 3 in the absence and presence of 3, 30 and 300 μM 4-iodobenzoate. Reproduced with permission from the Journal of Physical Chemistry B, submitted for publication, unpublished work copyright 2009 American Chemical Society.

At the AC/HSA ratio of 1 a decrease in the fluorescence intensity was seen on addition of 4-iodobenzoate (Figure 4.9a). At this ratio most AC is bound in site 1 and very little is bound to other sites. On addition of the inhibitor, AC is displaced from site 1 into the non-fluorescent site 2. At the higher AC/HSA ratio of 3, the fluorescence intensity increases, and the spectra broaden on addition of 4-iodobenzoate (Figure 4.9b). This is consistent with displacement of AC in site 1 to sites 3 – 5, as site 2 is already occupied at this ratio.

The steady-state fluorescence spectra of AC/HSA in the presence of warfarin are similarly consistent with the binding of warfarin to site 2 in HSA (Figure 4.10). At an AC/HSA ratio of 1 a small increase in intensity was seen on addition of warfarin (Figure 4.10a). Little change is expected at this ratio, since most AC is bound to site 1, but the small increase in intensity indicates that some AC is already bound to site 2 at this ratio. At the AC/HSA ratio of 3 the increase in intensity and broadening of the spectra are consistent with AC from site 2 displaced into sites 3-5 (Figure 4.10b).

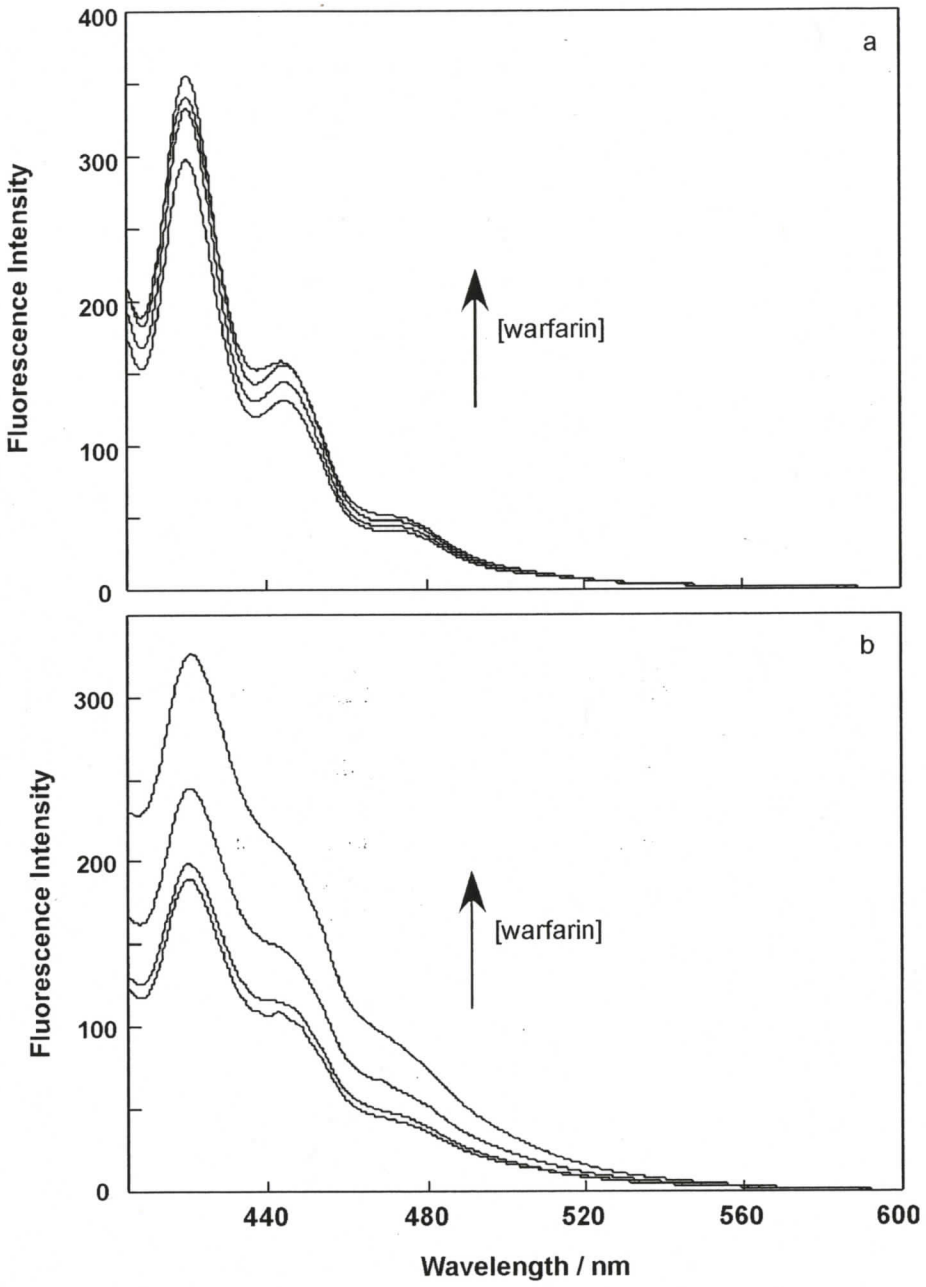


**Figure 4.10** Steady-state fluorescence spectra of (a) AC/HSA = 1 and (b) AC/HSA = 3 in the absence and presence 3, 30 and 300 μM of warfarin. Reproduced with permission from the Journal of Physical Chemistry B, submitted for publication, unpublished work copyright 2009 American Chemical Society.

### 4.3.7 AC/HSA time-resolved fluorescence in the presence of inhibitors

Fluorescence decays were obtained at AC/HSA ratios of 0.1, 1, 2 and 3 in the presence of various amounts of inhibitor. Similar behaviour was seen at all ratios and characteristic data is shown for an AC/HSA ratio of 3 in the presence of 4-iodobenzote (Table 4.5) and warfarin (Table 4.6).

**Table 4.5** Fluorescence lifetimes for an AC/HSA ratio of 3 in the presence of 4-iodobenzoate.

| [4-IB]/[AC] | $\tau_1$ / ns [a] | $A_1$ | $\tau_2$ / ns [a] | $A_2$ | $\tau_3$ / ns | $A_3$ |
|---|---|---|---|---|---|---|
| 0 | 1.8 | 0.64 | 4.0 | 0.27 | 15.9 | 0.094 |
| 0.1 | 1.8 | 0.62 | 4.0 | 0.27 | 15.7 | 0.11 |
| 1 | 1.8 | 0.49 | 4.0 | 0.27 | 15.4 | 0.25 |
| 3 | 1.8 | 0.28 | 4.0 | 0.32 | 14.9 | 0.41 |
| 6 | 1.8 | 0.14 | 4.0 | 0.30 | 15.0 | 0.56 |
| 10 | 1.8 | 0.084 | 4.0 | 0.27 | 15.2 | 0.65 |

[a] fixed for values at low AC/HSA ratios

**Table 4.6** Fluorescence lifetimes for an AC/HSA ratio of 3 in the presence of warfarin.

| [warfarin]/[AC] | $\tau_1$ / ns [a] | $A_1$ | $\tau_2$ / ns [a] | $A_2$ | $\tau_3$ / ns | $A_3$ |
|---|---|---|---|---|---|---|
| 0 | 1.8 | 0.64 | 4.0 | 0.27 | 15.9 | 0.094 |
| 0.1 | 1.8 | 0.64 | 4.0 | 0.27 | 15.9 | 0.094 |
| 1 | 1.8 | 0.51 | 4.0 | 0.33 | 15.6 | 0.16 |
| 10 | 1.8 | 0.36 | 4.0 | 0.40 | 15.4 | 0.24 |

[a] fixed for values at low AC/HSA ratios

As the amount of inhibitor was increased the contribution from the long-lived component was increased. The relative increase was higher in the case of 4-iodobenzoate, because AC was displaced from the fluorescent site 1, while in the case of warfarin, the amount of AC in site 1 is not changed, and the increase was due to AC displaced from the non-fluorescent site 2. At high inhibitor/AC ratios the ratio between

pre-exponential factors for AC in site 1 ($A_1$ and $A_2$) is changed. This is indicative of a fourth component with a lifetime close to 4 ns (see discussion below).

Fluorescence experiments were also performed in the presence of both inhibitors simultaneously. Similar trends were seen, but no additional information was obtained with both inhibitors present in solution.

### 4.3.8 AC/HSA fluorescence quenching by nitromethane in the presence of 4-iodobenzoate

Time-resolved quenching experiments were carried out for AC/HSA ratios of 1 and 3 in the presence of 10 equivalents of 4-iodobenzoate (Table 4.7 and Table 4.8). At a nitromethane concentration of 56 mM the lifetime of AC in water should be 2.6 ns. On addition of quencher the pre-exponential factor for the long-lived component decreased, indicating that some of the long-lived component is exposed to the bulk solution and quenched, but the presence of the 10 ns component at this nitromethane concentration suggests the presence of another AC species that is not quenched as efficiently as AC in water.

**Table 4.7** Fluorescence lifetimes for an AC/HSA ratio of 1 in the presence of 300 μM (10 equivalents) of 4-iodoenzoate.

| $[CH_3NO_2]$ / mM | $\tau_1$ / ns [a] | $A_1$ | $\tau_2$ / ns [a] | $A_2$ | $\tau_3$ / ns | $A_3$ |
|---|---|---|---|---|---|---|
| 0 | 1.8 | 0.26 | 4.0 | 0.37 | 12.27 | 0.37 |
| 55.7 | 1.8 | 0.32 | 4.0 | 0.47 | 9.91 | 0.21 |
| 92.8 | 1.8 | 0.39 | 4.0 | 0.41 | 9.43 | 0.20 |

[a] fixed for values at low AC/HSA ratios

**Table 4.8** Fluorescence lifetimes for an AC/HSA ratio of 3 in the presence of 300 μM (10 equivalents) of 4-iodoenzoate.

| $[CH_3NO_2]$ / mM | $\tau_1$ / ns [a] | $A_1$ | $\tau_2$ / ns [a] | $A_2$ | $\tau_3$ / ns | $A_3$ |
|---|---|---|---|---|---|---|
| 0 | 1.8 | 0.015 | 4.0 | 0.30 | 14.9 | 0.69 |
| 55.7 | 1.8 | 0.62 | 4.0 | 0.30 | 8.57 | 0.084 |
| 92.8 | 1.8 | 0.76 | 4.0 | 0.11 | 7.24 | 0.13 |

[a] fixed for values at low AC/HSA ratios

### 4.3.9 Fitting of fluorescence decays with FAST software

All the fluorescence decays were adequately fit to a sum of two or three exponentials, even though there was some indication of an additional AC species. This is not surprising as all the lifetimes are of similar magnitudes. Because of the evidence of another component, and because, for the lifetime experiments at high inhibitor concentrations, a fourth component could be resolved using the Edinburgh software (Table 4.9), further fitting of the data in the presence of inhibitors was carried out using the Edinburgh FAST software. This software allows the pre-exponential factors, $A_i$, which are related to the populations of each species, $i$, with lifetime $\tau_i$, to be fixed. Experiments at low AC/HSA ratios led us to believe that the relative populations of the 1.8 and 4.0 ns species should not change. By fixing the $A_1/A_2$ ratio we can attribute the correct populations to the short-lived species, and as a consequence should have a better chance of resolving the new component from the 4 ns component.

**Table 4.9** Fluorescence lifetimes of AC/HSA in the presence of 10 equivalents of 4-iodobenzoate (4 component fit in Edinburgh software).

| AC/HSA | $\tau_1$ / ns [a] | $A_1$ | $\tau_2$ / ns [a] | $A_2$ | $\tau_3$ / ns | $A_3$ | $\tau_4$ / ns | $A_4$ |
|---|---|---|---|---|---|---|---|---|
| 1 | 1.8 | 0.31 | 4.0 | 0.23 | 7.69 | 0.28 | 14.9 | 0.18 |
| 3 | 1.8 | 0.17 | 4.0 | 0.063 | 6.06 | 0.18 | 15.6 | 0.59 |

[a] fixed for values at low AC/HSA ratios

The fits were carried out with fixed pre-exponential factors by using the pre-exponential value obtained for the 1.8 ns component in the three component fit, and fixing the pre-exponential factor for the 4 ns component to what would be expected based on the ratio of these factors at low AC/HSA ratios ($A_1 = 0.76 \pm 0.04$, $A_2 = 0.24 \pm 0.04$; $A_1/A_2 = 3.2$). The first two lifetimes were fixed to those for AC in site 1 (1.8 ns and 4 ns), and the longest lifetime was fixed to that for AC in buffer (15.8 ns) (Figure 4.11). The lifetimes and pre-exponential factors recovered from these fits in the presence of 4-iodobenzoate at AC/HSA ratios of 0.1, 1, 2 and 3 are shown in Tables 4.10 – 4.13.

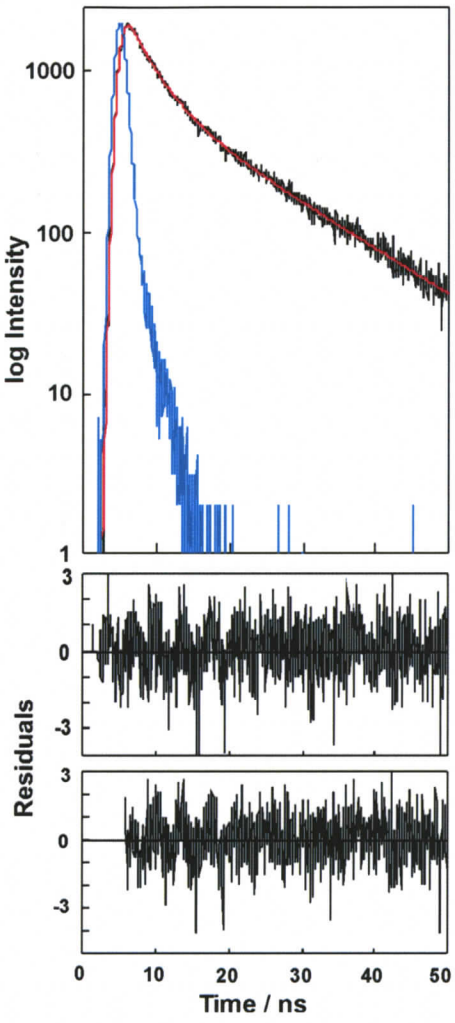


**Figure 4.11** Time-resolved fluorescence decay for an AC/HSA ratio of 3 fit to a sum of three exponentials using the Edinburgh software. The middle panel shows the residuals from the three exponential fit, and the lower panel shows the residuals of a fit to a sum of four exponentials, fixing the $A_1/A_2$ ratio using the FAST software.

**Table 4.10** Fluorescence lifetimes of an AC/HSA ratio of 0.1 in the presence of 4-iodobenzoate (fit with FAST software).

| [4-IB]/ [AC] | $\tau_1$ / ns [a] | $A_1$ [c] | $\tau_2$ / ns [a] | $A_2$ [c] | $\tau_3$ / ns | $A_3$ | $\tau_4$ / ns [b] | $A_4$ |
|---|---|---|---|---|---|---|---|---|
| 0 (1)[d] | 1.8 | 0.79 | 4.0 | 0.21 | - | - | - | - |
| 1 (1) | 1.8 | 0.79 | 4.0 | 0.21 | - | - | - | - |
| 10 (1) | 1.8 | 0.74 | 4.0 | 0.25 | - | - | 15.8 | 0.01 |
| 50 (1) | 1.8 | 0.36 | 4.0 | 0.12 | 6.8 | 0.36 | 15.8 | 0.15 |

[a] fixed to values at low AC/HSA ratios
[b] fixed to value in buffer
[c] $A_1/A_2$ ratio fixed to value at low AC/HSA ratios
[d] values in parentheses corresponds to the number of independent experiments

**Table 4.11** Fluorescence lifetimes of an AC/HSA ratio of 1 in the presence of 4-iodobenzoate (fit with FAST software).

| [4-IB]/ [AC] | $\tau_1$ / ns [a] | $A_1$ [c] | $\tau_2$ / ns [a] | $A_2$ [c] | $\tau_3$ / ns | $A_3$ | $\tau_4$ / ns | $A_4$ |
|---|---|---|---|---|---|---|---|---|
| 0 (2)[d] | 1.8 | 0.75 | 4.0 | 0.24 | - | - | 13.6 | 0.001 |
| 1 (2) | 1.8 | 0.73 | 4.0 | 0.24 | 7.7 | 0.014 | 15.8[b] | 0.02 |
| 2 (1) | 1.8 | 0.59 | 4.0 | 0.20 | 5.1 | 0.11 | 15.8[b] | 0.09 |
| 10 (6) | 1.8 | 0.23 | 4.0 | 0.08 | 6.1 | 0.46 | 15.8[b] | 0.23 |

[a] fixed to values at low AC/HSA ratios
[b] fixed to value in buffer
[c] $A_1/A_2$ ratio fixed to value at low AC/HSA ratios
[d] values in parentheses corresponds to the number of independent experiments

**Table 4.12** Fluorescence lifetimes of an AC/HSA ratio of 2 in the presence of 4-iodobenzoate (fit with FAST software).

| [4-IB]/ [AC] | $\tau_1$ / ns [a] | $A_1$ [c] | $\tau_2$ / ns [a] | $A_2$ [c] | $\tau_3$ / ns | $A_3$ | $\tau_4$ / ns | $A_4$ |
|---|---|---|---|---|---|---|---|---|
| 0 (1)[d] | 1.8 | 0.74 | 4.0 | 0.24 | - | - | 14.0 | 0.02 |
| 1 (1) | 1.8 | 0.50 | 4.0 | 0.17 | 3.7 | 0.25 | 15.8[b] | 0.08 |
| 10 (1) | 1.8 | 0.19 | 4.0 | 0.07 | 5.5 | 0.37 | 15.8[b] | 0.37 |

[a] fixed to values at low AC/HSA ratios
[b] fixed to value in buffer
[c] $A_1/A_2$ ratio fixed to value at low AC/HSA ratios
[d] values in parentheses corresponds to the number of independent experiments

**Table 4.13** Fluorescence lifetimes of an AC/HSA ratio of 3 in the presence of 4-iodobenzoate (fit with FAST software).

| [4-IB]/ [AC] | $\tau_1$ / ns [a] | $A_1$ [c] | $\tau_2$ / ns [a] | $A_2$ [c] | $\tau_3$ / ns | $A_3$ | $\tau_4$ / ns [b] | $A_4$ |
|---|---|---|---|---|---|---|---|---|
| 0 (1) [d] | 1.8 | 0.67 | 4.0 | 0.22 | 7.1 | 0.02 | 15.8 | 0.09 |
| 0.1 (1) | 1.8 | 0.64 | 4.0 | 0.22 | 7.1 | 0.04 | 15.8 | 0.09 |
| 1 (1) | 1.8 | 0.55 | 4.0 | 0.19 | 8.5 | 0.05 | 15.8 | 0.21 |
| 3 (1) | 1.8 | 0.41 | 4.0 | 0.13 | 7.5 | 0.13 | 15.8 | 0.34 |
| 6 (1) | 1.8 | 0.23 | 4.0 | 0.07 | 5.6 | 0.20 | 15.8 | 0.50 |
| 10 (2) | 1.8 | 0.14 | 4.0 | 0.05 | 5.7 | 0.25 | 15.8 | 0.57 |

[a] fixed to values at low AC/HSA ratios
[b] fixed to value in buffer
[c] $A_1/A_2$ ratio fixed to value at low AC/HSA ratios
[d] values in parentheses corresponds to the number of independent experiments

A 6 – 8 ns component is present in all four component fits, and the data show good reproducibility. The pre-exponential factor of this component, and the 15.8 ns component increased as the amount of inhibitor was increased, and the amount of AC in site 1 was decreased. Similar fits for data in the presence of warfarin at AC/HSA ratios greater than 2, and in the presence of both inhibitors simultaneously at all ratios, resulted in a similar 6 – 8 ns component. Additionally in the absence of any inhibitors the data for an AC/HSA ratio of 5 showed a similar 6 ns component (Table 4.14). This was the only AC/HSA ratio in the absence of inhibitors for which a fourth component could be resolved.

**Table 4.14** Fluorescence lifetimes of an AC/HSA ratio of 5 in the absence of inhibitors (fit with FAST software).

| $\tau_1$ / ns [a] | $A_1$ [c] | $\tau_2$ / ns [a] | $A_2$ [c] | $\tau_3$ / ns | $A_3$ | $\tau_4$ / ns [b] | $A_4$ |
|---|---|---|---|---|---|---|---|
| 1.8 | 0.29 | 4.0 | 0.087 | 6.1 | 0.13 | 15.8 | 0.49 |

[a]fixed to values at low AC/HSA ratios
[b]fixed to value in buffer
[c]$A_1/A_2$ ratio fixed to value at low AC/HSA ratios

### 4.3.10 Product Studies

Preliminary product studies for the AC photodimerization reaction were carried out in the presence of inhibitors to determine the feasibility of photoreaction experiments in the presence of inhibitors.

#### 4.3.10.1 Photodimerization of AC in the presence of inhibitors

The AC photoreaction was carried out in the presence of the inhibitors, 4-iodobenzoate and warfarin, in aqueous solution in the absence of HSA. The presence of

inhibitors had no observable effect on the product distribution, or the ee's obtained from HPLC analyses (Table 4.15). Both were, within error, the same as for the AC photoreaction in bulk solution in the absence of inhibitors, and no new peaks were observed in the HPLC trace (Figure 4.12). These results suggest that the inhibitors do not react with AC, and have no effect on the dimerization reaction.

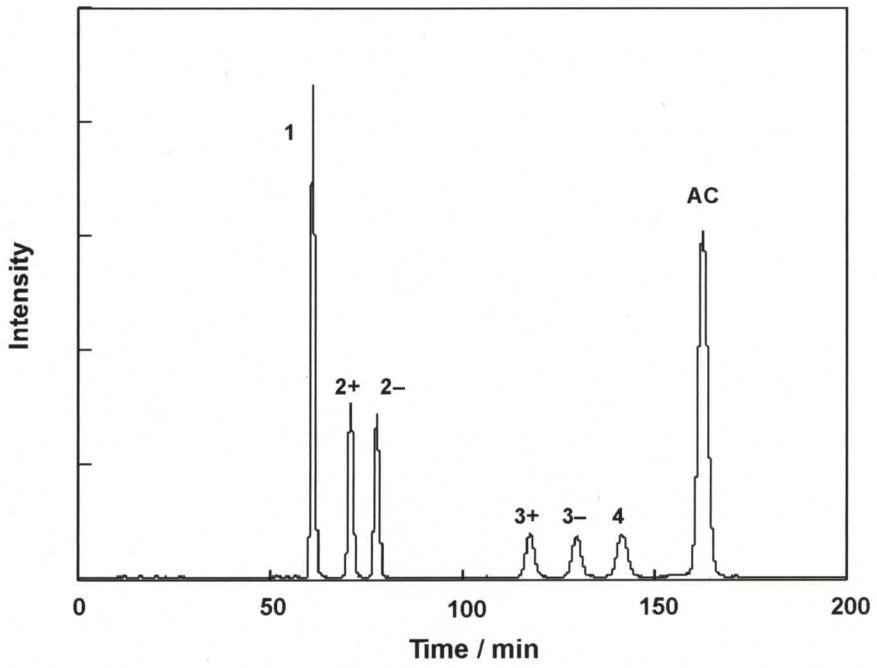


**Figure 4.12** Typical HPLC chromatogram obtained using the fluorescence detector for analysis of the AC photodimerization reaction ([AC] = 0.6 mM, [4-IB] = 0.6 mM). The assignment of **2+/2–** and **3+/3–** is not absolute and is based on the order in which the enantiomers are eluted.

**Table 4.15** Product distribution and ee for the photodimerization reaction of AC in aqueous solution in the presence of inhibitors.[a]

| Inhibitor | Conversion / % | Product Distribution / % | | | | ee / % | |
|---|---|---|---|---|---|---|---|
| | | **1** | **2** | **3** | **4** | **2** | **3** |
| 0.6 mM 4-iodobenzoate | 80 | 41 | 36 | 14 | 9 | 0.2 | -3 |
| 0.6 mM warfarin | 77 | 42 | 36 | 14 | 8 | 0.8 | 3 |
| None[b] | 88 | 43 | 36 | 14 | 7 | 0 | 0 |

[a] Irradiated at $\lambda > 320$ nm for 1 hr under Ar; [AC] = 0.6 mM, errors for product distribution ± 1 %, errors for ee ± 2 %

[b] data from reference 134

**4.3.10.2 Photodimerization of AC in the presence of HSA and inhibitors**

Photoreaction was carried out at an AC/HSA ratio of 1 in the presence of the inhibitors (Table 4.16). The presence of a third long-lived component in the photophysical data indicates that for AC/HSA = 1 in the presence of 4-iodobenzoate some AC is located in sites other than site 1 or site 2. The product distribution and ee obtained for AC/HSA = 1 in the presence of 1 equivalent of 4-iodobenzoate was not significantly different than the data obtained previously for AC/HSA = 3 in the absence of inhibitors. This may indicate that binding of 4-iodobenzoate to site 1 does not affect the reactivity at other sites. However, at higher equivalents of 4-IB (4-IB/AC = 5), a small decrease in the ee's obtained was observed.

Reaction was also carried out for AC/HSA = 1 in the presence of 4 equivalents of warfarin. Photophysical data indicates that there is very little AC located outside sites 1 or 2 under these conditions. The product distribution obtained was not significantly different than that obtained previously at AC/HSA = 3 in the absence of inhibitors, but the ee's obtained were somewhat lower.

**Table 4.16** Product distribution and ee for the photodimerization reaction of AC in the presence of HSA and inhibitors.[a]

| | Conversion / % | Product Distribution / % | | | | ee / % | |
|---|---|---|---|---|---|---|---|
| | | **1** | **2** | **3** | **4** | **2** | **3** |
| AC/HSA = 1 + 1 eq. 4-IB | 5 | 39 | 41 | 13 | 7 | 77 | 89 |
| AC/HSA = 1 + 5 eq. 4-IB | 8 | 42 | 41 | 11 | 7 | 70 | 71 |
| AC/HSA = 1 + 4 eq. warfarin | - | 44 | 42 | 10 | 5 | 68 | 65 |
| AC/HSA = 1 [b] | < 5 | - | - | - | - | - | - |
| AC/HSA = 3 [b] | 20 | 42 | 42 | 11 | 6 | 79 | 88 |

[a] Irradiated at $\lambda > 320$ nm for 1 hr under Ar; [AC] = 0.6 mM, errors for product distribution ± 1 %, errors for ee ± 2 %

[b] data from reference 134

**4.4 Discussion**

The fluorescence spectrum of AC bound to site 1 showed vibrational structure similar to that observed for protonated AC in nonpolar solvents. This result indicates that AC experiences a nonpolar environment in site 1 and could possibly be hydrogen bonded to an amino acid residue. AC in site 1 of HSA was shown to be well protected from the bulk solution and exhibited two lifetimes of 1.8 and 4.0 ns, similar to what was seen previously for AC bound to site 1 in BSA.[132]

Between the AC/HSA ratios of 1 and 2 the steady-state fluorescence intensity decreases, but the average lifetime is not shortened. This is indicative of static quenching of AC located in HSA binding site 2. This is likely due to a tryptophan residue located in the binding site, and as a result AC in site 2 is silent in fluorescence experiments. The comparison of steady-state intensities and average lifetimes at different AC/HSA ratios (Figure 4.6) showed the different behaviour of these two parameters at low ratios, and the subsequent lower fluorescence intensity seen at all AC/HSA ratios above 1. The difference between the fluorescence intensity and average lifetime does not increase as the AC/HSA ratio increases, indicating that the quenching of AC in site 2 is the only static process occurring, and the dimerization of AC in HSA is a dynamic process, similar to that seen in BSA.

At AC/HSA ratios greater than 2 the steady-state fluorescence plots for quenching by nitromethane were curved downward indicating the presence of multiple AC species, and time-resolved fluorescence experiments also exhibited multiple lifetimes. Experiments were focused on AC/HSA ratios between 2 and 5, as differentiation of AC bound to site 3 should be easiest at these ratios. The quenching data was consistent with two AC species: AC in site 1, and AC bound to HSA but fairly exposed to water. The

ratio of pre-exponential factors for the lifetimes of AC in site 1 ($A_1/A_2$) did not stay constant as the AC/HSA ratio increased, indicating the presence of an additional AC species with a lifetime close to 4 ns. Additionally, time-resolved nitromethane quenching experiments showed some suggestion of an AC species, with a lifetime longer than that for AC in site 1, that was well protected from quencher. However, no real distinction could be made between AC in sites 3, 4 or 5, or AC in bulk solution.

Since product studies showed little conversion at AC/HSA ratios below 2, AC in sites 1 and 2 are not involved in product formation, and therefore do not contribute to the ee. The sites in which chirogenesis manifests itself for the AC/HSA system (sites 3, 4 or 5) all appeared to be fairly exposed to the bulk solution in the initial fluorescence experiments. These sites are therefore much more similar than those in BSA, where differentiation between sites 2 and sites 3 + 4 was possible. In BSA the highest ee was observed for the moderate binding sites, and the same is likely true for HSA. The introduction of site 1 and site 2 inhibitors, 4-iodobenzoate and warfarin, was carried out in the hope that suppressing AC binding to these sites would augment any differences that may exist between sites 3, 4 and 5.

Fluorescence for AC/HSA in the presence of 4-iodobenzoate and warfarin confirmed the binding of these inhibitors to sites 1 and 2, respectively (Figures 4.9 and 4.10). Even at 10 equivalents of 4-iodobenzoate there is still some AC bound to site 1. This is not unexpected, as the binding affinity of AC for site 1 ($3.0 \times 10^8$ $M^{-1}$)[134] is greater than that for 4-iodobenzoate ($1.8 \times 10^6$ $M^{-1}$).[140] As AC in site 2 is silent in fluorescence experiments it is more difficult to establish how much AC is displaced by warfarin. The moderate increases seen in the fluorescence intensity on addition of warfarin suggest that

not all AC is displaced from site 2. This implies that the binding constant for AC in site 2 is of the same magnitude as, or larger than, that for warfarin ($3.3 \times 10^5$ $M^{-1}$).[38]

More compelling evidence for an additional AC species was obtained from time-resolved fluorescence experiments in the presence of 4-iodobenzoate. Though evidence of an additional AC species is present in the data with either inhibitor, the data in the presence of 4-iodobenzoate is stronger. This is not unexpected, as inhibition of AC binding to site 1 decreases the relative amount of fluorescence emission from site 1, thus enhancing the emission from other sites. Binding of warfarin displaces AC from a site that is silent in fluorescence experiments, and thus should effectively result in behaviour similar to that of a higher AC/HSA ratio in the absence of inhibitors.

As the amount of 4-iodobenzoate added to AC/HSA solutions was increased the $A_1/A_2$ ratio in the three exponential fit changed. At an AC/HSA ratio of 3 (Table 4.5) the pre-exponential factor for the 1.8 ns component decreased, while the pre-exponential factor for the 4.0 ns component changed very little. There are two possibilities that could explain this trend. Either AC is displaced from site 1 into a site that has a lifetime similar to 4 ns, or 4-iodobenzoate preferentially displaces AC from one of the site 1 'sub-sites'. Because a similar trend in pre-exponential factors was seen with increasing AC/HSA ratios in the absence of inhibitors, and in the presence of increasing amounts of the site 2 inhibitor, warfarin, the first explanation is more probable. No decrease was seen for the lifetime of the long component as the amount of inhibitor was increased. Even though the inhibitors are efficient quenchers of AC in bulk solution, this is not an issue under the experimental conditions in the presence of HSA. At the highest concentration of inhibitor used (300 μM) a 15.8 ns lifetime would be expected to decrease < 3% if all the

inhibitor was available as quencher in the bulk solution. Further, the lack of quenching of the long-lived component indicates that excess inhibitor is not binding to HSA in close proximity to AC.

Nitromethane quenching experiments for AC/HSA in the presence of 10 equivalents of 4-iodobenzoate revealed the presence of an 8 – 9 ns component that was not efficiently quenched by nitromethane. This experiment showed both the presence of an additional AC species with an intermediate lifetime, and that this species is well protected from the bulk solution.

On the basis of the evidence for an additional component in the fluorescence decays for AC/HSA in the presence of inhibitors, the decays were fit to a sum of four exponentials, while fixing the lifetimes for AC in site 1 and in bulk solution, and fixing the ratio of pre-exponentials factors for site 1 to the value expected from experiments at low AC/HSA ratios. A fourth component with a lifetime of 6 – 8 ns was consistently seen at all AC/HSA ratio studied in the presence of 4-iodobenzoate, at ratios greater than 2 in the presence of warfarin, and at an AC/HSA ratio of 5 in the absence of inhibitors. The pre-exponential factor for this component increased as the amount of inhibitor in solution increased. The longer lived component, corresponding to AC exposed to the bulk solution, is always present when the 6 – 8 ns component is present. However, at the lower AC/HSA ratios studied there is relatively less of the long-lived component compared to the 6 – 8 ns component, while at the higher AC/HSA ratios there is more of the long-lived component. This implies that the 6 – 8 ns component corresponds to AC bound to site 3 in HSA. The fact that the pre-exponential factors for both this component and the long-lived component increase as inhibitor is added indicates that the binding

affinity for AC in site 3 may not be much greater than that for the binding of AC to the more exposed sites 4 and 5.

There is evidence that guest binding to one binding site in HSA can result in conformational changes in the protein that can affect binding to other sites.[143,144] The trends seen in the absence or presence of inhibitors were quite similar, and four component fits of the fluorescence decay data in the presence of either inhibitor, or in the absence of inhibitor at an AC/HSA ratio of 5 all resolved a similar 6 – 8 ns AC species. This indicates that, though there may be effects from binding of 4-iodobenzoate and warfarin to sites 1 and 2, the effects are not significantly different from binding of AC to these same sites.

Product studies on the AC photoreaction in bulk solution in the presence of inhibitors showed that the inhibitors do not react directly with AC. The dimerization reaction of AC bound to HSA also seemed to be affected very little by the presence of inhibitors. These control experiments show promise that product studies could be carried out under conditions where AC in site 3 is the prominent fluorescent species, in order to isolate products formed by reaction in this site.

**4.5 Conclusions**

The AC dimerization reaction in HSA is a dynamic reaction with products resulting from reaction in sites 3, 4 and 5. These sites are much more difficult to differentiate in photophysical experiments than the AC binding sites in BSA. Differentiation of AC in site 3 of HSA was made possible through the use of site 1 and/or site 2 inhibitors, and quenching experiments with nitromethane. AC in site 3 is very

protected from the bulk solution, and has a lifetime of 6 – 8 ns, which is shorter than that of AC exposed to bulk solution in sites 4 and 5. The high ee's observed at low AC/HSA ratios likely result from reaction of this newly discriminated AC species in site 3. The moderately high ee's observed even at high AC/HSA ratios are more a chance result due to preferential production of the same enantiomer in all sites and limited AC free in bulk solution.

# 5. SUMMARY

Though there is some previous knowledge of binding dynamics of certain small molecules with DNA, focus has been on dynamic processes on millisecond to second timescales. There also has been little in the way of systematic studies to reveal the structural feature relevant to modulation of association and dissociation rate constants for the binding of small molecules to DNA.

Laser flash photolysis experiments with the aminoxanthones showed that the reactivity of guest molecules towards DNA can be reduced through appropriate substitution. However, this strategy also led to a decrease in triplet excited state energies. This made determination of association and dissociation rate constants using the laser flash photolysis quenching methodology impossible, though dynamics occurring on microsecond timescales were revealed, showing that experimental techniques that span a wide dynamic range are needed to study dynamics in small molecule – DNA systems.

Our laser temperature jump system was shown to have the ability to measure dynamics on timescales from hundreds of nanoseconds to seconds. Detection of signals by either fluorescence or absorption has been realized, though improvement of the signal quality is still needed. Systematic studies on how structure affects the binding dynamics will only be possible when implementation of this technique is completed.

Proteins have the ability to act as host molecules for photochirogenic reactions, but previous studies had only looked at the effect on unimolecular reactions. The AC dimerization reaction in the presence of human serum albumin produced products in high enantiomeric excesses. A combination of photophysical studies and product studies on

this bimolecular reaction in the presence of serum albumin proteins revealed that it is a dynamic reaction and both the strength of binding and mobility of reactants are important. Fluorescence studies on AC in the presence of HSA were able to successfully differentiate between AC bound to different binding sites in the protein, which will allow determination of which bound species is responsible for the high ee's. The experimental strategies employed were effective in uncovering mechanistic details in this system, and should be applicable to other systems.

# 6. REFERENCES

(1) Lehn, J.-M. *Angew. Chem. Int. Ed. Engl.* **1988**, *27*, 89-112.

(2) Bohne, C. *Langmuir* **2006**, *22*, 9100-9111.

(3) Kleinman, M. H.; Bohne, C. In *Molecular and Supramolecular Photochemistry*; Ramamurthy, V., Schanze, K. S., Eds.; Marcel Dekker Inc.: New York, 1997; Vol. 1, p 391-466.

(4) Liao, Y.; Frank, J.; Holzwarth, J. F.; Bohne, C. *J. Chem. Soc., Chem. Commun.* **1995**, 199-200.

(5) Crooks, J. E. *J. Phys. E: Sci. Instrum.* **1983**, *16*, 1142-1147.

(6) Marcandalli, B.; Winzek, C.; Holzwarth, J. F. *Ber. Bunsen Ges. Phys. Chem.* **1984**, *88*, 368-374.

(7) Monaco, R. R.; Gardiner, W. C. *Biochem. Biophys. Res. Commun.* **1993**, *196*, 975-983.

(8) Strehlow, H. *Rapid Reactions in Solution*; VCH: Weinheim, 1992.

(9) Porschke, D. *Ber. Bunsen Ges. Phys. Chem.* **1996**, *100*, 715-720.

(10) Callender, R.; Dyer, R. B. *Curr. Opin. Struct. Biol.* **2002**, *12*, 628-633.

(11) Gruebele, M.; Sabelko, J.; Ballew, M.; Ervin, J. *Acc. Chem. Res.* **1998**, *31*, 699-707.

(12) Holzwarth, J. F.; Schmidt, A.; Wolff, H.; Volk, R. *J. Phys. Chem.* **1977**, *81*, 2300-2301.

(13) Ma, H.; Wan, C.; Zewail, A. H. *J. Am. Chem. Soc.* **2006**, *128*, 6338-6340.

(14) Caldin, E. F.; Crooks, J. E.; Robinson, B. H. *J. Phys. E: Sci. Instrum.* **1971**, *4*, 165-189.

(15) Ameen, S. *Rev. Sci. Instrum.* **1975**, *46*, 1209-1215.

(16) Turner, D. H.; Flynn, G. H.; Sutin, N.; Beitz, J. V. *J. Am. Chem. Soc.* **1972**, *94*, 1554-1559.

(17) Williams, A. P.; Longfellow, C. E.; Freier, S. M.; Kierzek, R.; Turner, D. H. *Biochemistry* **1989**, *28*, 4283-4291.

(18) Yamamoto, K.; Mizutani, Y.; Kitagawa, T. *Biophys. J.* **2000**, *79*, 485-495.

(19) Berger, R. L.; Balko, B.; Borcherdt, W.; Friauf, W. *Rev. Sci. Instrum.* **1968**, *39*, 486-493.

(20) Thurn, T.; Bloor, D. M.; Wyn-Jones, E. In *Mixed Surfactant Systems (2nd Edition)*; Abe, M., Scamehorn, J. F., Eds.; CRC Press: 2005, p 709-768.

(21) Verrall, R. E. *Chem. Soc. Rev.* **1995**, *24*, 135-142.

(22) Green, R. J.; Frazier, R. A.; Shakesheff, K. M.; Davies, M. C.; Roberts, C. J.; Tendler, S. J. B. *Biomaterials* **2000**, *21*, 1823-1835.

(23) Englebienne, P.; Van Hoonacker, A.; Verhas, M. *Spectroscopy* **2003**, *17*, 255-273.

(24) Schuck, P. *Annu. Rev. Biophys. Biomol. Struct.* **1997**, *26*, 541-566.

(25) Thompson, N. L. In *Topics in Fluorescence Spectroscopy Volume 1 Techniques*; Lakowicz, J. R., Ed.; Plenum Press: New York, 1991, p 337-378.

(26) Webb, W. W. In *Fluorescence Correlation Spectroscopy*; Rigler, R., Elson, E. S., Eds.; Springer: Berlin, 2001, p 305-330.

(27) Felekyan, S.; Kühnemuth, R.; Kudryavtsev, V.; Sandhagen, C.; Becker, W.; Seidel, C. A. M. *Rev. Sci. Instrum.* **2005**, *76*, 083104.

(28) Freeman, R. *A Handbook of Nuclear Magnetic Resonance*; John Wiley & Sons, Inc.: New York, 1988.

(29) Perrin, C. L.; Dwyer, T. J. *Chem. Rev.* **1990**, *90*, 935-967.

(30) Blackburn, G. M.; Gait, M. J.; Loakes, D.; Williams, D. M. *Nucelic Acids in Chemistry and Biology*; RSC Publsihing: Cambridge, 2006.

(31) Sinden, R. R. *DNA structure and function*; Academic Press, Inc.: San Diego, 1994.

(32) Kumar, C. V. In *Photochemistry in Organized and Constrained Media*; Ramamurthy, V., Ed.; VCH Publishers, Inc.: New York, 1991, p 783-816.

(33) Ihmels, H.; Otto, D. *Top. Curr. Chem.* **2005**, *258*, 161-204.

(34) Denny, W. A. In *DNA and RNA Binders: From Small Molecules to Drugs*; Demeunynck, M., Bailly, C., Wilson, W. D., Eds.; VHC: Weinheim, 2003, p 482-502.

(35) Wemmer, D. E. *Biopolymers* **1999/2000**, *52*, 197-211.

(36) Lacy, E. R.; Madsen, E. M.; Lee, M.; Wilson, W. D. In *DNA and RNA Binders: From Small Molecules to Drugs*; Demeunynck, M., Bailly, C., Wilson, W. D., Eds.; VHC: Weinheim, 2003, p 384-413.

(37) Noble, M. *Proteins: structures and molecular properties*; W. H. Freeman and Company: New York, 1993.

(38) Peters Jr., T. *All about Albumin: Biochemistry, Genetics, and Medical Applications*; Academic Press, Inc.: San Diego, 1996.

(39) Algrem, M.; Grieser, F.; Thomas, J. K. *J. Am Chem. Soc.* **1979**, *101*, 279-291.

(40) Scaiano, J. C.; Selwyn, J. C. *Photochem. and Photobiol.* **1981**, *34*, 29-32.

(41) Scaiano, J. C.; Selwyn, J. C. *Can. J. Chem.* **1981**, *59*, 2368-2372.

(42) Okano, L. T.; Barros, T. C.; Chou, D. T. H.; Bennet, A. J.; Bohne, C. *J. Phys. Chem. B* **2001**, *105*, 2122-2128.

(43) Cramer, F.; Saenger, W.; Spatz, H.-C. *J. Am Chem. Soc.* **1967**, *89*, 14-20.

(44) Pace, T. C. S.; Monahan, S. L.; MacRae, A. I.; Kaila, M.; Bohne, C. *Photochem. Photobiol.* **2006**, *82*, 78-87.

(45) Denny, W. A.; Atwell, G. J.; Baguley, B. C.; Wakelin, L. P. G. *J. Med. Chem.* **1985**, *28*, 1568-1574.

(46) Feigon, J.; Denny, W. A.; Leupin, W.; Kearns, D. R. *J. Med. Chem.* **1984**, *27*, 450-465.

(47) Fox, K. R.; Wakelin, L. P. G.; Waring, M. J. *Biochemistry* **1981**, *20*, 5768-5779.

(48) Gabbay, E. J.; Grier, D.; Fingerle, R. E.; Reimer, R.; Levy, R.; Pearce, S. W.; Wilson, W. D. *Biochemistry* **1976**, *15*, 2062-2070.

(49) Pace, T. C. S.; Bohne, C. *Adv. Phys. Org. Chem.* **2008**, *42*, 167-223.

(50) Waring, M. J. *J. Mol. Biol.* **1965**, *13*, 269-282.

(51) Magde, D.; Elson, E. S.; Webb, W. W. *Phys. Rev. Lett.* **1972**, *29*, 705-708.

(52) Mandal, C.; Englander, S. W.; Kallenbach, N. R. *Biochemistry* **1980**, *19*, 5819-5825.

(53) Macgregor Jr., R. B.; Clegg, R. M.; Jovin, T. M. *Biochemistry* **1987**, *26*, 4008-4016.

(54) Meyer-Almes, F. J.; Porschke, D. *Biochemistry* **1993**, *32*, 4246-4253.

(55) Bresloff, J. L.; Crothers, D. M. *J. Mol. Biol.* **1975**, *95*, 103-123.

(56) Wakelin, L. P. G.; Waring, M. J. *J. Mol. Biol.* **1980**, *144*, 183-214.

(57) Geacintov, N. E.; Waldmeyer, J.; Kuzmin, V. A.; Kolubayev, T. *J. Phys. Chem.* **1981**, *85*, 3608-3613.

(58) Steenken, S.; Jovanovic, S. V. *J. Am. Chem. Soc.* **1997**, *119*, 617-618.

(59) Murov, S. L.; Carmichael, I.; Hug, G. L. *Handbook of Photochemistry*; 2nd, revised and expanded ed.; Marcel Dekker, Inc.: New York, 1993.

(60) Abuin, E. B.; Scaiano, J. C. *J. Am. Chem. Soc.* **1984**, *106*, 6274-6283.

(61) Barra, M. *Supramol. Chem.* **1997**, *8*, 263-266.

(62) Barra, M.; Bohne, C.; Scaiano, J. C. *J. Am. Chem. Soc.* **1990**, *112*, 8075-8079.

(63) Liao, Y.; Bohne, C. *J. Phys. Chem.* **1996**, *100*, 734-743.

(64) Liao, Y.; Frank, J.; Holzwarth, J. F.; Bohne, C. *J. Chem. Soc., Chem. Commun.* **1995**, 2435-2436.

(65) Atwell, G. J.; Rewcastle, G. W.; Baguley, B. C.; Denny, W. A. *J. Med. Chem.* **1990**, *33*, 1375-1379.

(66) Ibrom, W. G. A.; Frahm, A. W. *Arzneim.-Forsch./Drug Res.* **1997**, *47*, 662-667.

(67) Ignatushchenko, M. V.; Winter, R. W.; Bächinger, H. P.; Hinrichs, D. V.; Riscoe, M. K. *FEBS Lett.* **1997**, *409*, 67-73.

(68) Lin, C.-N.; Hsieh, H.-K.; Liou, S.-J.; Ko, H.-H.; Lin, H.-C.; Chung, M.-I.; Ko, F.-N.; Liou, H.-W.; Teng, C.-M. *J. Pharm. Pharmacol.* **1996**, *48*, 887-890.

(69) Lin, C.-N.; Liou, S.-J.; Lee, T.-H.; Chuang, Y.-C.; Won, S.-J. *J. Pharm. Pharmacol.* **1996**, *48*, 539-544.

(70) Liou, S.-S.; Shieh, W.-L.; Cheng, T.-H.; Won, S.-J.; Lin, C.-N. *J. Pharm. Pharmacol.* **1993**, *45*, 791-794.

(71) Wang, T.-C.; Chen, Y.-L.; Tzeng, C.-C.; Liou, S.-S.; Chang, Y.-L.; Teng, C.-M. *Helv. Chim. Acta* **1996**, *79*, 1620-1626.

(72) Hirakawa, K.; Yoshida, M.; Oikawa, S.; Kawanishi, S. *Photochem. Photobiol.* **2003**, *77*, 349-355.

(73) Monahan, S. L., University of Victoria, 1999.

(74) Syromyatnikov, V. G.; Yashchuk, V. M. N.; Ogul'chansky, T. Y.; Novikova, O. O.; Piryatinsky, Y. P.; Kolendo, O. Y. *J. Fluoresc.* **1999**, *9*, 93-98.

(75) McGhee, J. D.; von Hippel, P. H. *J. Mol. Biol.* **1974**, *86*, 469-489.

(76) Bohne, C.; Redmond, R. W.; Scaiano, J. C. In *Photochemistry in Organized and Constrained Media*; Ramamurthy, V., Ed.; VCH Publishers: New York, 1991, p 79-132.

(77) Ireland, J. F.; Wyatt, P. A. H. *J. Chem. Soc., Faraday Trans. 1* **1972**, *68*, 1053-1058.

(78) Pownall, H. J.; Huber, J. R. *J. Am. Chem. Soc.* **1971**, *93*, 6429-6436.

(79) Abdullah, K. A.; Kemp, T. J. *J. Photochem. Photobiol., A: Chem.* **1986**, *32*, 49-57.

(80) Boch, R.; Whittlesey, M. K.; Scaiano, J. C. *J. Phys. Chem.* **1994**, *98*, 7854-7857.

(81) Elisei, F.; Favaro, G.; Görner, H. *J. Photochem. Photobiol., A: Chem.* **1991**, *59*, 243-253.

(82) Okano, L. T.; Ovans, R.; Zunic, V.; Moorthy, J. N.; Bohne, C. *Can. J. Chem.* **1999**, *77*, 1356-1365.

(83) Janata, E.; Schuler, R. H. *J. Phys. Chem.* **1982**, *86*, 2078-2084.

(84) Carmichael, I.; Hug, G. L. *J. Phys. Chem. Ref. Data* **1986**, *15*, 1-250.

(85) Treinin, A.; Hayon, E. *J. Am. Chem. Soc.* **1976**, *98*, 3884-3891.

(86) Ju, C.; Bohne, C. *J. Phys. Chem.* **1996**, *100*, 3847-3854.

(87) Inoue, H.; Hida, M.; Nakashima, N.; Yoshihara, K. *J. Phys. Chem.* **1982**, *86*, 3184-3186.

(88) Moog, R. S.; Burozski, N. A.; Desai, M. M.; Good, W. R.; Silvers, C. D.; Thompson, P. A.; Simon, J. D. *J. Phys. Chem.* **1991**, *95*, 8466-8473.

(89) Biczók, L.; Bérces, T.; Inoue, H. *J. Phys. Chem. A* **1999**, *103*, 3837-3842.

(90) Biczók, L.; Bérces, T.; Linschitz, H. *J. Am. Chem. Soc.* **1997**, *119*, 11071-11077.

(91) Flom, S. R.; Barbara, P. F. *J. Phys. Chem.* **1985**, *89*, 4489-4494.

(92) Waissbluth , O. L.; Morales., M., C.; Bohne, C. *Photochem. Photobiol.* **2006**, *82*, 1030-1038.

(93) Marcandalli, B.; Stange, G.; Holzwarth, J. F. *J. Chem. Soc., Faraday Trans. 1* **1988**, *84*, 2807-2819.

(94) Goldmints, I.; Holzwarth, J. F.; Smith, K. A.; Hatton, T. A. *Langmuir* **1997**, *13*, 6130-6134.

(95) Kositza, M. J.; Bohne, C.; Alexandridis, P.; Hatton, T. A.; Holzwarth, J. F. *Macromolecules* **1999**, *32*, 5539-5551.

(96) Peacocke, A. R. In *The Chemistry of Heterocyclic Compounds: Acridines*; Acheson, R. M., Ed.; John Wiley and Sons, Inc.: 1973, p 723-757.

(97) Holzwarth, J. F.; Eck, V.; Genz, A. In *Spectroscopy and the Dynamics of Molecular Biological Systems*; Bayley, P. M., Dale, R. E., Eds.; Academic Press Inc.: London, 1985, p 351-377.

(98) Biver, T.; Secco, F.; Tinè, M. R.; Venturini, M. *Arch. Biochem. Biophys.* **2003**, *418*, 63-70.

(99) Corin, A. F.; Jovin, T. M. *Biochemistry* **1986**, *25*, 3995-4007.

(100) Dourlent, M.; Hogrel, J. F. *Biochemistry* **1976**, *15*, 430-436.

(101) Li, H. J.; Crothers, D. M. *J. Mol. Biol.* **1969**, *39*, 461-477.

(102) Ramstein, J.; Ehrenberg, M.; Rigler, R. *Biochemistry* **1980**, *19*, 3938-3948.

(103) Sakoda, M.; Hiromi, K.; Akasaka, K. *Biopolymers* **1971**, *10*, 1003-1012.

(104) Genz, A.; Holzwarth, J. F. *Eur. Biophys. J.* **1986**, *13*, 323-330.

(105) Inoue, Y.; Dong, F.; Yamamoto, K.; Tong, L. H.; Tsuneishi, H.; Hakushi, T.; Tai, A. *J. Am. Chem. Soc.* **1995**, *117*, 11033-11034.

(106) Inoue, Y.; Wada, T.; Sugahara, N.; Yamamoto, K.; Kimura, K.; Tong, L. H.; Gao, X. M.; Hou, Z. J.; Liu, Y. *J. Org. Chem.* **2000**, *65*, 8041-8050.

(107) Lu, R. H.; Yang, C.; Cao, Y. J.; Wang, Z. Z.; Wada, T.; Jiao, W.; Mori, T.; Inoue, Y. *Chem. Commun.* **2008**, 374-376.

(108) Nakamura, A.; Inoue, Y. *J. Am. Chem. Soc.* **2003**, *125*, 966-972.

(109) Nakamura, A.; Inoue, Y. *J. Am. Chem. Soc.* **2005**, *127*, 5338-5339.

(110) Rao, V. P.; Turro, N. J. *Tetrahedron Lett.* **1989**, *30*, 4641-4644.

(111) Tamaki, T.; Kokubu, T. *J. Inclusion Phenom.* **1984**, *2*, 815-822.

(112) Tamaki, T.; Kokubu, T.; Ichimura, K. *Tetrahedron* **1987**, *43*, 1485-1494.

(113) Yang, C.; Fukuhara, G.; Nakamura, A.; Origane, Y.; Fujita, K.; Yuan, D.-Q.; Mori, T.; Wada, T.; Inoue, Y. *J. Photochem. Photobiol., A: Chem.* **2005**, *173*, 375-383.

(114) Yang, C.; Nakamura, A.; Fukuhara, G.; Origane, Y.; Mori, T.; Wada, T.; Inoue, Y. *J. Org. Chem.* **2006**, *71*, 3126-3136.

(115) Yang, C.; Nakamura, A.; Wada, T.; Inoue, Y. *Org. Lett.* **2006**, *8*, 3005-3008.

(116) Joy, A.; Ramamurthy, V.; Scheffer, J. R.; Corbin, D. R. *Chem. Commun.* **1998**, 1379-1380.

(117) Joy, A.; Scheffer, J. R.; Ramamurthy, V. *Org. Lett.* **2000**, *2*, 119-121.

(118) Wada, T.; Shikimi, M.; Inoue, Y.; Lem, G.; Turro, N. J. *Chem. Commun.* **2001**, 1864-1865.

(119) Bach, T.; Bergmann, H.; Grosch, B.; Harms, K. *J. Am. Chem. Soc.* **2000**, *124*, 7982-7990.

(120) Cauble, D. F.; Lynch, V.; Krische, M. J. *J. Org. Chem.* **2003**, *68*, 15-21.

(121) Grosch, B.; Orlebar, C. N.; Herdtweck, E.; Massa, W.; Bach, T. *Angew. Chem. Int. Ed.* **2003**, *42*, 3693-3696.

(122) Mizoguchi, J.; Kawanami, Y.; Wada, T.; Kodama, K.; Anzai, K.; Yanagi, T.; Inoue, Y. *Org. Lett.* **2006**, *8*, 6051-6054.

(123) Tanaka, K.; Fujiwara, T. *Org. Lett.* **2005**, *7*, 1501-1503.

(124) Festa, C.; Levi-Minzi, N.; Zandomeneghi, G. *Gazz. Chim. Ital.* **1996**, *136*, 599-603.

(125) Levi-Minzi, N.; Zandomeneghi, M. *J. Am. Chem. Soc.* **1992**, *114*, 9300-9304.

(126) Ouchi, A.; Zandomeneghi, G.; Zandomeneghi, M. *Chirality* **2002**, *14*, 1-11.

(127) Jiménez, M. C.; Miranda, M. A.; Vayá, I. *J. Am Chem. Soc.* **2005**, *127*, 10134-10135.

(128) Lhiaubet-Vallet, V.; Sarabia, Z.; Boscá, F.; Miranda; M. A. *J. Am. Chem. Soc.* **2004**, *126*, 9538-9529.

(129) Vay, I.; Jiménez, M. C.; Miranda, M. A. *J. Phys. Chem. B* **2008**, *112*, 2694-2699.

(130) Monti, S.; Manet, I.; Manoli, F.; Sartino, S. *Photochem. and Photobiol. Sci.* **2007**, *6*, 462-470.

(131) Bouas-Laurent, H.; Castellan, A.; Desvergne, J.-P.; Lapouyade, R. *Chem. Soc. Rev.* **2001**, *30*, 248-263.

(132) Nishijima, M.; Pace, T. C. S.; Nakamura, A.; Mori, T.; Wada, T.; Bohne, C.; Inoue, Y. *J. Org. Chem.* **2007**, *72*, 2707-2715.

(133) Wada, T.; Nishijima, M.; Fujisawa, T.; Sugahara, N.; Mori, T.; Nakamura, A.; Inoue, Y. *J. Am. Chem. Soc.* **2003**, *125*, 7492-7493.

(134) Nishijima, M.; Wada, T.; Mori, T.; Pace, T. C. S.; Bohne, C.; Inoue, Y. *J. Am. Chem. Soc.* **2007**, *129*, 3478-3479.

(135) Kragh-Hansen, U. *Pharmacol. Rev.* **1981**, *33*, 17-53.

(136) Mi, Z.; Burke, T. G. *Biochemistry* **1994**, *33*, 12540-12545.

(137) Sulkowska, A. *J. Mol. Struct.* **2002**, *614*, 227-232.

(138) Ghuman, J.; Zaunszain, P. A.; Petitpas, I.; Bhattacharya, A. A.; Otagiri, M.; Curry, S. *J. Mol. Biol.* **2005**, *353*, 38-52.

(139) Sugio, S.; Kashima, A.; Mochizuki, S.; Noda, M.; Kobayashi, K. *Protein Eng.* **1999**, *12*, 439-446.

(140) Tabachnick, M.; Korcek, L. *Arch. Biochem. Biophys.* **1979**, *198*, 403-405.

(141) Inoue, Y.; Nishijima, M., Personal Communication.

(142) Eftink, M. R. In *Topics in Fluorescence Spectroscopy. Vol. 2, Principles*; Lakowicz, J. R., Ed.; Plenum Press: New York, 1991, p 53-126.

(143) Chadborn, N.; Bryant, J.; Bain, A. J.; O'Shea, P. *Biophys. J.* **1999**, *76*, 2198-2207.

(144) Nicoletti, F. P.; Howes, B. D.; Fittipaldi, M.; Fanali, G.; Fasano, M.; Ascenzi, P.; Smulevich, G. *J. Am. Chem. Soc.* **2008**, *130*, 11677-11688.